Progress in Retinal and Eye Research 104 (2025) 101320

Contents lists available at ScienceDirect

Progress in Retinal and Eye Research

journal homepage: www.elsevier.com/locate/preteyeres

Extensive macular atrophy with pseudodrusen-like appearance (EMAP) clinical characteristics, diagnostic criteria, and insights from allied inherited retinal diseases and age-related macular degeneration

Alessio Antropoli [a,b,c,1], Lorenzo Bianco [a,b,c,1], Francesco Romano [d], Andrea Trinco [d], Alessandro Arrigo [c,e], Amine Benadji [b], Raphaël Atia [b], Oana Palacci [b], Dorothée Dagostinoz [b], Céline Devisme [b], Christel Condroyer [a], Aline Antonio [a], Francesca Bosello [f], Stefano Casati [f], Anna Paola Salvetti [d], Chiara Zaffalon [d,f], Alain Gaudric [g,h], José-Alain Sahel [i], Giovanni Staurenghi [d], Francesco Bandello [c], Florian Sennlaub [a], Christina Zeitz [a], Isabelle Meunier [j], Maurizio Battaglia Parodi [c], Isabelle Audo [a,b,*]

[a] Sorbonne Université, INSERM, CNRS, Institut de la Vision, Paris, France
[b] CHNO des Quinze-Vingts, Centre de Référence Maladies Rares REFERET and DHU Sight Restore, INSERM-DGOS CIC1423, Paris, France
[c] Department of Ophthalmology, IRCCS San Raffaele Scientific Institute, Milan, Italy
[d] Eye Repair Unit, Division of Neuroscience, IRCCS San Raffaele Scientific Institute, Milan, Italy
[e] Eye Clinic, Department of Biomedical and Clinical Science, Luigi Sacco Hospital, University of Milan, Milan, Italy
[f] Ophthalmic Unit, Department of Neurosciences, Biomedicine and Movement Sciences, University of Verona, Verona, Italy
[g] Ophthalmology Center for Imaging and Laser, Paris, France
[h] Department of Ophthalmology, AP-HP, Hôpital Lariboisière, Université Paris Cité, Paris, France
[i] Department of Ophthalmology, The University of Pittsburgh School of Medicine, Pittsburgh, PA, 15213, USA
[j] National Reference Center for Inherited Sensory Diseases, University Hospital of Montpellier, University of Montpellier, Montpellier, France

ARTICLE INFO

Keywords:
Extensive macular atrophy with pseudodrusen-like appearance
Multimodal imaging
Retinal electrophysiology
Diffuse-trickling geographic atrophy
Age-related macular degeneration
Inherited retinal diseases

ABSTRACT

Extensive macular atrophy with pseudodrusen-like appearance (EMAP) was first described in France in 2009 as a symmetric and rapidly progressive form of macular atrophy primarily affecting middle-aged individuals. Despite the recent identification of a significant number of cases in Italy and worldwide, EMAP remains an under-recognized condition. The clinical triad typical of EMAP consists of vertically oriented macular atrophy with multilobular borders, pseudodrusen-like deposits across the posterior pole and mid-periphery, and peripheral pavingstone degeneration. Nonetheless, recent research has portrayed EMAP as a highly stage-dependent condition, allowing the identification of novel disease hallmarks, including a diffuse separation between the Bruch's membrane and the retinal pigment epithelium, along with consistent sparing of a region temporal to the macula. Additionally, retinal electrophysiology is particularly useful in distinguishing EMAP from age-related macular degeneration (AMD).

Supported by unpublished data from the largest EMAP cohorts worldwide, this review aims to provide a comprehensive and updated description of EMAP, now recognized as a severely blinding disease characterized by diffuse chorioretinal atrophy and photoreceptor dysfunction. Furthermore, we propose a set of diagnostic criteria that incorporate clinical, imaging, and functional tests, to facilitate the recognition of this clinical entity. Lastly, we aim to shed light on its pathogenesis by comparing it with AMD and monogenic retinal disorders exhibiting similar phenotypes.

* Corresponding author. Sorbonne Université, INSERM, CNRS, Institut de la Vision, Paris, France.
E-mail address: isabelle.audo@inserm.fr (I. Audo).
[1] Joint first authors, listed in alphabetical order.

https://doi.org/10.1016/j.preteyeres.2024.101320
Received 14 April 2024; Received in revised form 19 November 2024; Accepted 21 November 2024
Available online 25 November 2024

List of abbreviations

AF	Autofluorescence
AMD	Age-Related Macular Degeneration
BCVA	Best-corrected visual acuity
BLamD	Basal Laminar Deposits
BLinD	Basal Linear Deposits
BM	Bruch's membrane
CAM	Classification of Atrophy Meeting
CFP	Color Fundus Photograph
cRORA	complete retinal pigment epithelium and outer retinal atrophy
DA	Dark-adapted
DDAF	Definitely Decreased Autofluorescence
DTGA	Diffuse-Trickling Geographic Atrophy
EMAP	Extensive Macular Atrophy with Pseudodrusen-like appearance
FA	Fundus Albipunctatus
ERG	electroretinogram
ICGA	Indocyanine green angiography
IRD	Inherited Retinal Diseases
ISCEV	International Society for Clinical Electrophysiology of Vision
L-ORD	Late-Onset Retinal Degeneration
LA	Light-adapted
MA	Macular Atrophy
MDAF	Moderately Decreased Autofluorescence
MNV	Macular Neovascularization
NIR-AF	Near-infrared Autofluorescence
NIR	Near Infrared Reflectance
OCT	Optical Coherence Tomography
OCTA	Optical coherence tomography angiography
PXE	Pseudoxanthoma elasticum
qAF	quantitative Autofluorescence
QDAF	Questionably Decreased Autofluorescence
RPA	Retinitis Punctata Albescens
RPD	Reticular pseudodrusen
RPE	Retinal Pigment Epithelium
SDD	Subretinal drusenoid deposit
SFD	Sorsby Fundus Dystrophy
SW-AF	Short-wavelength autofluorescence
UWF	Ultra-widefield

1. Introduction

In 2009, Hamel et al. described in France a rapidly progressive form of macular atrophy (MA) which they named "extensive macular atrophy with pseudodrusen-like appearance (EMAP)" (Hamel et al., 2009). The disease symmetrically affected both eyes of middle-aged patients and was characterized by three key features: (1) a large, vertically-oriented MA with multilobular borders, (2) a lattice of yellowish pseudodrusen-like deposits spread throughout the posterior pole and mid-periphery, and (3) pavingstone degeneration in the far periphery. While the consistent association of these features was unique to EMAP, the close resemblance to other genetic retinal diseases, such as Sorsby fundus dystrophy (SFD) and late-onset retinal degeneration (L-ORD), soon elicited skeptical opinions (Boon et al., 2009). Additional analogies emerged also between EMAP and the diffuse-trickling pattern of geographic atrophy (DTGA) secondary to age-related macular degeneration (AMD) (Holz et al., 2007). These included a diffuse retinal pigment epithelium (RPE)-Bruch's membrane (BM) separation on optical coherence tomography (OCT), a peculiar "grayish" appearance of MA on short-wavelength autofluorescence (SW-AF), and an exceptionally fast growth rate.

Subsequently, the findings from the French multicentric "EMAP Case-Control National Clinical Trial" proved instrumental in identifying numerous potential risk factors in affected patients (Douillard et al., 2016, 2018). Indeed, in the recent years, other large cohorts of patients have been documented in Italy, contributing further to the literature regarding the natural history and imaging features of EMAP (Antropoli et al., 2023; Battaglia Parodi et al., 2023; Bianco et al., 2023; Romano

Fig. 1. *Hallmarks of EMAP on multimodal retinal imaging*. The central macular lesion is better documented using short-wavelength fundus autofluorescence because of its unique features (moderately decreased autofluorescence with predominant vertical axis and multilobular borders). Optical coherence tomography demonstrates thick hyporeflective deposits separating the retinal pigmented epithelium (RPE) from Bruch's membrane (BM) in the macular region surrounding the atrophic lesion. Widespread yellowish pseudodrusen-like deposits in the posterior pole and mid-periphery, as well as areas of peripheral pavingstone-like degeneration, are seen on pseudocolor ultrawide-field retinography.

et al., 2021; Romano et al., 2023c). Additional cases outside Europe have been reported (Sato et al., 2022a; Vilela and Battaglia Parodi, 2022; Watanabe et al., 2023), confirming that EMAP might be "*rare but not exceptional*" (Puech et al., 2014). Despite these advances, EMAP is still considered a "niche" diagnosis, and many patients in their sixties are mistakenly diagnosed with AMD.

The aim of this review is to provide a comprehensive and updated description of EMAP, now recognized as a severely blinding disease characterized by diffuse chorioretinal atrophy and photoreceptor dysfunction. Furthermore, EMAP can be distinguished using multimodal retinal imaging by a set of hallmark features, as illustrated in Fig. 1 and discussed in detail herein. To make our case, we will present unpublished data collected from two large European cohorts: 79 patients followed at IRCCS San Raffaele Scientific Institute in Milan, Luigi Sacco Hospital in Milan, and Borgo Roma Hospital in Verona (Italy), alongside 89 patients followed at the rare disease center REFERET of Quinze-Vingts Hospital in Paris (France) (Supplementary Material). Building on this detailed discussion, we will next delve into its similarities with AMD and monogenic retinal conditions to shed light on its pathogenesis. In the final chapter, we will propose the first diagnostic criteria for EMAP.

2. Environmental and genetic risk factors

Seven years following its initial description, the first results of the "EMAP Case-Control National Clinical Trial" conducted in France were published (Douillard et al., 2016, 2018). The study included a total of 115 patients diagnosed with EMAP - 61% being women - alongside 415 healthy controls and investigated the environmental and genetic risk factors of EMAP. Interestingly, most patients were born immediately after the end of World War II, between 1946 and 1950, with a notable peak in 1948 (Douillard et al., 2018). The disease prevalence was higher in geographic regions characterized by intensive farming or industrial activities. Occupational exposure to toxic compounds was identified as a risk factor (Douillard et al., 2018), along with a family history of glaucoma or AMD (Douillard et al., 2016). Abnormal erythrocyte sedimentation rate, increased plasma concentration of complement component 3 (C3), as well as other biomarkers of systemic inflammation (eosinophilia, lymphocytosis) were associated with EMAP. Interestingly, a reduced serum activity of classical complement pathway (measured as the CH_{50}) was also noted. Conversely, no association was found with known risk factors for AMD, such as cardiovascular diseases, hypercholesterolemia, hypertension, and smoking (Douillard et al., 2016). Genetic variants previously associated with AMD were evaluated in a subgroup of 65 patients (Douillard et al., 2018). The only genetic variant demonstrating a significant association was the rs2230199 variant in the *C3* gene (Yates et al., 2007), which increased the probability of being affected by EMAP by 50% (Douillard et al., 2018). The authors concluded that EMAP may be a neurodegenerative disease resulting from chronic inflammation and abnormal complement pathway activation with a toxic contribution (Douillard et al., 2018).

Given the diverse etiologies that have been hypothesized for EMAP, we reviewed the available medical histories of patients from the French Quinze-Vingts cohort. Beyond the cardiovascular risk factors, such as high blood pressure and hypercholesterolemia, approximately half of these patients exhibited a silent medical history. The remaining half presented at least one additional comorbidity, frequently related to endocrine-metabolic conditions (notably, diabetes and thyroid diseases), as well as neoplastic, rheumatic, or immune-related diseases. Interestingly, around 20% of patients suffered from two or more additional comorbidities. A comprehensive report detailing the patients' medical histories is available in the Supplementary Material.

The above-mentioned cluster of patients born around 1948, coupled with the uneven case distribution across France, positioned EMAP as a phenomenon confined in time and space, much like an outbreak. However, a similar distribution of EMAP cases has been observed in Northern Italy, where a significant number of cases has been identified. More specifically, the Italian EMAP cases are clustered in the Po Valley region and were born between 1955 and 1965, with 1960 emerging as the most frequent birth year (Fig. 2A). It must be acknowledged that the clusters observed in 1948 (France) and 1960 (Italy), as well as the regional differences, may be attributed to a selection bias. Indeed, EMAP patients typically seek consultation with a retina specialist around age 60 when they first notice symptoms. The first description of EMAP in France in 2009 coincided with individuals born around 1948 reaching the age of 60, which might explain the prominence of this birth year in the French cohorts (Fig. 2B). Subsequently, recognition of the disease in Italy trailed, with a considerable number of diagnoses around 2020, the year in which those born in 1960 turned the very same age of 60. Therefore, it is critical to recognize the possibility that EMAP may have been misdiagnosed as AMD in the past years, as well as the existence of younger asymptomatic individuals with EMAP who have not yet been diagnosed.

Furthermore, although EMAP has predominantly been considered a regional phenomenon observed in Europe, documented cases from other continents have emerged recently. A cohort of 18 patients affected by EMAP has been described in Brazil (Watanabe et al., 2023). In their study, Watanabe et al. reported an association between EMAP and rheumatic fever, with 17 out of 18 patients having received prolonged penicillin treatment for rheumatic fever prevention. Moreover, roughly half of their patients also suffered from a systemic inflammatory condition, and 22% of them had at least one autoimmune disease (Moreira-Neto et al., 2024). These findings led the authors to hypothesize an autoimmune etiology (Watanabe et al., 2023). Formally, only one case of EMAP has been documented in Japan (Sato et al., 2022b), although some of the 6 patients described by Tsunoda et al. in 2019 as being affected by progressive trickle-like macular degeneration with peripheral flecks might also meet the criteria for EMAP (Tsunoda et al., 2019). Indeed, all these patients presented between 49 and 71 years of age and exhibited rapidly progressive MA, a diffuse RPE-BM separation on OCT, pseudodrusen and confluent drusen-like deposits, decreased scotopic full-field ERG responses recovering after prolonged dark adaptation (see section 6), and no pathogenic variants in IRD-associated genes detected by whole-exome sequencing. Despite these similarities, EMAP was not recognized as a possible diagnosis by the authors (Tsunoda et al., 2019).

Overall, to date no definitive evidence exists on the etiology and risk factors for EMAP, with many hypotheses deserving further investigation. However, since the disease mainly affects middle-aged individuals, it is conceivable that EMAP is not strictly related to aging. In this regard, prospective cohort studies and laboratory investigations focusing on the systemic inflammatory and immune profile of these patients are highly warranted. Lastly, considering that EMAP is a bilateral and symmetric disease, pangenomic studies will offer an opportunity to dig deeper into the genetic determinants of this disease.

3. Clinical presentation

The onset of the first visual symptoms in EMAP generally ranges between 45 and 60 years, with the most frequent complaints including photophobia (83%), night blindness (56–95%), dyschromatopsia (67%), or scotoma/visual field loss (33–67%) (Hamel et al., 2009; Romano et al., 2021; Watanabe et al., 2023). A decrease in visual acuity does not represent the most frequent complaint (28%), and it is rarely reported as the sole symptom (Hamel et al., 2009). Indeed, best-corrected visual acuity (BCVA) is highly variable in EMAP, ranging from light perception to 20/20 Snellen, depending on the extent of foveal involvement and the potential development of an eccentric fixation point (Romano et al., 2023c). Unlike AMD, metamorphopsia is not a typical presenting symptom in EMAP, likely due to the absence of large soft drusen and the uncommon occurrence of neovascular complications. EMAP is associated with myopia, present in 77% (53/69) of patients belonging to the

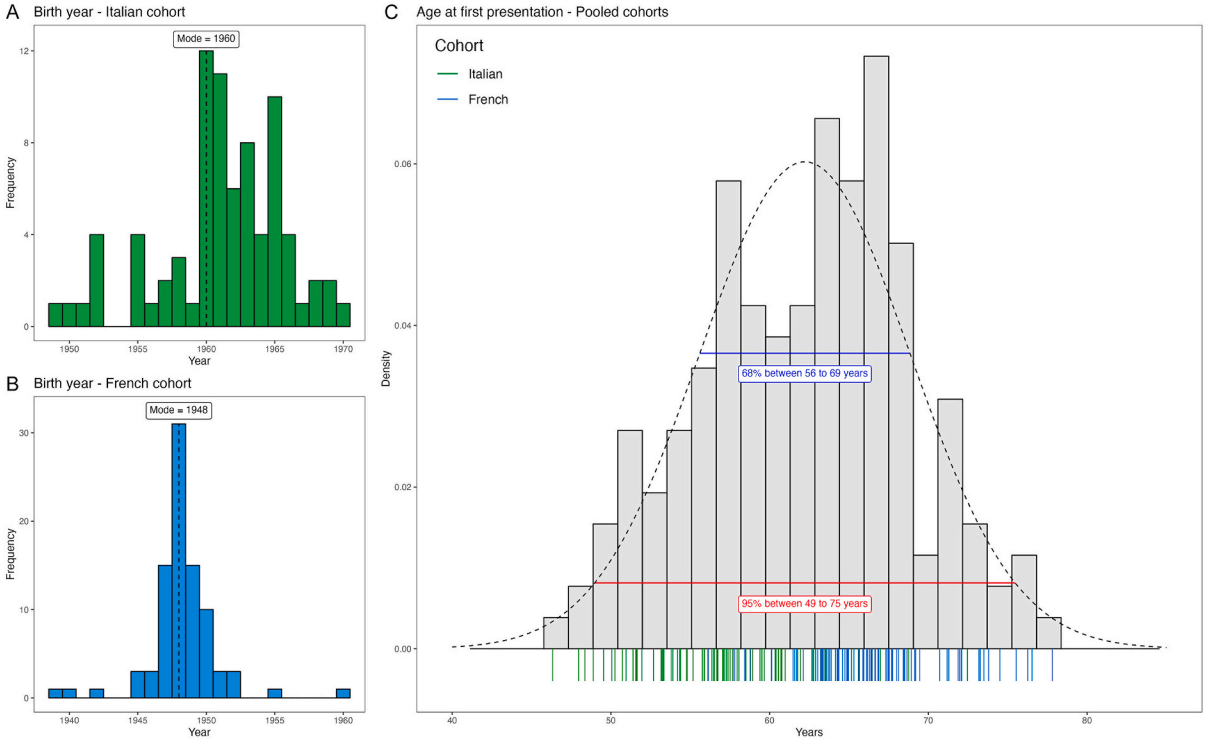

Fig. 2. *Demographic characteristics of the Italian and French EMAP cohorts.* (A, B) Frequency of birth year in the Italian and French Quinze-Vingts EMAP cohorts. (C) Density plot for the age at first presentation in the pooled EMAP cohort. Segments below the x-axis represent individual patients and are color-coded according to the cohort of origin. This variable follows a normal distribution (P = .28 for the Shapiro-Wilk normality test) with a mean ± SD of 62.2 ± 6.6 years (overlaid dotted black curve).

French Quinze-Vingts cohort, with a mean refractive error (spherical equivalent) of −1.4 diopters (95% CI -0.88 to −1.91 diopters; P < .001) in phakic eyes.

Nonetheless, the onset of symptoms and the presenting complaint are subjective and, thus, susceptible to recall bias. Indeed, 28% of patients in the original cohort by Hamel et al. were not able to specify an age of onset (Hamel et al., 2009). Additionally, even in conditions such as retinitis pigmentosa, where night blindness and dark adaptation are typically the earliest symptoms, these issues may remain unrecognized, as artificially illuminated environments at night are more prevalent than in previous decades (Verbakel et al., 2018). On the contrary, while the age at presentation in a reference center for retinal diseases may not accurately reflect the precise onset of the disease, it is less susceptible to bias. Data on the age at first visit collected from the pooled Italian and French Quinze-Vingts cohorts resulted in a normal distribution (Fig. 2C), allowing for some inferences to be made. The mean (SD) age was 62.2 (6.6) years, meaning that most patients presented between 56 and 69 years, yet a not-negligible proportion between 49 and 56 years or between 69 and 75 years. This latter circumstance deserves careful consideration since these patients are more likely to be misdiagnosed as GA secondary to AMD. Indeed, EMAP cases with a later presentation but clear phenotypic features have already been published in the literature (Puech et al., 2014). Thus, we advocate against relying solely on an age threshold as criterion for differentiating EMAP and AMD, without considering the phenotypic features observable on multimodal retinal imaging.

4. Hallmarks on multimodal retinal imaging

The classic diagnostic triad, consisting of MA, pseudodrusen-like deposits, and pavingstone degeneration as described by Hamel et al., was primarily based on observations made through fundus examination and conventional flash-based color fundus photography (CFP) (Hamel et al., 2009). However, the recent diffusion of additional imaging modalities, specifically OCT and ultra-widefield (UWF) retinography, has allowed for a more precise characterization of these pathologic features. In the upcoming sections, we will elaborate on the original triad, delving into the multifaced complexity of these distinctive features to establish a foundation for a set of diagnostic criteria that can accommodate both early and late stages of the disease.

4.1. Macular atrophy

MA in EMAP is bilateral and largely symmetric. On CFP, atrophy appears as a well-demarcated area of hypopigmentation, due to RPE and choriocapillaris loss, with a major vertical axis and multilobular borders, and is surrounded by pseudodrusen-like deposits. In all cases of the original series by Hamel et al., the size of MA was larger than 6 disc areas (Hamel et al., 2009). However, the features of MA in EMAP are highly stage-dependent, given the fast-progressing nature of this disease. The earliest atrophic changes are localized in the superior parafoveal or perifoveal region, and are associated with a diffuse RPE-BM separation at the macula on OCT (see section 4.2) (Fragiotta et al., 2022; Puech et al., 2014; Romano et al., 2023c). Subsequently, the lesion enlarges along the vertical axis until it encroaches upon the fovea, typically occurring after a median of 3.4 years (Antropoli et al., 2024) (Fig. 3). This span of the natural history of EMAP has been summarized in a three-stage disease classification proposed by Romano F et al. (Fig. 4), which also includes potential complications such as MNV (see section 4.6) and correlates with macular sensitivity (see section 6.2) (Romano et al., 2023a, 2023c). Shortly after foveal involvement, MA in EMAP expands outside the posterior pole (Antropoli et al., 2024). Indeed, the central macular lesion expands both centrifugally and through the *de novo* formation of small circular patches of RPE atrophy in the mid-periphery, which is abundant in pseudodrusen-like deposits (Bianco et al., 2023). Due to the peculiar distribution of the deposits along the

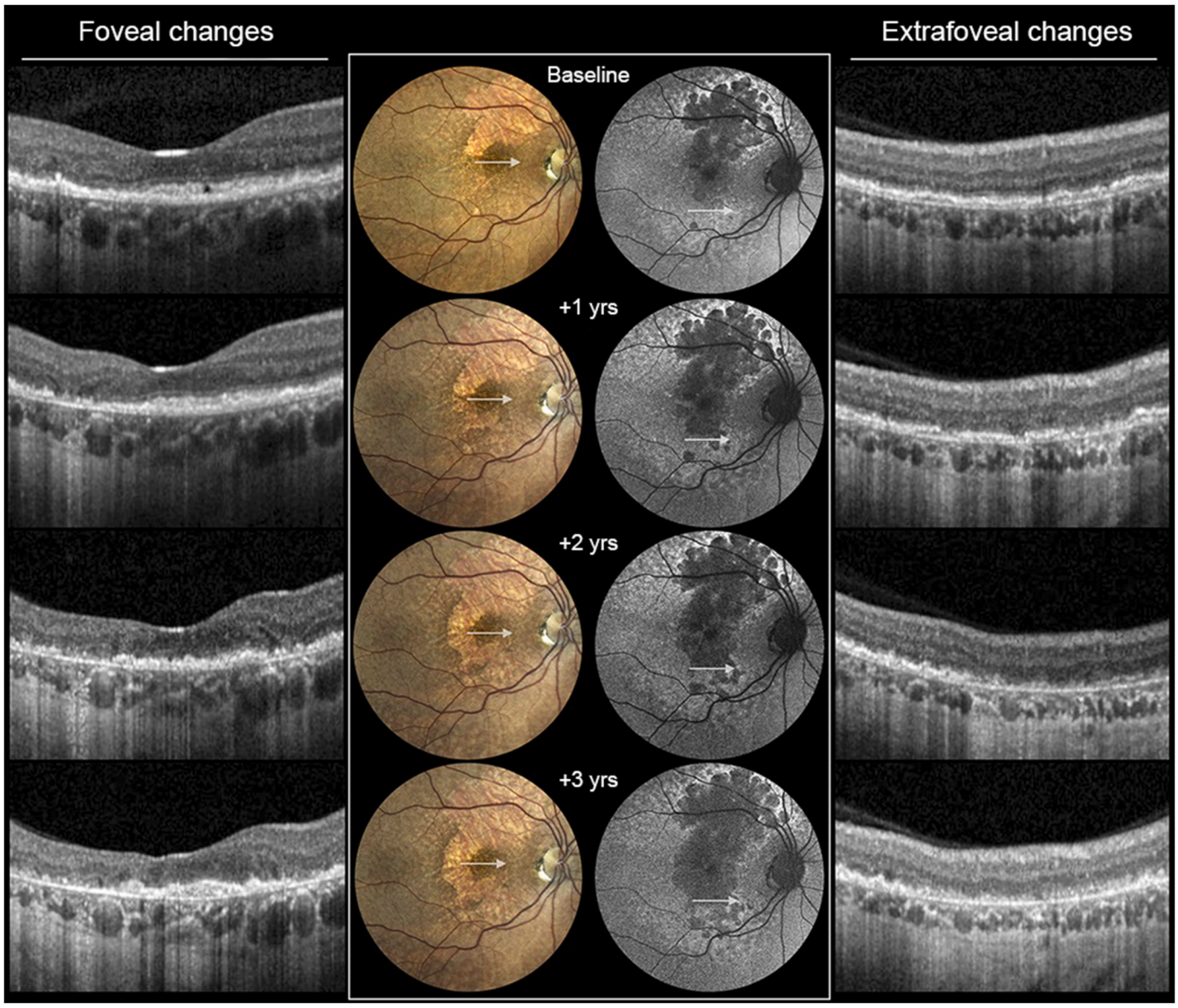

Fig. 3. *Progression of macular atrophy in EMAP over 3 years of follow-up*. (Central panel, fundus changes on color photography and short-wavelength autofluorescence) At baseline, the atrophic lesion is confined at the level of the temporal vascular arcade and parafoveal region. Thereafter, predominant enlargement along the vertical axis leads to loss of foveal sparing by year 2 of follow-up. (Left panel, foveal changes on optical coherence tomography). Severe disruption of the ellipsoid zone (EZ) in the foveal area is present at baseline and progresses toward EZ disappearance by year 2 of follow-up. Conversely, disruption of the external limiting membrane (ELM) and the retinal pigment epithelium (RPE) appears later during the disease course (year 2) and rapidly leads to the development of RPE atrophy with a collapse of the inner retinal layers (year 3). Please note the development of a subfoveal fibrotic nodule shortly after the loss of foveal sparing, between year 2 and year 3. (Right panel, extrafoveal changes on optical coherence tomography) Significant thinning of the outer nuclear layer and diffuse disruption of the EZ are observed at baseline above areas of separation between the RPE and the Bruch's membrane. Focal areas of RPE atrophy progressively appear (year 1) and coalesce over the follow-up (years 2–3). Finally, the inner retinal layers subside, leaving the typical subretinal hyperreflective debris (year 3). [Adapted with permission from "Romano, F., Cozzi, M., Monteduro, D., Oldani, M., Boon, C.J.F., Staurenghi, G., Salvetti, A.P., 2023c. Natural course and classification of Extensive Macular Atrophy with Pseudodrusen-like appearance. Retina 43, 402."].

vertical axis, the atrophy deviates, encircling the optic disc and often mfulling with preexistent patches of atrophy on the nasal side. Conversely, on the temporal side, the atrophy expands toward the mid-periphery, almost invariably leaving an island of spared retinal tissue across the median *raphae*. Thus, in the late stages of EMAP, the atrophy acquires a distinctive "leaf-shaped" silhouette, with the major vertical axis transitioning to a horizontal orientation as the macular lesion expands nasally to the optic nerve and also into the temporal mid-periphery. An exemplary case illustrating the full natural history of EMAP – from small parafoveal lesions to extensive atrophy of the entire posterior pole – was published by Puech & de Laey five years after the initial description of the disease, and it is reproduced in Fig. 5 (Puech et al., 2014). Additionally, areas of peripheral pavingstone-like degeneration grow centripetally and, in some cases, merge with atrophy at the posterior pole and mid-periphery, most often from the temporal sector (Battaglia Parodi et al., 2023) (see section 4.4).

However, imaging modalities such as fundus autofluorescence and OCT hold a critical importance to highlight stage-independent features of MA in EMAP and in enhancing the recognition of the disease, particularly in its early stages.

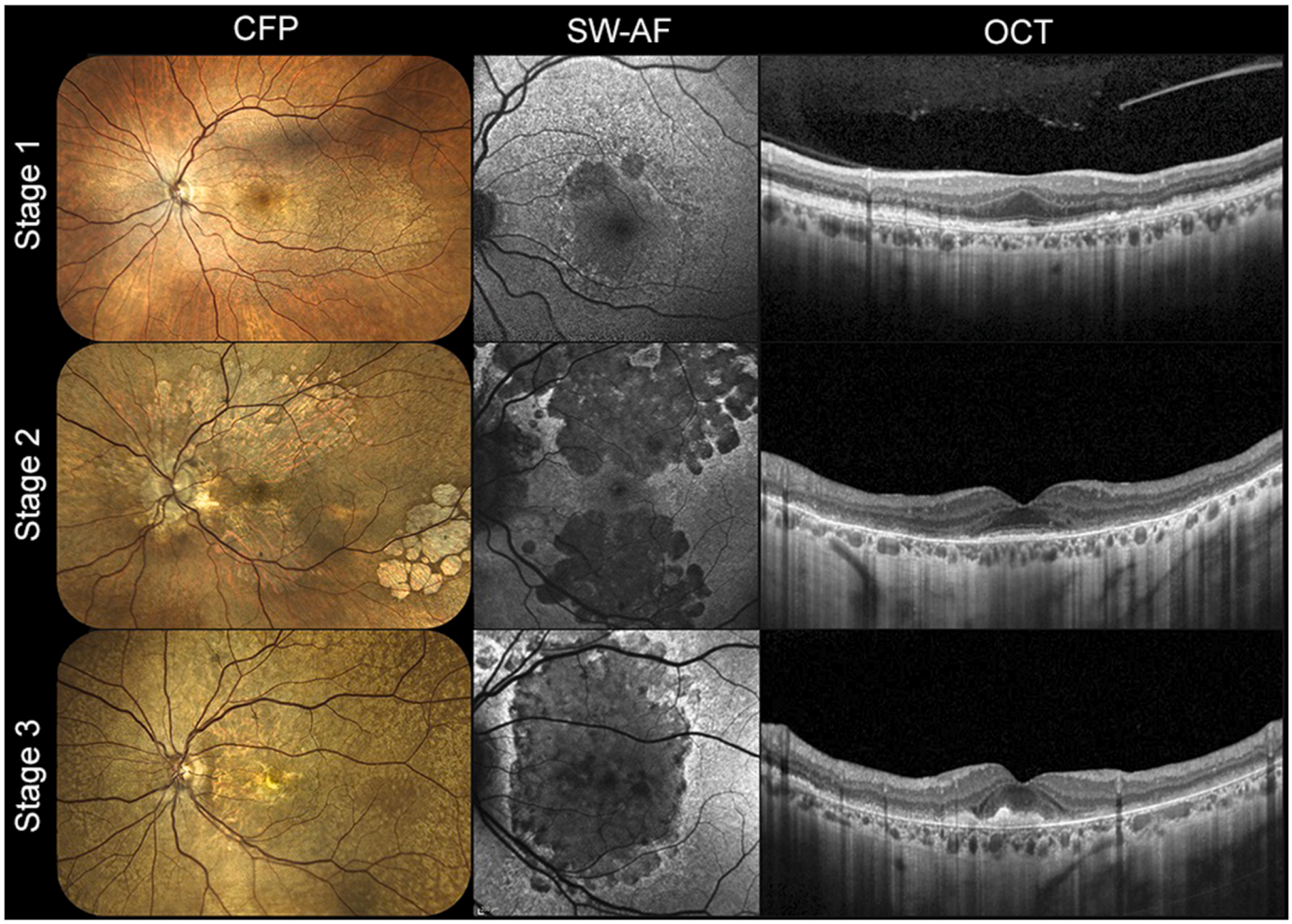

Fig. 4. *Three-stage classification of Extensive Macular Atrophy with Pseudodrusen-Like Appearance (EMAP)*. For each stage, color fundus photograph (CFP), short-wavelength autofluorescence (SW-AF), optical coherence tomography (OCT) images are shown. Stage 1 is characterized by diffuse pseudodrusen-like deposits and a few nonconfluent areas of macular atrophy, generally in the superior parafovea. OCT demonstrates a diffuse separation between the retinal pigment epithelium and the Bruch's membrane with overlying disruption of the ellipsoid zone. In stage 2, the macular atrophy is larger, vertically-oriented, and extends towards the temporal vascular arcades without affecting the fovea. Stage 3 is instead characterized by the loss of foveal sparing (3a), which can be accompanied by the formation of subfoveal fibrosis (3b). At any moment, macular neovascularization may complicate the disease course ("+" feature). [Adapted with permission from "Romano, F., Cozzi, M., Monteduro, D., Oldani, M., Boon, C.J.F., Staurenghi, G., Salvetti, A.P., 2023c. Natural course and classification of Extensive Macular Atrophy with Pseudodrusen-like appearance. Retina 43, 402."].

4.1.1. Short-wavelength autofluorescence

Fundus autofluorescence (AF) imaging allows for non-invasive *en face* visualization of endogenous fluorophores present in the retina, either physiologically or pathologically. The most common form of AF utilizes excitation light in the spectrum of blue light - hence termed SW-AF - with the major fluorophore being lipofuscin, which accumulates physiologically in the RPE cells as part of the normal aging process. Consequently, a uniform AF signal is observed over the posterior pole in a healthy retina, while retinal vessels and the optic nerve head exhibit hypoAF due to blood absorption or the absence of RPE cells, respectively. Similarly, regions of RPE atrophy appear hypoAF on SW-AF imaging, with the degree of hypoAF varying among different macular diseases (Schmitz-Valckenberg et al., 2021). The most unambiguous way to describe the degree of to which AF signal is lost is by comparison with a reference, given that specific instruments are necessary to perform a quantitative analysis of SW-AF images (*see* section 4.1.3). For instance, in the context of *ABCA4*-associated retinopathy, atrophic lesions are graded on a grayscale in reference to the optic nerve head (considered as 100% black). Two distinct types of hypoAF lesions have been distinguished: definitely decreased autofluorescence (DDAF), where the darkness level exceeds 90%, and questionably decreased autofluorescence (QDAF), where the darkness level ranges between 50% and 90% (Strauss et al., 2017). Most diseases featuring RPE atrophy, whether hereditary or acquired, exhibit distinct lesions with a profoundly hypoAF signal, similar to DDAF. In contrast, areas of RPE atrophy in EMAP are hypoAF only relative to the surrounding retina, but not when compared to major retinal vessels, which remain clearly discernible from the background RPE atrophy (Fig. 6). This appearance of atrophy in EMAP has often been referred to as "grayish" in the literature. However, despite its extensive use in previous publications, including those from our groups, this term is not entirely accurate, as all findings on SW-AF imaging should described in terms of grayscale. Although the darkness level of atrophic lesions in EMAP generally falls within the range of QDAD, this term also seems inadequate, as it was originally intended to differentiate between two types of atrophy detectable in the same eye, each with different prognostic implications in *ABCA4*-associated retinopathy. In contrast, EMAP presents with only one type of hypoAF signal which, though it may appear inhomogeneous within the central lesion, "unquestionably" corresponds to RPE atrophy. Therefore, we propose the term "moderately decreased autofluorescence" (MDAF) to designate atrophic lesions in EMAP, where the average gray value falls between that of the optic nerve head and the

Fig. 5. *Long-term natural history of macular atrophy in EMAP.* (Upper panel) This woman was 45 years old at baseline, and complained of progressive vision loss, photophobia, night blindness, and dyschromatopsia. Both eyes showed small parafoveal patches of chorio-retinal atrophy, typical of early-stages of EMAP (arrowheads). Full-field ERG already demonstrated a reduction of both scotopic and photopic responses. (Lower panel) After 14 years of follow-up, the atrophic lesions bilaterally progressed to involve the whole posterior pole and reach the mid-peripheral retina, morphing into the characteristic "leaf" shape accompanied by a temporal sparing (arrowheads). Pavingstone-like degeneration can be documented in the temporal periphery. Furthermore, both eyes developed a Bruch's membrane rupture that crossing horizontally the macula. Corresponding fluorescein angiography and short-wavelength fundus autofluorescence images are shown below. [Adapted with permission from "Puech, B., De Laey, JJ. (2014). Extensive Macular Atrophy with Pseudodrusen-Like Appearance. In: Puech, B., De Laey, JJ., Holder, G. (eds) Inherited Chorioretinal Dystrophies. Springer, Berlin, Heidelberg"].

surrounding retina. The origin of this unique MDAF signal may be attributed to unidentified fluorophores within sub-RPE deposits, which persist above the BM after RPE atrophy, in addition to the severe choroidal thinning unmasking scleral AF (Romano et al., 2023d). For a detailed discussion on the use of SW-AF images to quantify the area of MA and estimate its longitudinal growth rate, we refer the reader to section 5.3.

The AF pattern at the border of MA, often termed the "junctional pattern", is hyperAF in 72% of eyes and isoAF in 28% relative to the surrounding retina with intact RPE (Romano et al., 2021). Beyond MA, the posterior pole shows a heterogeneous appearance, with diffuse fine granular or stippled faintly hyperAF lesions (Fig. 6). This latter pattern may correspond to mid-peripheral pseudodrusen-like deposits and precede the *de novo* formation of small circular patches of RPE atrophy, which later coalesce with the main lesion, contributing to its multilobular borders. Notably, the aforementioned mid-peripheral temporal island retains a normal AF signal, possibly explaining its long-term resistance to RPE atrophy and the predominant vertical expansion of MA toward the vascular arcades (Fig. 7).

4.1.2. *Near-infrared autofluorescence*

Near-infrared autofluorescence (NIR-AF), unlike SW-AF, utilizes an excitation light in the red end of the visible spectrum, enabling the visualization of different fluorophores, attributed to melanin within the RPE and choroid (Keilhauer and Delori, 2006). However, in over 80% of EMAP cases, the contours of MA are not easily discernible on NIR-AF images. Instead, the entire posterior pole shows a diffuse loss of AF signal, with large choroidal vessels becoming visible due to the unmasking of fluorescence from the underlying choroidal stroma (Antropoli et al., 2024) (Fig. 8). This phenomenon may result from

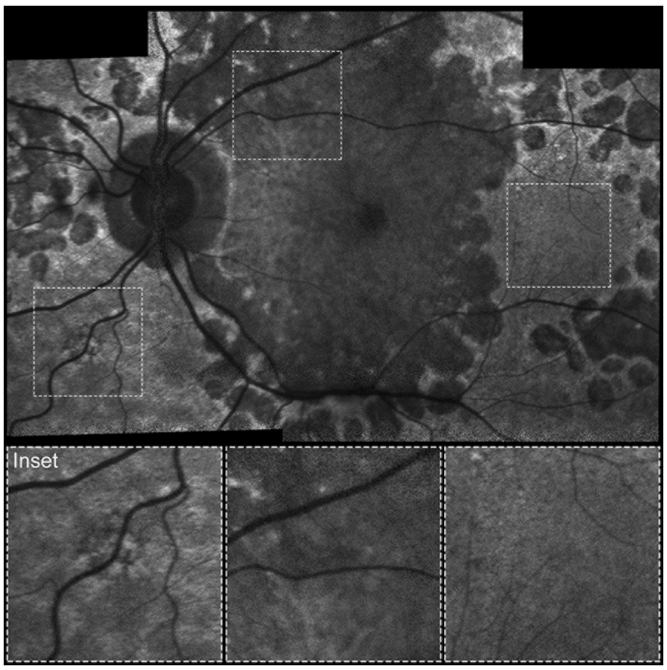

Fig. 6. *Typical features of macular atrophy in EMAP using short-wavelength autofluorescence*. In addition to the predominant vertical axis and multilobular borders, the atrophic lesion exhibits characteristic moderately decreased hypoautofluorescence (MDAF), allowing the course of the overlying retinal vessels to be easily identified (central inset). The surrounding retina has a heterogeneous granular or marbleized appearance, being covered by diffuse hyperAF lesions, upon which new atrophic patches may develop (left inset). A temporal sparing showing nearly normal autofluorescence can be recognized in almost all cases (right inset).

melanin loss due to severe choroidal atrophy, diffuse RPE damage extending beyond the MA, or a combination of both. Notably, the first hypothesis is supported by the observation that in eyes with occasional normal choroidal thickness, the AF signal from the surrounding retina appears almost normal, exhibiting enhanced contrast with the atrophic lesion (Antropoli et al., 2024). However, it must be acknowledged that all IRDs characterized by primary RPE impairment due to mutations in visual cycle enzymes often display a similar abnormal visibility of the choroidal vessel on NIR-AF despite having normal choroids and an intact RPE band on OCT (Bianco et al., 2024) (see section 8.1), and further research is required to clarify the significance of this finding in EMAP. Nonetheless, NIR-AF is an invaluable imaging modality for the recognition of the earliest alterations in EMAP. In particular, pigment abnormalities may be observed in the parafoveal region before MA develops, appearing as reticular hyperAF lesions on NIR-AF (Romano et al., 2023b). Furthermore, NIR-AF facilitates the identification of foveal sparing, which may not be readily apparent on SW-AF due to masking from macular pigments (Fig. 8).

4.1.3. Quantitative autofluorescence

As already mentioned, conventional SW-AF imaging provides spatial distribution of the autofluorescence signal by assigning a grayscale value ranging from 0 to 255 to each pixel (Schmitz-Valckenberg et al., 2021). The spectral properties and distribution of this signal suggest that autofluorescence originates from bisretinoid compounds such as A2E, A2-glycerophosphoethanolamine, and A2-dihydropyridine-phosphatidylethanolamine (Kim and Sparrow, 2018), though the level of these compounds have been demonstrated to be higher in the retinal periphery than in the macula (Kotnala et al., 2022). However, performing comparisons between serial images of the same individual or across different individuals becomes challenging due to various inherent factors, like signal normalization within each SW-AF image. To overcome this limitation, the quantitative autofluorescence (qAF) approach utilizes images captured in non-normalized mode, followed by signal calibration using an internal, instrument-mounted autofluorescent reference (Delori et al., 2011). Specifically, qAF values are obtained using a formula that accounts for laser power, offset, sensitivity, refractive errors, and variations in media structures. Given the absorption spectrum of macular pigment in the 400–540 nm range, qAF measurement is recommended at 7–9° of eccentricity (qAF_8 ring) (Sparrow et al., 2020), where the influence of macular pigment is negligible (Bone et al., 1988); however, the qAF8 ring may overlook early pathologies under the fovea (Berlin et al., 2024). Nonetheless, these measurements serve as valuable tools for enhancing our understanding of disease pathogenesis, assessing genotype-phenotype correlations in IRDs, and serving as efficacy measures (Duncker et al., 2014, 2015; Müller et al., 2021; Parrulli et al., 2022). To date, the application of qAF in EMAP remains unexplored, yet it holds considerable promise. For instance, qAF values have been reported to change significantly in areas with SDD in AMD and in the nasal sectors of patients affected by pseudoxanthoma elasticum (PXE) (Gliem et al., 2016b, 2017). Comparative studies with other forms of retinal degeneration could facilitate the diagnostic process, considering that the rapid and severe outer retinal degeneration seen in EMAP is likely accompanied by a significant slowdown of the visual cycle. Additionally, although not its primary purpose, qAF assessment of atrophic areas may shed light on the origins of the MDAF signal detected in patients with EMAP, as illustrated in Fig. 9.

4.1.4. Infrared reflectance

Near-infrared reflectance (NIR) is an often-overlooked imaging modality that holds key importance in the deep phenotyping of EMAP. It relies on the differential scattering and absorption of an 815-nm laser light by various retinal structures and interfaces. The major responsible for light absorption is the RPE (Elsner et al., 1996), while the choroidal stroma and/or sclera unmasked by RPE atrophy reflect incident light (Cideciyan et al., 2015). Consequently, MA in EMAP appears distinctly hyper-reflective on NIR imaging, resulting from localized loss of RPE absorption and a subsequent "window effect" that allows the backscattering of light from the choroid and sclera. Based on our experience, NIR images may allow a better recognition of atrophic areas compared to SW-AF, particularly in the early stages of the disease when small patches of RPE atrophy have already formed, but thick sub-RPE deposits persist above the BM, as we will explore further in the following section.

4.1.5. MultiColor imaging

MultiColor is a novel imaging modality developed by Heidelberg Engineering (Heidelberg, Germany), which utilizes confocal scanning laser ophthalmoscopy (cSLO) to achieve higher resolution and to address some of the limitations associated with traditional flash-based CFP (Ben Moussa et al., 2015; Tan et al., 2016). The simultaneous acquisition of three reflectance images using specific monochromatic laser sources facilitates the creation of a composite image that includes features from different retinal layers. Specifically, the blue reflectance component (488 nm) enhances the visualization of the inner retina and vitreoretinal interface (Charbel Issa et al., 2008), the green reflectance (515 nm) offers insights into deeper structures such as retinal blood vessels and intraretinal lipids (Tan et al., 2016), while the infrared component (820 nm) aids in assessing alterations in the outer retina, RPE, and the choroid, including drusen and pigment abnormalities (Alten et al., 2014). Although the use of MultiColor mode in examining EMAP remains underexplored, potential applications for these patients are emerging (Fig. 10). For instance, there is growing evidence supporting that MultiColor may outperform CFP in detecting reticular pseudodrusen (RPD), which appear more distinct with a hyperreflective/yellowish core surrounded by a hyporeflective halo (Alten et al., 2014; Rabiolo et al., 2017). Additionally, RPE atrophy boundaries in GA are delineated more distinctly with MultiColor imaging, yielding

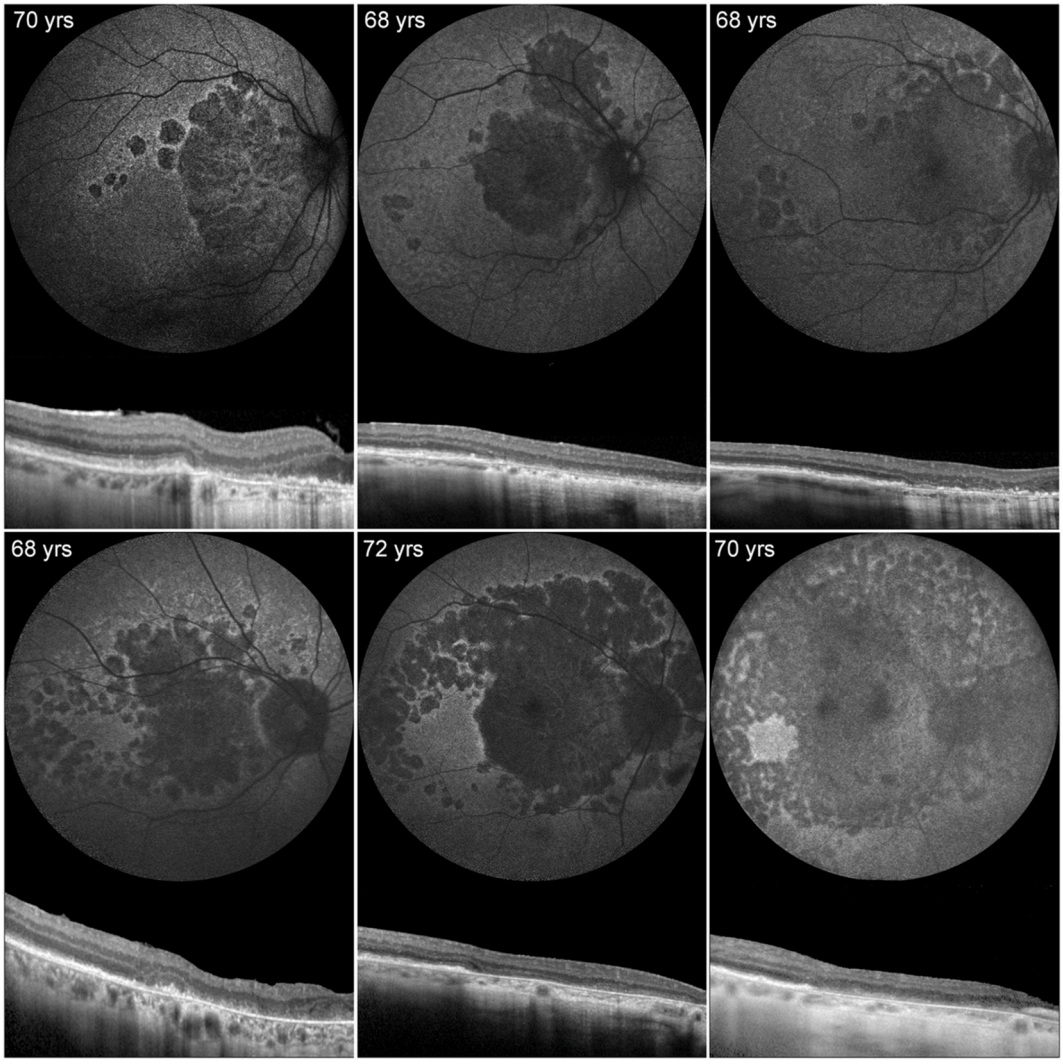

Fig. 7. *Temporal sparing in EMAP at different disease stages*. Over the course of its natural history, atrophy in EMAP consistently spares a small circular patch of retinal tissue straddling the outer temporal border of the macula and the mid-periphery, as seen on short-wavelength autofluorescence. As shown in these 6 patients at different stages, the main macular lesion expands towards the mid-periphery through the formation and subsequent coalescence of smaller atrophic foci, that progressively extend temporally but never crossing the horizontal *raphae*. The temporal sparing is most visible in the late-stage cases (lower-right panel), in which the whole posterior pole is covered by atrophy, and it remains the only residual source of "normal" autofluorescence. This finding may prove particularly useful in the differential diagnoses with similar forms of extensive macular atrophy. As expected, horizontal optical coherence tomography scans of the macula demonstrate absence of the retinal pigment epithelium layer and choroidal hypertransmission in the foveal and temporal paracentral sectors of the macula, ending abruptly at the temporal sparing observed on SW-AF.

intra- and inter-grader repeatability that surpasses CFP and is possibly comparable to SW-AF (Ben Moussa et al., 2015; Crincoli et al., 2022). This modality also proves effective in detecting retinal hemorrhages, which indicate the development of MNV, a rare but treatable complication of EMAP (*see* section 4.6.1). However, MultiColor mode is not without drawbacks, including chromatic aberration due to the different focal planes of the three wavelengths, and the occurrence of a "ghost" artifact – a central hyperreflective spot not corresponding to any discernible lesion but associated with intraocular lenses (Pang and Freund, 2014; Tan et al., 2016).

4.2. RPE-Bruch's membrane separation

On OCT, the presence of a diffuse, relatively hyporeflective material located between the RPE and BM in the macula is considered a hallmark of EMAP and precedes the formation of MA. This characteristic finding is frequently referred to as "RPE-BM separation" but will be used interchangeably with "sub-RPE deposits" in this review. This separation is typically thickest at the fovea and gradually thins towards the peripheral macula, where it is usually associated with subretinal drusenoid deposits (SDDs). Due to its topographic distribution, reflectivity properties, and the absence of soft drusen (Sura et al., 2020), it has been proposed that the RPE-BM separation may mirror the presence of basal laminar deposits (BLamD) (Fragiotta et al., 2022; Romano et al., 2023b), as described in histological studies of AMD (Curcio et al., 2005; Khan et al., 2020; Sura et al., 2020). However, the lack of histological studies specific to EMAP makes the assumption merely speculative. Recently, the SPECTRALIS high-resolution OCT device from Heidelberg Engineering (Heidelberg, Germany) has been employed to investigate *in vivo* the composition of these deposits in the earliest stage of EMAP (Romano et al., 2023b). According to the authors, two layers with different reflectivity properties could be identified within the RPE-BM separation: (1) a slightly hyporeflective layer right beneath the RPE, and (2) more hyperreflective deposits with a triangular shape immediately above BM (Fig. 11). It is important to note, however, that these observations are limited to the RPE and BM layers as visualized on OCT, which currently

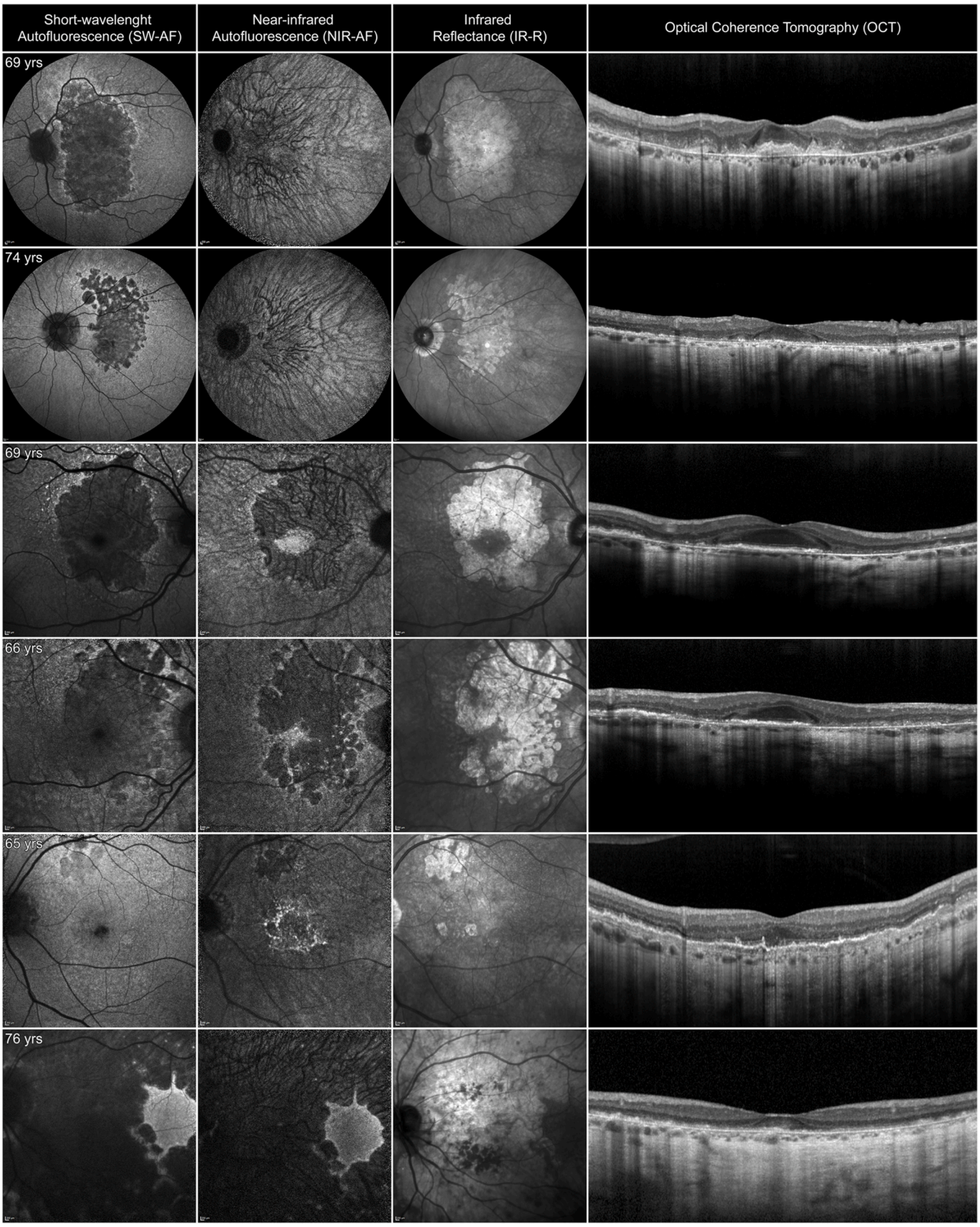

(caption on next page)

Fig. 8. *Features of macular atrophy in EMAP using multimodal retinal imaging.* The hallmark features of macular atrophy in EMAP are all recognizable using short-wavelength autofluorescence (SW-AF) and infrared reflectance (IR). Conversely, in the majority of cases the contours of macular atrophy in EMAP cannot be identified on near-infrared autofluorescence (NIR-AF) because the whole posterior pole is characterized by a diffuse loss of autofluorescent signal with abnormal visibility of large choroidal vessels. This can be at least partly attributed to the severe choroidal thinning (as seen by the relative optical coherence tomography scans). Nonetheless, NIR-AF is extremely useful in early or late-stage cases of EMAP. In particular, some pigment deposits visible as speckled hyperautofluorescence can be observed in the parafoveal region in the pre-atrophic stage or early atrophic stage of the disease, while they are poorly visible on SW-AF. Furthermore, NIR-AF allows the immediate identification of foveal sparing, which may be not recognized using SW-AF because of physiological masking from the macular pigments. Lastly, in very advanced cases NIR-AF is able to highlight the typical temporal sparing.

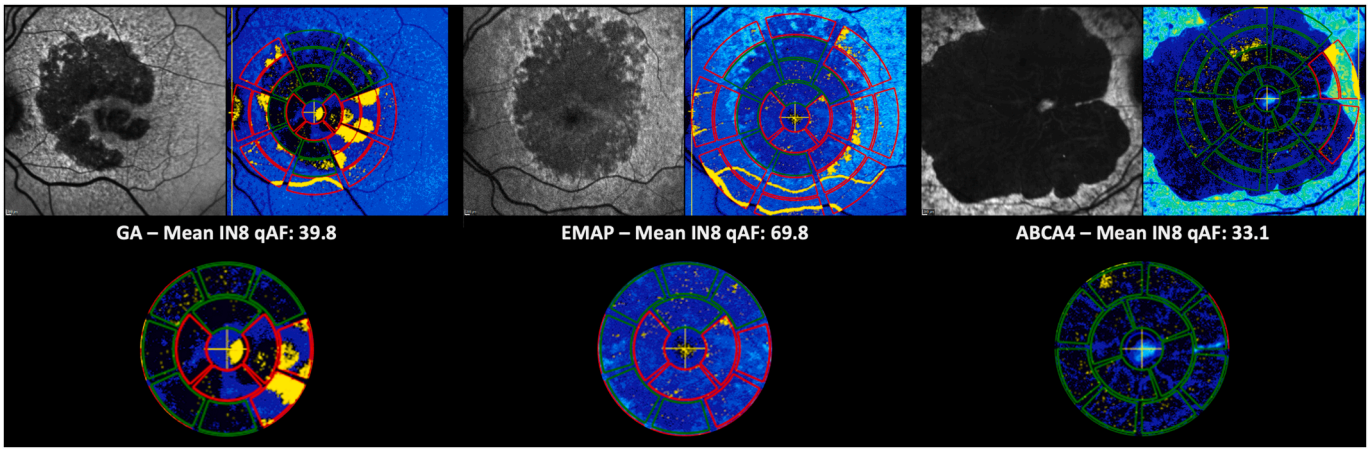

Fig. 9. *Quantitative autofluorescence (qAF) changes in extensive macular atrophy with pseudodrusen (EMAP), geographic atrophy (GA) secondary due age-related macular degenerations, and ABCA4 retinopathy.* The short-wavelength autofluorescence (SW-AF) and qAF images with overlapped measurement grid are presented for the three described conditions. The analyzed segments for qAF quantification are highlighted in green. Notably, the assessment of atrophy signal within the 8-segment inner ring shows significantly higher qAF values in the EMAP case, corresponding to the typical moderately decreased autofluorescence. Yellow areas within the atrophic regions represent artifacts related to the 'off-label' use of qAF, as they indicate regions too dark for accurate measurement, such as retinal vessels, which are typically excluded in standard qAF calculations.

does not allow for the discrimination of whether these deposits reside within RPE cells, above their basal lamina, or within the BM (*see* section 8.2).

Although the precise composition of these deposits remains elusive, Romano et al. were able to capture the transition from RPE-BM separation to complete RPE and outer retinal atrophy (cRORA) (Romano et al., 2023c) (Fig. 3). Indeed, the sub-RPE deposits seen as RPE-BM separation on OCT may represent the precursor lesions of MA in EMAP. Initially, thinning of the outer nuclear layer and diffuse disruption of the ellipsoid zone (EZ) become visible above regions with a thick RPE-BM separation. Subsequently, the RPE gradually disappears, leading to the persistence of the deposits underneath, which can be seen as "debris" of hyperreflective heterogeneous material above the bare BM (Fig. 12). This is a unique finding, and if these sub-RPE deposits are inherently AF when excited with blue-light, it could explain why atrophic lesions are characterized by MDAF on SW-AF, as suggested for DTGA (Fleckenstein et al., 2011). As already mentioned, the RPE-BM separation can be detected in the peripheral macula, even relatively far from the atrophic lesion (Antropoli et al., 2023). This is of uttermost importance when atrophy has already encroached on the fovea and the RPE-BM separation is no longer discernible. Thus, based on our experience, large-volume scans of the posterior pole, rather than fovea-centered horizontal line scans, are essential for accurately identifying such finding in late-stage cases of EMAP. Indeed, the RPE-BM separation is generally most visible peripherally to the superior boundary of the MA, while it is never present temporally, which corresponds to the region of temporal sparing described on SW-AF (Fig. 7). However, such sub-RPE deposits with a diffuse RPE-BM separation are not unique to EMAP but can also be found in IRDs such as SFD and L-ORD, and their histological composition will be discussed in section 7.2.

4.3. Pseudodrusen-like deposits

In EMAP, the so-called "pseudodrusen-like appearance" refers to the presence of several ill-defined and interlacing yellowish/hypopigmented lesions arranged in a reticular pattern ("pseudodrusen-like deposits"). These deposits affect the entire mid-peripheral retina beyond the posterior pole, although their density and anterior extension may vary among patients, and their visibility according to the utilized imaging modality (Douillard et al., 2016) (Fig. 13). It must be emphasized that pseudodrusen-like deposits likely represent a different type of outer retinal deposit than RPD, which correspond to SDDs on OCT (Zweifel et al., 2010), despite the misleading implication of their name. Nonetheless, in the original publication on EMAP Hamel et al. used several different terms to describe the pseudodrusen-like appearance, sometimes interchangeably with "pseudodrusen" (Hamel et al., 2009). To make even more confusing, pseudodrusen-like deposits and RPD/SDDs typically occur simultaneously in EMAP, while other types of drusen are generally absent. On OCT, pseudodrusen-like deposits found in the peripheral retina correspond to large, flat, highly reflective lesions at the level of the RPE causing an undulation of the ellipsoid zone band (Fig. 14). However, the resolution of current OCT devices employed for clinical use is not sufficient to resolve whether the deposits are located above or below the RPE, and their composition has not been clarified by histology, unlike RPD/SDDs. Thus, we opted to retain the name proposed in the original publication on EMAP (Hamel et al., 2009) to ensure consistency in the literature while awaiting further research. As mentioned, conventional "dot" RPD/SDDs are also present in EMAP and appear as whitish, discrete, punctiform lesions. These are predominantly localized in the macula, i.e. the central 6 mm region (Curcio et al., 2024), and its immediate surroundings, tend to be visible in the early stages of the disease but may no longer be detectable once extensive MA develops. NIR images aid in the recognition of these lesions particularly

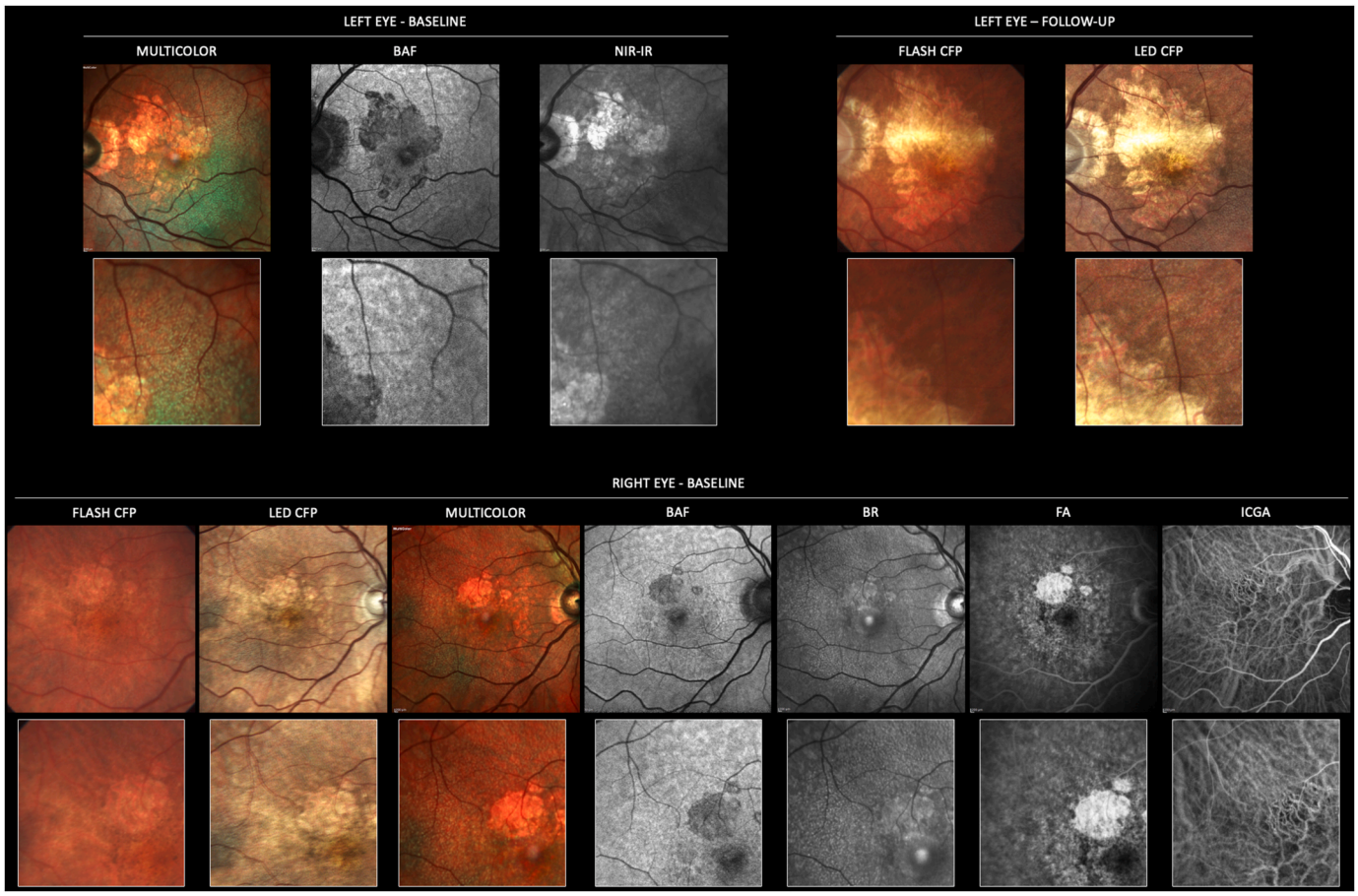

Fig. 10. *Comprehensive multimodal imaging evaluation of pseudodrusen and pseudodrusen-like deposits in extensive macular atrophy with pseudodrusen-like appearance (EMAP) at baseline and follow-up (left eye only).* Compared to traditional flash-based fundus cameras, MultiColor mode, near-infrared reflectance, confocal blue reflectance and the LED-based color fundus photographs appear more sensitive tools for detecting the discrete dot pseudodrusen. Conversely, short-wavelength autofluorescence, MultiColor mode and LED-based fundus photographs more effectively highlight the extra-macular "marbling" appearance of pseudodrusen-like deposits. **Fundus cameras used**: flash-based fundus camera (FF 450 Plus; Carl Zeiss MediTec, Jena, Germany), confocal fundus imaging system (Spectralis HRA + OCT2; Heidelberg Engineering GmbH, Heidelberg, Germany), and LED-based color fundus camera (EIDON; CenterVue, Padua, Italy).

in myopic eyes in which the thin choroid precludes adequate contrast. "Dot" RPD/SDDs appear as small hyperreflective spots surrounded by an hyporeflective halo, often referred to as "target configuration" (Suzuki et al., 2014). In EMAP, "dot" RPD/SDDs can often be found above regions characterized by thick RPE-BM separation (see section 4.2). Large and flat "ribbon" RPD/SDDs can also be seen in EMAP as interlacing hyporeflective structures (Suzuki et al., 2014) in the peripheral region of the macula. We can thus affirm that EMAP is characterized by a widespread accumulation of drusenoid deposits in the outer retina, presumably located both above (SDDs) and beneath ("RPE-BM separation") the RPE. At least at the posterior pole, the distribution of the SDDs and sub-RPE deposits seems to follow that of rod and cone photoreceptors, respectively (Curcio et al., 2013), while the localization and composition of the pseudodrusen-like deposits remain to be elucidated. The overlapping characteristics between EMAP and AMD, including the presence of RPD/SDDs, are explored in greater detail in Section 6 of this review. Interestingly, similar deposits are also found in IRDs characterized by a defective visual cycle, which will be discussed in Section 7. From now on, the term RPD will be used when referring to AMD, and SDDs in all other instances throughout this review, even though they can be considered equivalent.

4.4. Pavingstone-like degeneration

Pavingstone degeneration is a core component of the classical triad of EMAP. Indeed, in the original paper all patients exhibited this finding, predominantly in the infero-temporal periphery of the retina (Hamel et al., 2009). Since peripheral atrophy in EMAP exhibits specific characteristics, we will utilize the term "pavingstone-like degeneration" when referencing EMAP-related lesions, while "pavingstone degeneration" will serve as a broader term. To date, our understanding of pavingstone degeneration (occasionally termed "cobblestone degeneration") remains limited. This is generally considered a benign finding frequently observed in myopic eyes of elderly individuals (Karlin and Curtin, 1976; O'Malley et al., 1965). Fundus examination of the retinal periphery reveals well-defined, yellowish, punched-out lesions that tend to coalesce, forming a circular pattern around the outermost periphery, approximately 1-to-2 disc diameters posterior to the ora serrata and predominantly in the inferotemporal sector (Karlin and Curtin, 1976). In a histological study published by O'Malley et al. in 1965, it was proposed that pavingstone degeneration may be linked to inadequate blood supply stemming from the terminal arteriolar branches of the recurrent choroidal arteries, with additional evidence supporting their occurrence beyond the equator of the eye (O'Malley et al., 1965). Despite the introduction of UWF imaging in recent years, which has enabled a comprehensive assessment of the retinal periphery, few studies have systematically investigated pavingstone degeneration in healthy individuals (Vatavuk et al., 2018). Conversely, Battaglia Parodi et al. conducted the first study on the peripheral findings in EMAP using UWF imaging, documenting the progression of pavingstone-like degeneration over time (Battaglia Parodi et al., 2023) (Fig. 15). In accordance with previous descriptions in both healthy and EMAP-affected eyes, the

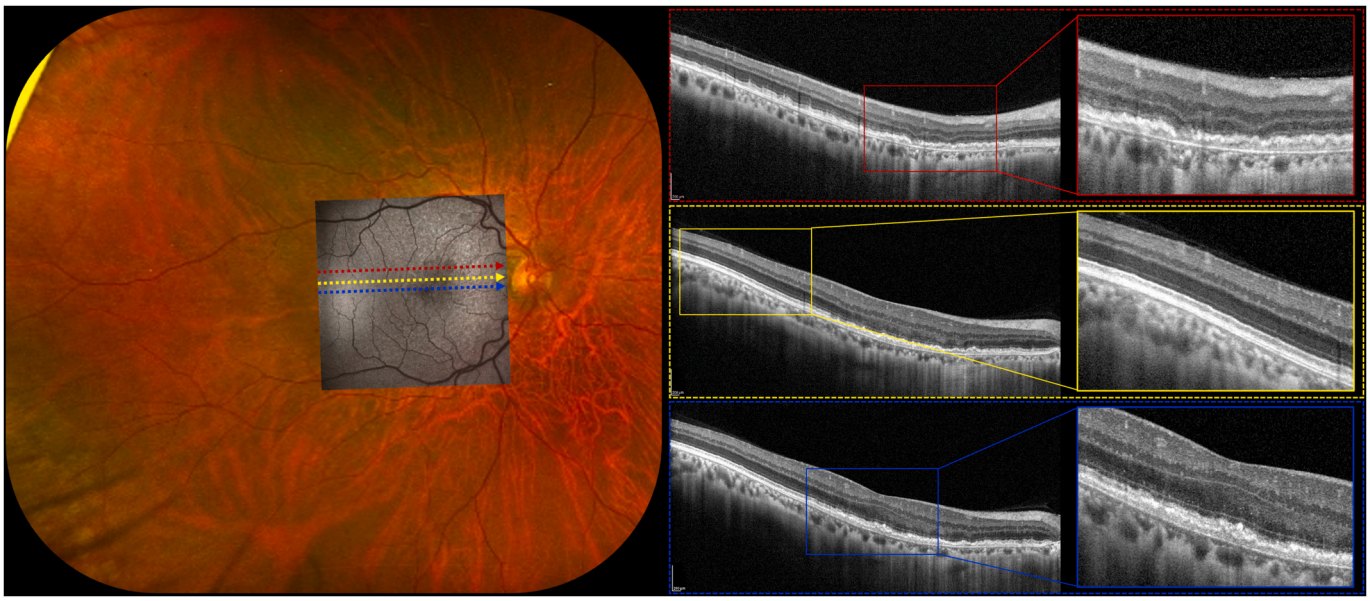

Fig. 11. *High-resolution optical coherence tomography (Hi-Res OCT) findings in stage 1 extensive macular atrophy with pseudodrusen-like appearance (EMAP).* The ultra-widefield fundus photograph, enhanced with fundus autofluorescence overlay, reveals diffuse pseudodrusen-like deposits, a small area of retinal pigment epithelium (RPE) atrophy located supero-nasal to the fovea, and evidence of peripheral pavingstone-like degeneration. The Hi-Res OCT scan passing through the atrophic area demonstrates marked disruption of the ellipsoid zone (EZ) situated above a diffuse separation between RPE and Bruch's membrane, with numerous lesions atop the RPE resembling pseudodrusen (red box). Discontinuity of the external limiting membrane, accompanied by initial subsidence of the outer plexiform layer, can be observed above the small RPE atrophy area. Comparable findings are noted in the two additional, more inferior Hi-Res OCT scans. Specifically, the EZ appears disrupted at the fovea above areas of RPE-Bruch's membrane separation, while the temporal macula results largely unaffected by these lesions (yellow box). The subfoveal RPE layer exhibits nodular thickening (blue box). Notably, across all scans, the material beneath the RPE displays dual reflectivity; a less hyperreflective layer immediately underneath the RPE and a more hyperreflective layer above the Bruch's membrane.

infero-temporal sector emerged as the most frequently involved area. Similar to MA, peripheral degeneration was generally symmetrical between the two eyes of each patient. The range of findings encompassed pseudodrusen-like deposits, pavingstone-like degeneration, and pigmented chorioretinal atrophy. Notably, using autofluorescence with a green excitation laser, not only were the peripheral pseudodrusen-like deposits faintly hyperAF but also the pavingstone-like degeneration, possibly due to scleral exposure (Battaglia Parodi et al., 2023). Furthermore, in two patients in the pre-atrophic stage (or EMAP stage 1), Romano et al. were able to image with UWF-OCT the pseudodrusen-like deposits adjacent to the peripheral pavingstone-like degeneration (Romano et al., 2023b). Interestingly, peripheral OCT scans passing through these lesions showed highly hyperreflective deposits at the level of the RPE, similar to the mid-peripheral ones described in the previous chapter. Additionally, the extent to which the macular region and the retinal periphery are affected seems to be independent of each other. Indeed, as observed by Battaglia Parodi et al., a subgroup of patients may present with a "predominantly central" disease, with minimal to no signs of pavingstone-like degeneration in the peripheral retina (Battaglia Parodi et al., 2023). Conversely, other patients may have a "predominantly peripheral" involvement, with pavingstone-like degeneration extending to the equator at presentation. Such peripheral atrophy could further extend towards the posterior pole, eventually merging with MA through radial spokes – most often from the temporal side – to form a "confluent" pattern (Fig. 16). The latter represents the potential final stage of EMAP, although the reason why not all patients experience this degree of retinal involvement remains unanswered. Future prospective studies featuring UWF imaging will expand our understanding of the origin of the peripheral atrophy and investigate its significance in EMAP.

4.5. Subretinal fibrosis, Bruch's membrane ruptures, and additional findings

Even after cRORA has developed in the macula, OCT enables the identification of further pathological changes that take place within the atrophic lesion. Among these, a subfoveal hyperreflective material, fundoscopically compatible with fibrosis, forms in up to two-thirds of eyes and in roughly half of the cases bilaterally (Antropoli et al., 2024). In such cases, multimodal imaging fails to detect an MNV within the fibrotic lesion (Romano et al., 2023c). Nonetheless, it must be acknowledged that rapidly regressing MNV or networks below the detection threshold of current imaging techniques could contribute to this complication (for the description of clinical and angiographic characteristics of MNV in EMAP we refer the reader to section 4.6.1). Anyway, non-neovascular subfoveal fibrosis represents a cause of additional visual acuity loss in EMAP (Romano et al., 2023c).

Another phenomenon that has been demonstrated to occur within the atrophic area in EMAP is the development of BM ruptures, either with or without a concurrent MNV (Antropoli et al., 2024). These BM ruptures are usually large linear steaks that cross the macula vertically (Fig. 17) or horizontally (Figs. 5 and 18). Due to the extreme choroidal thinning, these lesions appear pale – rather than dark red typical of "angioid streaks" in PXE - because of scleral exposure. BM ruptures in EMAP appear as sharp hyperreflective streak on NIR imaging, providing sufficient contrast for accurate identification of their margins. Vice versa, SW-AF is not optimal for detecting a BM rupture, as it presents as an area of "dark" hypoAF within the context of a MDAF lesion typical of EMAP (Antropoli et al., 2024). Of note, this latter observation suggests that the source of the residual AF signal in the atrophic lesion does not reside in the sclera but above the BM, as already discussed in section 4.2. Besides NIR and SW-AF imaging, OCT is particularly useful in the identification of further small BM ruptures, which tend to be more irregular and with jagged margins and can be easily missed on other imaging modalities. In the second part of this review, we will delve into

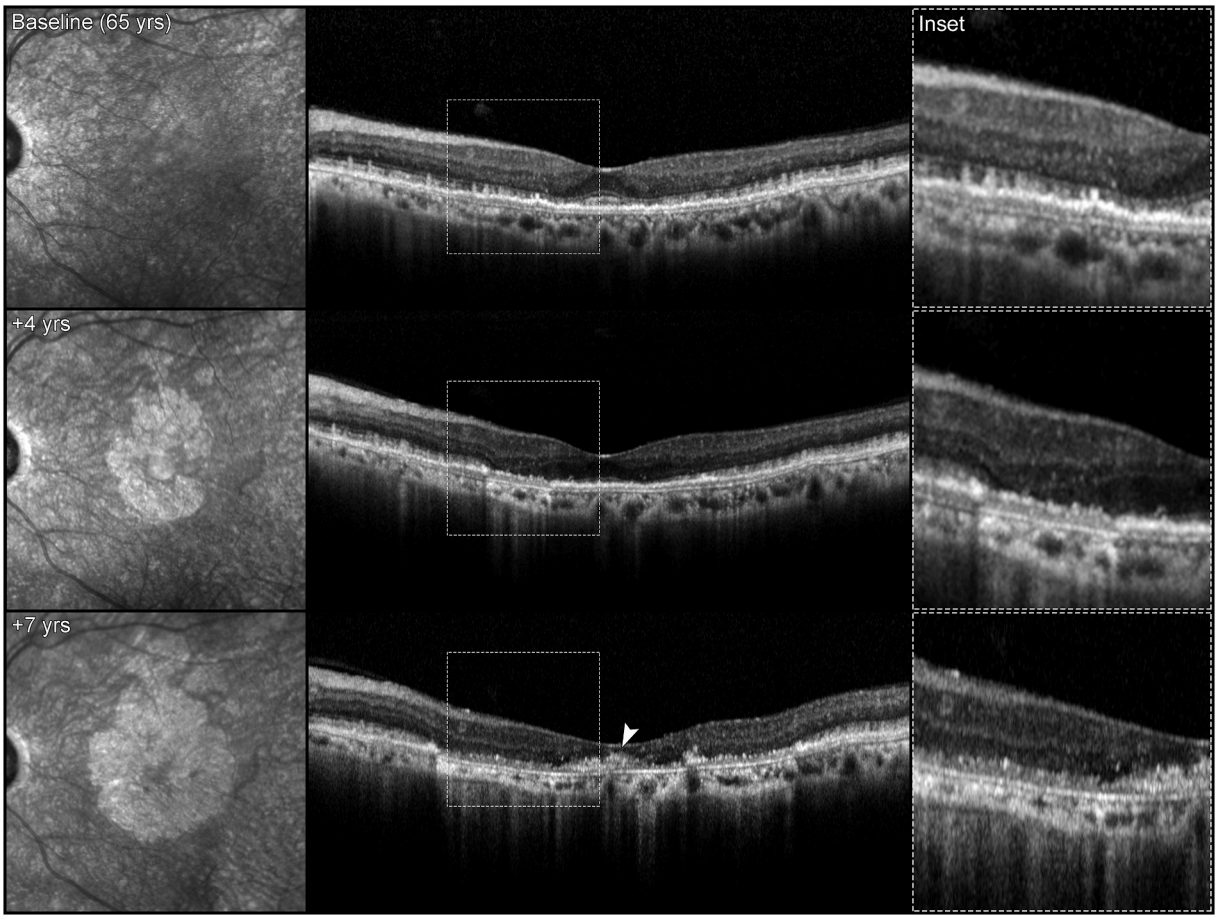

Fig. 12. *Retinal pigment epithelium (RPE)-Bruch's membrane (BM) separation in the pre-atrophic stage of EMAP*. At baseline examination, no macular atrophy is noted on infrared reflectance while thick deposits located below the RPE and above the BM, along with copious subretinal drusenoid deposits in the parafoveal and perifoveal regions, can be seen on optical coherence tomography. After 4 years of follow-up, circumferential perifoveal atrophy has developed, corresponding on OCT to loss of the RPE layer with persistence of epi-BM deposits and subsidence of inner retinal layers. A foveal sparing of the RPE layer is still present, even though the ellipsoid zone has already disappeared. After 3 additional years of progression, atrophy expanded to all sectors of the macula, including the fovea. OCT images of the central macula show subretinal hyperreflective deposits in the areas of atrophy, along with a presumably fibrotic hyperreflective subfoveal nodule (white arrowhead).

IRDs featuring a primary impairment of the BM (PXE, L-ORD, and SFD), to extrapolate on the possible mechanisms leading to the development of BM ruptures in EMAP (*see* section 7). Further insights on the differential diagnosis of BM ruptures in EMAP and PXE will also be provided.

Additionally, hyperreflective pyramidal structures (HPS) may develop within the MA in up to 30% of eyes affected by EMAP, typically occurring later in the disease course (Antropoli et al., 2024). These lesions have been identified in AMD in 2014 (Bonnet et al., 2014), but can also be found in IRDs akin to EMAP, such as L-ORD and SFD (Khan et al., 2016; Soumplis et al., 2013). In AMD, HPS have been shown to correspond to calcific nodules within drusen, capped by thick BLamD (Tan et al., 2018). In contrast, in EMAP they are interpreted as the calcified form of the hyperreflective "debris" that persists over the bare BM after RPE atrophy has already occurred, differing from AMD (Antropoli et al., 2024).

In the area of MA, OCT can also identify less frequent and specific abnormalities, including intraretinal pseudocysts and outer retinal tubulations (Romano et al., 2021). Notably, EMAP features a progressive choroidal thinning with the formation of rounded, hyporeflective choroidal structures known as choroidal caverns or lipid globules (Antropoli et al., 2023; Romano et al., 2021). Whether the choroidal thinning is a cause (through a vascular insufficiency) or a consequence (signaling a decline in the metabolic demands of the outer retina) of MA in EMAP still remains to be investigated (Antropoli et al., 2023). Interestingly, small hyperreflective neuroretinal foci - commonly understood as activated microglial aggregates and an inflammatory signature biomarker in diabetic retinopathy (Midena et al., 2021) - were not found to be increased in EMAP compared to GA (Pilotto et al., 2024).

4.6. Neovascular complications and angiographic findings

4.6.1. Macular neovascularization

MNV is a rare but significant complication of EMAP, potentially leading to further visual impairment at any stage of the disease (Romano et al., 2023c). Owing to this variability, MNV has been categorized as a '+' feature in the recent classification proposed by Romano F et al. Literature on this topic is limited, mostly comprising of a few case reports. All documented cases report an acute visual loss in the affected eye, a symptom that is uncommon among EMAP patients due to the significant visual dysfunction present from the early stages of the disease. In 2015, Battaglia Parodi and Querques reported a case of bilateral MNV in a 53-year-old woman presenting with a large disciform scar in her right eye and a juxtafoveal lesion surrounded by the typical extensive MA in her left eye (Battaglia Parodi and Querques, 2015). More recently, Romano D et al. described a unilateral MNV case in a 54-year--old woman precipitated by a BM rupture extending linearly from the peripapillary area to the fovea (Romano et al., 2023). Treatment with a single anti-vascular endothelial growth factor (VEGF) injection led to regression of the MNV and significant, though incomplete, visual acuity restoration. The only study in literature including data from multiple

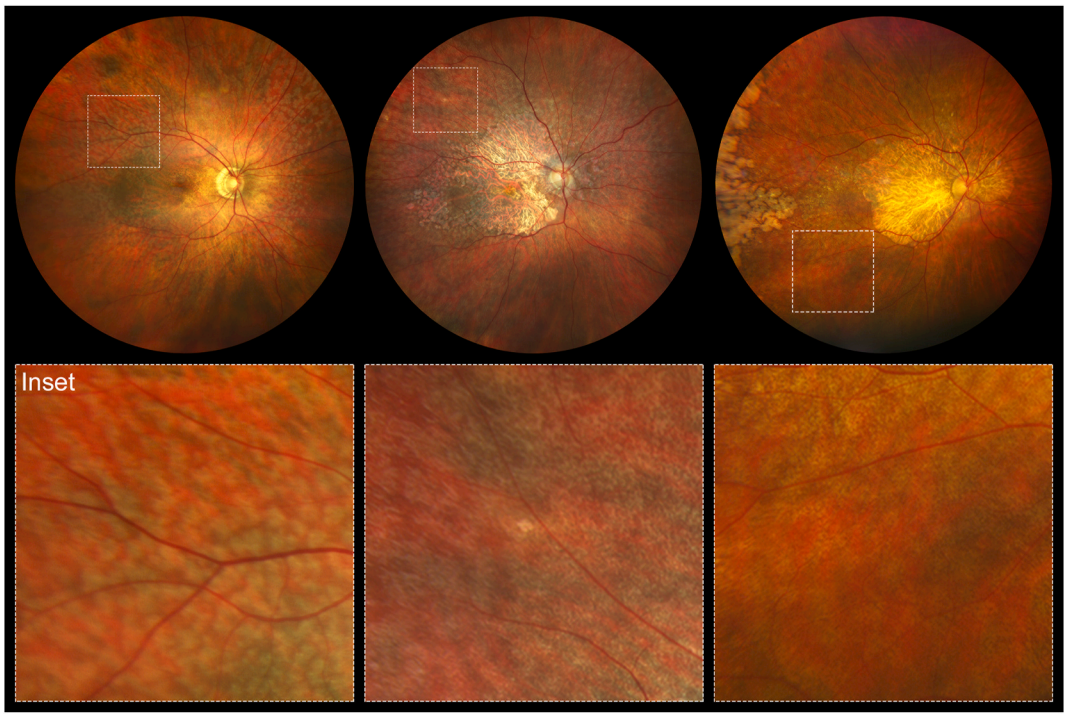

Fig. 13. *Fundus appearance of pseudodrusen-like deposits in EMAP.* Pseudodrusen-like deposits are ill-defined yellowish/hypopigmented lesions arranged in a lattice that extends from the outermost boundary of the posterior pole to the equator. Lesions towards the posterior pole are generally smaller and more discrete, while become larger and interlacing towards the equator. These are most abundant in the temporal quadrant of the retinal mid-periphery, while are scant in the inferior one. The anterior extension of pseudodrusen-like deposits may vary among patients, also depending on the posterior extension of pavingstone-like degeneration.

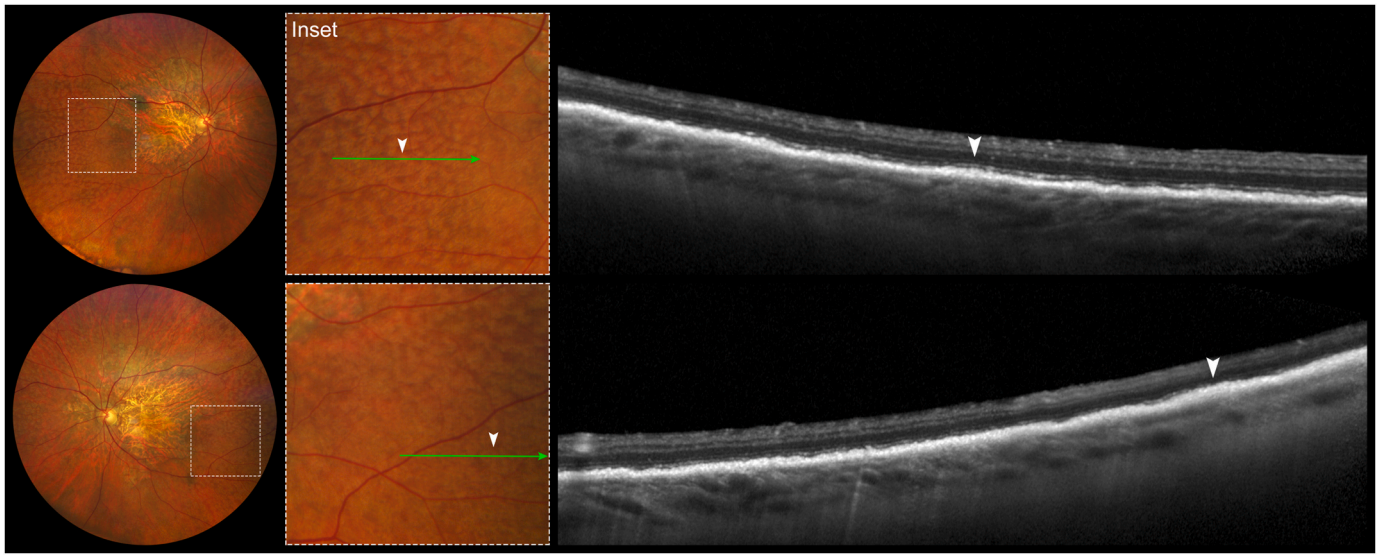

Fig. 14. *Optical coherence tomography (OCT) scans of pseudodrusen-like deposits in EMAP.* The interlacing network of hypopigmented lesions forming pseudodrusen-like deposits in the retinal mid-periphery corresponds to numerous large, flat hyperreflective lesions at the level of the retinal pigment epithelium (RPE) (arrowheads). These are interrupted by segments with normal outer retinal configuration, that give rise to the lattice appearance on retinography. The resolution of current OCT devices does not allow to accurately discern whether these are located above (subretinal drusenoid deposits), below the RPE ("separation"), or both. Thus, pending further evidence, we refrain from changing nomenclature and stick with the original description.

patients was conducted by Kamami-Levy and colleagues (Kamami-Levy et al., 2014). In their series of 19 patients, MNV occurred in 4 eyes of 3 patients, showing a prevalence of ~10%. All identified neovascular complications were classified as type 2 (or classic) MNVs, exhibiting signs of active leakage in both early and late phases, along with pooling of intraretinal fluid. With an improved understanding of EMAP natural history, distinguishing MNV from the non-neovascular fibrosis typical of stage 3 patients has become a critical diagnostic challenge (Romano et al., 2023c). In such cases, the sudden onset of visual loss and the identification of a neovascular network and/or clear exudative signs through a multimodal imaging approach are instrumental in the diagnosis (Fig. 19). Therefore, a thorough characterization of MNV features becomes essential to standardize treatment protocols and optimize follow-up strategies for these patients. This is particularly relevant

Fig. 15. *Fundus appearance and progression of peripheral pavingstone-like degeneration in EMAP.* (A) Baseline examination reveals the macular atrophy and the temporal sector affected by the peripheral degeneration. (B) At the 3-year follow-up examination, a limited enlargement of the macular atrophy can be noted, whereas the peripheral degeneration now covers the entire periphery, except for a small portion of the inferior quadrant. (C) At the 5-year follow-up examination, a further centripetal progression of the peripheral degeneration is observed, which merges with the macular atrophy in a radiating manner, while maintaining the characteristic temporal sparing. [Adapted with permission from: "Battaglia Parodi, M., Antropoli, A., Bianco, L., Arrigo, A., Pili, L., Saladino, A., Bandello, F., 2023. Peripheral Retinal Involvement in Extensive Macular Atrophy with Pseudodrusen-Like Deposits. Ophthalmol Retina 7, 910–917"].

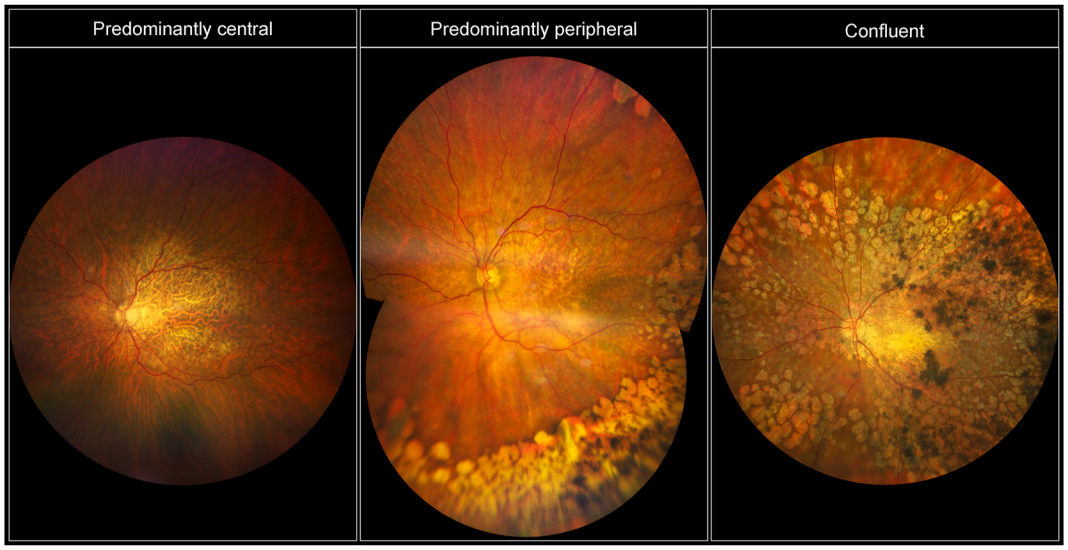

Fig. 16. *Topographic patterns of retinal atrophy progression in EMAP.* "Predominantly central" (left image): a 63-year-old patient with extensive posterior pole atrophy contoured by pseudodrusen-like deposits. No pavingstone-like degeneration is visible in the 130° field of view. "Predominantly peripheral" (center image): a 75-year-old woman with a minimal patch of macular atrophy superior to the fovea and extensive pavingstone-like degeneration approaching the posterior pole. "Confluent" pattern (right image): a 78-year-old subject with extensive retinal atrophy. A distinct boundary between the central and peripheral atrophy is lacking. Note the relatively spared region in the temporal mid-periphery.

considering the potential application of the recently approved intravitreal anti-complement therapies for GA (*see* section 9.3), which have been shown to increase the rate of MNV development in treated eyes. Consequently, longitudinal data from the Italian EMAP cohort, including 79 patients, aimed to shed light on the incidence, characteristics, and visual outcomes of eyes developing MNV (Trinco et al., under review). We observed signs of MNV in 14 eyes (8.9%) of 10 patients, with a 4-year cumulative incidence of 15.2%. Consistent with prior reports, most MNVs were type 2 (or subretinal, 85.7%) and located in the sub-foveal or juxtafoveal area at the time of diagnosis. This distribution may reflect a significant ischemic insult occurring in the fovea of these patients and/or an increased fragility of the RPE-BM complex, which hinders its ability to prevent the growth of pathological neovascular complexes. Indeed, when stratifying for the size of RPE atrophy at the time of MNV occurrence, we identified two distinct incidence peaks with potential pathogenetic implications. The first peak occurred early in the disease course, where the already compromised RPE and subsequent outer retinal alterations might promote neovascular growth. The second one was observed in advanced cases, where ruptures in the BM or loss of the outer retinal barrier integrity could facilitate MNV occurrence. Interestingly, the occurrence of MNV in our large cohort did not seem to impact long-term visual outcomes in these eyes, nor did it the growth rate of macular atrophy.

4.6.2. Fluorescein angiography and indocyanine-green angiography

Fluorescein and indocyanine green (ICGA) angiography have historically played an essential role for complementing the clinical examination of chorioretinal disorders (Gass et al., 1967). However, the advent of newer imaging modalities like fundus autofluorescence and OCT, coupled with its invasive nature, has progressively reduced their use in routine clinical practice (Sadda et al., 2018; Schmitz-Valckenberg et al., 2021). Despite this, dye angiographies remain crucial for ruling out macular neovascularization and formulating hypotheses on disease pathogenesis (Fleckenstein et al., 2018; Giani et al., 2012). On fluorescein angiography, MA in EMAP is characterized by well-demarcated hyperfluorescent areas evident since the early phases resulting from

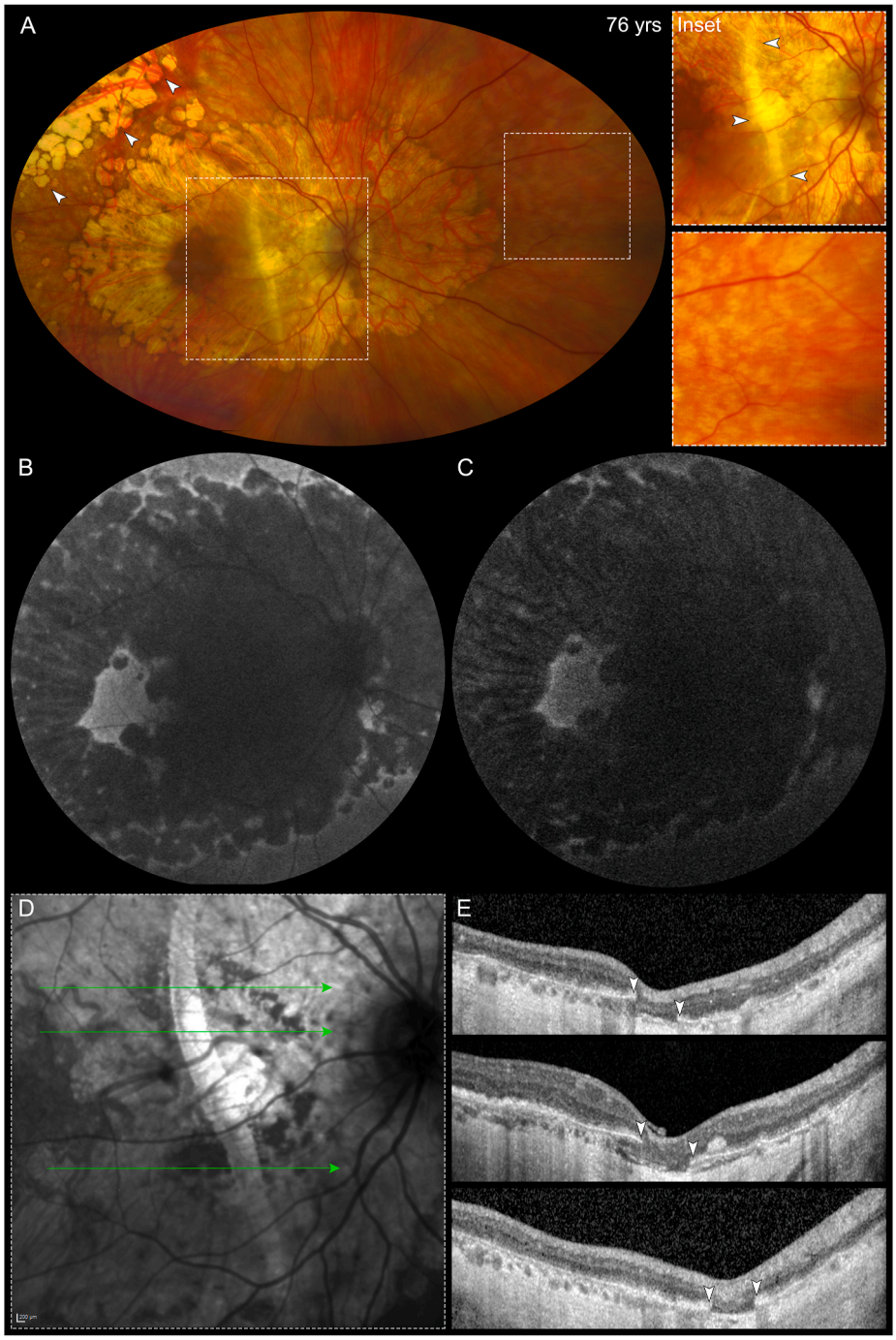

Fig. 17. *Bruch's membrane (BM) ruptures in EMAP.* (Right panel) Case associated macular neovascularization. (A) Ultrawide-field retinography shows the typical "leaf-shaped" atrophy with temporal sparing, as well as pavingstone-like degeneration invading the temporal mid-periphery. A large hypopigmented linear streak with vertical orientation crosses the center of the macula. Please note the relatively low visibility of mid-peripheral pseudodrusen-like deposits in the context of a myopic fundus. However, magnification allows the identification of such lesions in the nasal mid-periphery. The linear streak cannot be distinguished from RPE atrophy on both short-wavelength (B) and near-infrared (C) fundus autofluorescence. Conversely, infrared reflectance (D) of the macula allows the identification of a linear hyperreflective lesion. Optical coherence tomography (E) demonstrates that the borders of the streak correspond to BM ruptures (arrowheads) in the context of a severe atrophy of the outer retinal layers and choroid. The exposure of underlying scleral tissue explains the appearance of the streak as hypopigmented on retinographies, as well as the hyperreflectivity on infrared reflectance.

the "window effect" caused by severe RPE loss (Romano et al., 2021). Surrounding these atrophic areas, a reticular hypo-/hyper-fluorescent pattern often emerges, indicative of RPE changes occurring above the material separating the RPE layer from the BM. In the late phases, while the margins of the atrophic lesions remain stable, their delineation can become less distinct due to the concurrent staining of the adjacent choroidal stroma (Fig. 20). In early ICGA, atrophic areas display hypofluorescence and are less defined, revealing the underlying larger choroidal vessels due to RPE and choriocapillaris atrophy. In later phases, an increase in hyperfluorescence is observed as the dye slowly diffuses from the large choroidal vessels, staining the residual choriocapillaris (Romano et al., 2021). In advanced EMAP stages, a persistent late hypofluorescent signal, mimicking "dark atrophy" may appear over extra-foveal atrophic lesions, indicative of profound choroidal atrophy

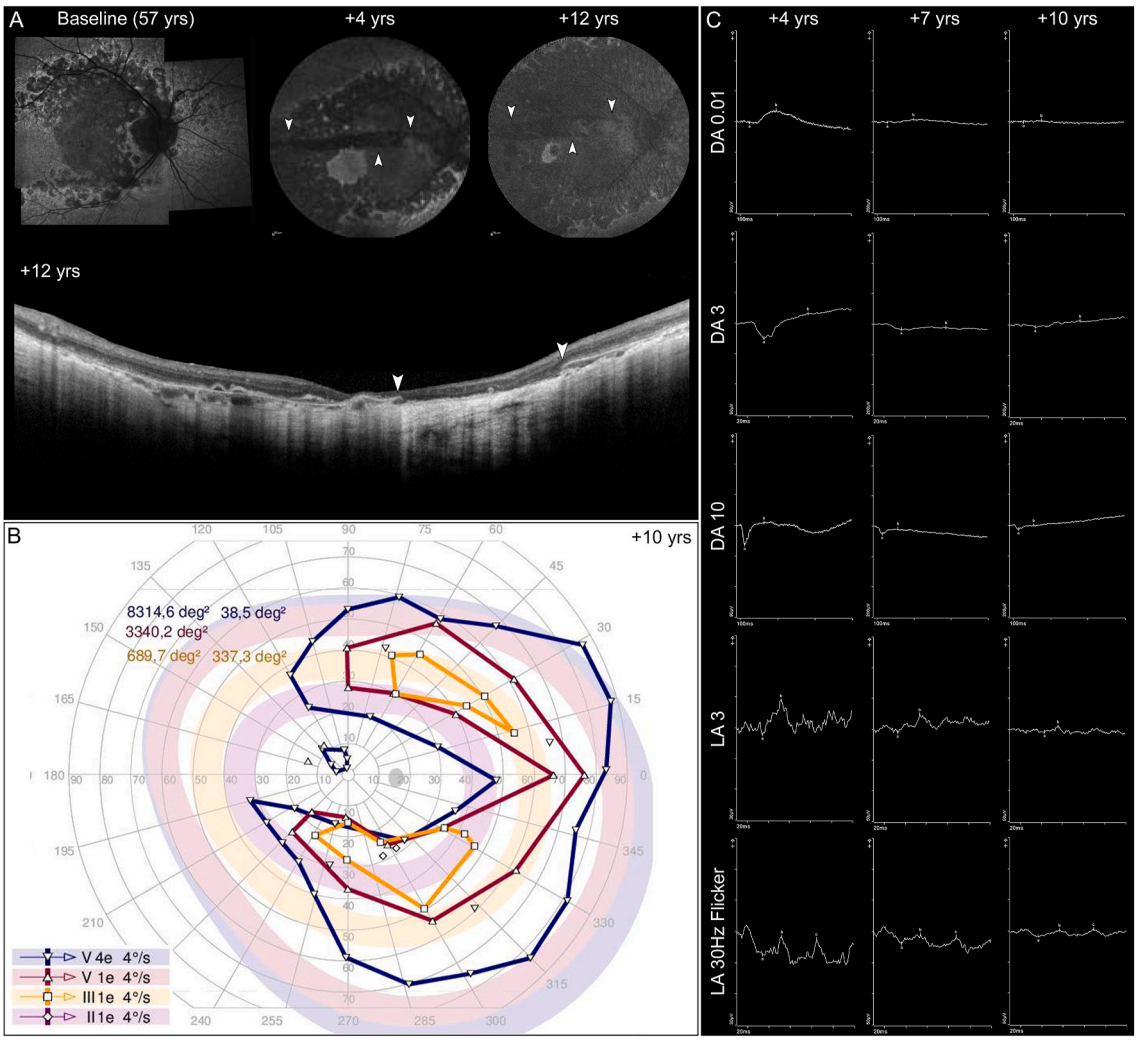

Fig. 18. *Progression of EMAP in a 57-year-old patient over 12 years of follow-up.* (A) On SW-AF images, macular atrophy progressively spreads to the entire posterior pole over the follow-up. A large linear BM break horizontally crossing the macula developed during at the fourth year of follow-up. The margins of the rupture (white arrowheads) can be easily identified also on a vertical macular OCT scan. Please note the persistence of a small temporal sparing until the very late disease stage. (B) Interestingly, the temporal sparing corresponds to an island of vision within an absolute scotoma on kinetic perimetry. The peripheral visual field is constricted, mostly in the nasal hemifield corresponding to the temporal retinal periphery, where the pavingstone-like degeneration is usually found. (C) Longitudinal ERG recordings demonstrate a profound worsening of waveform amplitudes under dark-adapted conditions over 3 years of follow-up, in which the DA 10 ERG response acquires a pseudo-electronegative configuration because of the complete loss of rod system activity and consequent exposure of residual cone responses under dark-adapted conditions. After 3 additional years of follow-up, also light-adapted recordings show a profound amplitude depression. Note the LA 30 Hz flicker implicit time is already delayed (32.5 ms) at the baseline visit [the upper limit of normality (95th percentile) being 31.5 ms].

and scleral exposure (Fig. 20). Notably, pseudodrusen-like deposits present as scattered, nummular hypofluorescent lesions, more prominent in the early-middle phases but possibly persisting through the late angiograms, suggesting the presence of hydrophobic neutral lipids (Chen et al., 2018). Additionally, ultra-widefield application of fluorescein angiography and ICGA enable a more comprehensive characterization of the peripheral pavingstone-like lesions observed in EMAP. Specifically, fluorescein angiography reveals these pavingstone-like areas as well-defined, markedly hyperfluorescent due to a window effect, while surrounding hyperreflective lesions exhibit mild staining in the late phases. Conversely, ICGA highlights more numerous and confluent hypofluorescent spots, likely reflecting a combination of choriocapillaris atrophy and a masking effect from the hyperreflective lesions (Fig. 21).

4.6.3. OCT angiography

The advent of OCTA has revolutionized the medical retina field enabling for depth-resolved and non-invasive assessment of retinal and choroidal layers (Laíns et al., 2021; Spaide et al., 2018). As an emerging imaging modality in the study of retinal disorders, OCTA has introduced novel imaging biomarkers supplementing traditional methodologies (Arrigo et al., 2023). Although OCTA cannot completely replace dye angiographies due to its inability to capture dynamic information (e.g., leakage and staining) and its susceptibility to artifacts, it has proven invaluable in various clinical and research settings. This is particularly relevant in understanding the intimate relationship linking SDD with choriocapillaris alterations, particularly considering that the appearance of MA in EMAP resembles the lobular structure of the choriocapillaris. The first study on OCTA findings in EMAP, published by Rajabian et al. and including 14 eyes, identified significant vascular alterations in all retinal vascular plexa in EMAP compared to controls. The authors suggested an early involvement of the deep capillary plexus, along with progressive choriocapillaris rarefaction from atrophic to non-atrophic areas (Rajabian et al., 2020). More recently, Romano F et al. explored the relationship between structural findings and microperimetry in a large cohort of 88 EMAP eyes (Romano et al., 2023a).

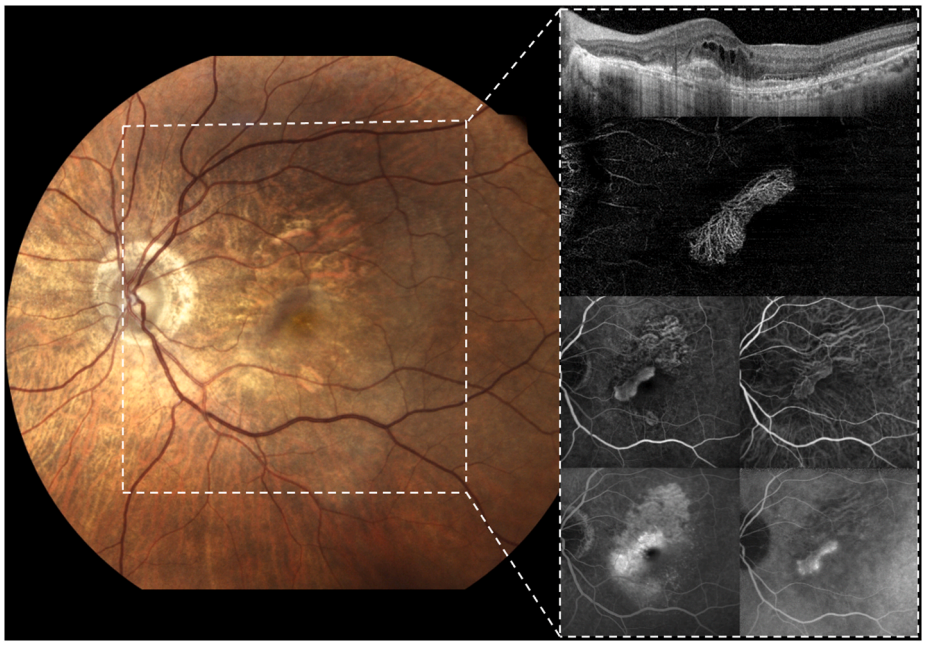

Fig. 19. *Multimodal retinal imaging of extensive macular atrophy with pseudodrusen (EMAP) complicated by macular neovascularization (MNV).* True color fundus photograph of the posterior pole shows a faint, whitish lesion supero-nasal to the fovea, located at the border of a large area of retinal pigment epithelium (RPE) atrophy (EIDON; CenterVue, Padua, Italy). Dotted white box: the horizontal optical coherence tomography (OCT) scan through the fovea reveals intra- and subretinal exudation above a hyperreflective subretinal lesion. The MNV can be visualized in the subretinal space using a customized *en face* OCT angiography slab. Fluorescein angiography shows the neovascular lesion as hyperfluorescent from the early phases, attributable to its subretinal location, with diffuse leakage apparent in the late phases. Indocyanine green angiography further delineates a neovascular network exhibiting progressive staining in the late phases.

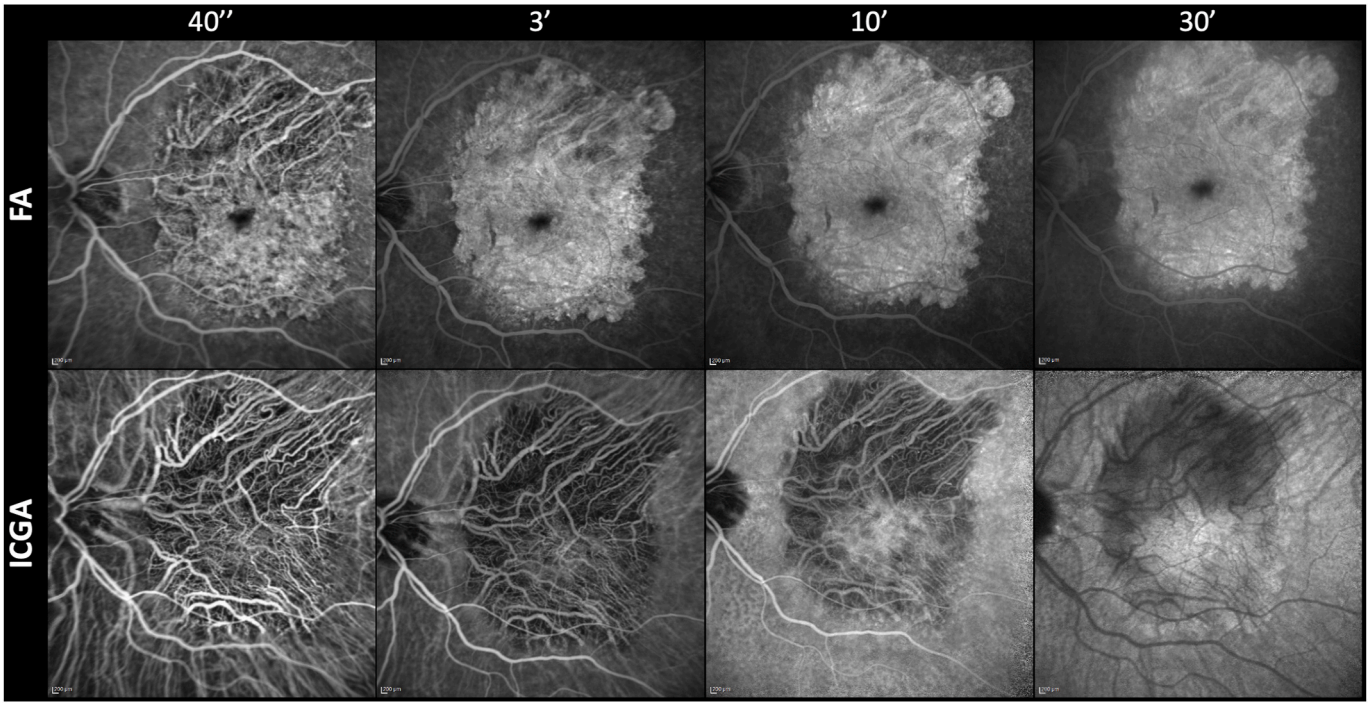

Fig. 20. *Fluorescein (FA) and indocyanine green (ICGA) angiography in extensive macular atrophy with pseudodrusen (EMAP).* On FA imaging, atrophic areas become progressively hyperfluorescent and sharply defined, reflecting the window effect resulting from the retinal pigment epithelium (RPE) loss. The boundaries of the atrophic areas appear less distinct in the later phases of the angiogram, a consequence of the dye diffusion and simultaneous staining of the nearby choroidal stroma. Early ICGA phases reveal diffuse hypofluorescence over the atrophic areas, attributable to the severe atrophy of both the RPE and choriocapillaris, which enhances the visualization of the underlying large choroidal vessels. In the angiography late phase, the atrophic areas exhibit variable fluorescence, presumably due to the faint staining of the residual choriocapillaris. Notably, during this phase, the fovea is iso-fluorescent, and the surrounding pseudodrusen are more distinctly visible.

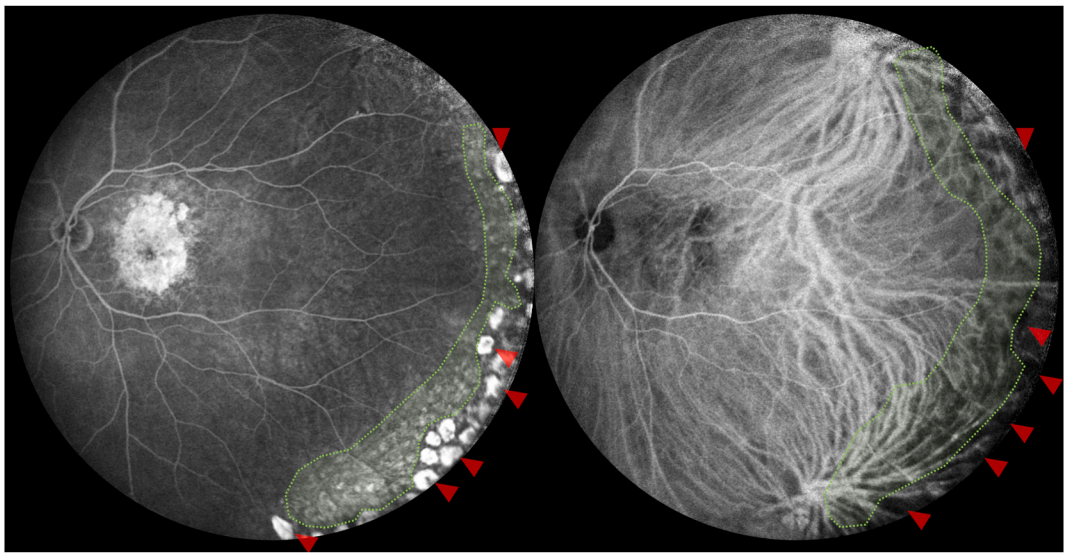

Fig. 21. *Fluorescein (FA) and indocyanine (ICGA) angiography findings in peripheral pavingstone-like lesions and surrounding areas.* Widefield FA images, captured 10 min after dye injection, reveal well-defined hyper-fluorescent spots that correspond to pavingstone degeneration (dark red arrowhead – Spectralis HRA2, 102° × 102° field of view; Heidelberg Engineering GmbH, Heidelberg, Germany). Adjacent to the pavingstone lesions, a diffuse area of faint hyperfluorescence can be noticed, aligning with areas where hyperreflective lesions have been identified using peripheral optical coherence tomography (light green dotted area). On simultaneously acquired ICGA images, the pavingstone-like degeneration and the posterior hyperreflective lesions appear as markedly and slightly hypofluorescent, respectively.

This analysis included data on choriocapillaris flow deficits, finding that choriocapillaris rarefaction progressively increased in advanced stages of the disease, and correlated significantly with diminished scotopic retinal sensitivity, a phenomenon previously described in AMD. Furthermore, the same group qualitatively assessed choriocapillaris alterations in a small series of stage 1 eyes without RPE atrophy (Romano et al., 2023b). All examined eyes exhibited multiple large flow voids at the choriocapillaris level, predominantly located in the perifovea, and with a relative sparing of the fovea. Based on our clinical experience, choriocapillaris alterations tend to rapidly advance over time, leading to clearer visibility of the underlying Sattler and Haller's layers (Fig. 22). In the end stage of the disease, visualization of the short posterior cilio-retinal arteries becomes more pronounced. As already mentioned regarding choroidal thinning, whether these changes are primary effects or occur secondary to the extensive retinal degeneration or the thick sub-RPE deposits remains unclear. Still, it is important to acknowledge that OCTA accuracy in assessing choriocapillaris diminishes in more advanced stages due to challenging segmentation and marked choroidal thinning. Lastly, as previously indicated, OCTA is instrumental in accurately differentiating MNV from the non-neovascular fibrosis seen in most stage 3 eyes (Trinco et al., under review).

5. Natural history

5.1. Visual acuity

Visual acuity is a measure of the eye's ability to resolve fine spatial details at a given distance. Although subjective in nature and highly reliant on foveal status, visual acuity is the most common endpoint used in clinical trials in ophthalmology (Schmetterer et al., 2023).

Half of the patients affected by EMAP attain a visual acuity of 20/200 Snellen or less within approximately 4 years after diagnosis (Douillard et al., 2016; Romano et al., 2021). This finding was recently corroborated by Antropoli et al., who demonstrated that within 4 years of diagnosis, 50% of EMAP patients met the legal blindness criteria set by the United States Social Security Administration (≤20/200 Snellen), coinciding with the onset of foveal atrophy (Antropoli et al., 2024). However, when applying the WHO definition of blindness, the median time to reach a visual acuity of <20/400 was approximately 7 years, with many patients not reaching this endpoint during the observation period. These data correspond to incidence rates of blindness of 3.95/100-subjects-year following US criteria and 1.54/100-subjects year according to the WHO. It is still important to note that the exclusion of patients with baseline BCVA below the established thresholds may have led to an underestimation of the true incidence rates. At the end of the study, after a mean disease duration of 5.7 ± 4.4 years, one-third to two-thirds of EMAP patients had become blind, depending on the definition considered (Antropoli et al., 2024). The yearly rate of BCVA decline has been estimated at 7.4 ± 5.8 ETDRS letters/year in a retrospective cohort study (Romano et al., 2021), and subsequently confirmed at 7.7 ± 5.2 ETDRS letters/year in a 3-year prospective observational trial including 9 patients (Romano et al., 2023c).

5.2. Visual field

Kinetic perimetry involves the presentation of moving visual stimuli to map the patients' visual field by drawing different isopters. These are generated by connecting all the locations where stimuli of the same dimensions (from "*I*" to "*V*") and intensity (from "1" to "4") are first seen, allowing to create a two-dimensional representation of the patient's "hill of vision". This technique is particularly useful for evaluating peripheral visual field defects and retinal sensitivity changes with steep gradients, such as those related to atrophic lesions. It is also adept at identifying islands of vision, such as that located in the area of temporal sparing (Fig. 18), with potential implications for low vision rehabilitation. The simultaneous presence of MA expanding beyond the vascular arcades and peripheral pavingstone-like degeneration encroaching centripetally into the posterior pole makes kinetic perimetry one of the most effective tools for monitoring disease progression in EMAP, particularly as the atrophy can grow so large that its measurement becomes unreliable. Hamel et al. reported central scotomas ranging from 10 to 20° in diameter, as evaluated with the I4 stimulus, which correlated with the area of MA (Hamel et al., 2009). Conversely, the peripheral visual field boundaries were preserved in all eyes. More recently, we investigated the kinetic visual fields of 27 patients from the French Quinze-Vingts cohort aged 70.5 ± 6.5 years (Antropoli et al., 2024). All of them had central scotomas, generally displaying a major diameter of 30° or less in binocular testing with the III4e stimulus.

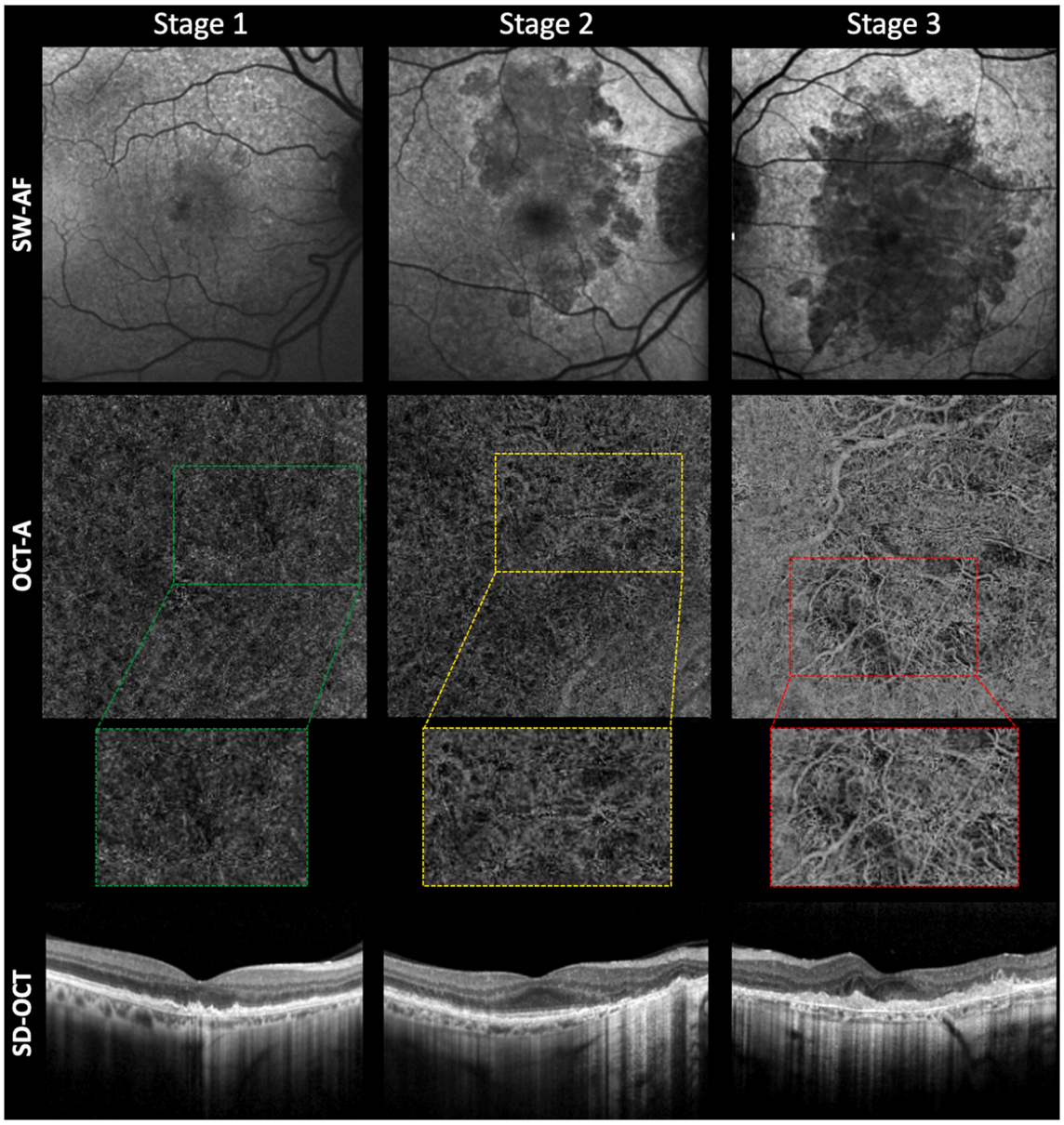

Fig. 22. *Qualitative optical coherence tomography angiography (OCTA) features across the three stages of extensive macular atrophy with pseudodrusen-like appearance (EMAP).* Stage 1 is characterized by the absence or isolated, non-confluent patches of retinal pigment epithelium (RPE) atrophy, alongside severe rarefaction and numerous flow voids within the choriocapillaris layer. In stage 2, as RPE atrophy becomes confluent, a notable increase in flow voids can be documented, with choriocapillaris atrophy becoming apparent in the perifoveal area. By stage 3, choriocapillaris atrophy extends widely, adopting an annular pattern, thereby enhancing the visibility of the underlying larger choroidal vessels.

However, the proportion of wider scotomas rapidly increased when testing each eye separately, particularly when considering the V1e stimulus. Moreover, contrary to Hamel et al., we found a peripheral visual field constriction in about 20% of the patients, likely attributable to the high prevalence of pavingstone-like degeneration.

5.3. Macular atrophy growth rate

Concerning the size of MA in EMAP, Hamel et al. reported that it involved the entire posterior pole and was larger than 6 papillary areas in all eyes of their 18 patients aged 49–60 years (Hamel et al., 2009). However, in the recent years color fundus photographs have been progressively superseded by SW-AF for the quantitative measurement of MA, owing to its enhanced contrast in delineating the lesion borders and the advent of highly reproducible semi-automated image processing tools (Schmitz-Valckenberg et al., 2011). Indeed, SW-AF-based measurements of MA are now accepted as primary outcome measures in clinical trials for GA secondary to AMD and Stargardt disease (Schmetterer et al., 2023). Despite its MDAF signal, it is generally feasible to delineate the lesion boundaries on SW-AF images (Bianco et al., 2023). Only recently, some monocentric studies on the Italian EMAP cohort attempted to measure MA growth rates in EMAP using SW-AF (BluePeak®) images acquired through Heidelberg SPECTRALIS instruments. The estimates varied from 2.9 to 4.7 mm^2/year (Antropoli et al., 2023; Bianco et al., 2023; F. Romano et al., 2023c; Romano et al., 2021), all of which exceeded those measured in GA secondary to AMD (1.52 mm^2/year) (Holz et al., 2007) and in genetic macular dystrophies, such as *ABCA4*-associated retinopathy/Stargardt disease (0.76 mm^2/year) (Strauss et al., 2019). Conversely, growth rates in EMAP were similar to the 3.02 mm^2/year reported for DTGA (Fleckenstein et al., 2014). However, these estimates were not adjusted for the baseline area of MA, which is often associated with its own growth rate

(Schmitz-Valckenberg et al., 2016b; Strauss et al., 2019). Consequently, since the mean MA area can vary greatly among different diseases and also across different cohorts of patients affected by the same disease, growth rates are difficult to compare with each other unless a square root transformation of MA areas is applied (Yehoshua et al., 2011). Since we had access to individual-level data from both the Italian and French Quinze-Vingts EMAP cohorts, we performed quantitative measurements and statistical analyses to yield a more accurate knowledge of the kinetics of MA progression in EMAP (Supplementary Material). Using pooled SW-AF data from both cohorts (294 eyes of 150 patients), the median (IQR) area of MA at baseline was 12.61 (5.02–22.3) mm^2 at a median (IQR) age of 62.7 (57.1–66.4) years, with a high correlation between right and left eyes ($r = 0.95$; $P < .001$), confirming that EMAP is not only bilateral but also highly symmetric. As illustrated by the scatterplot in Fig. 23A, the patient's age was positively associated with the area of MA ($P < .001$), meaning that older patients on average showed larger lesions. We also estimated the mean MA area based on the patient's age (1188 observations), as this could be valuable for estimating the likelihood of an EMAP diagnosis when suggestive phenotypic features are present. The mean age at the first onset of MA was predicted to be 58.4 years (95% CI, 57.4 to 59.5; $P < .001$), while a MA area of 25 mm^2 – roughly corresponding to 9 disc areas (Elledge et al., 2005) – was predicted to be reached by a mean age of 64.9 years (95% CI, 63.9 to 65.9; $P < .001$). Regarding the longitudinal progression of MA, we attempted to retrospectively estimate its annual growth rate in the two independent EMAP cohorts. In the Italian cohort, 609 observations over a median (IQR) follow-up of 3.7 (1.7–6.2) years were available from 116 eyes. The mean growth rate of square root transformed MA areas was estimated at 0.452 mm/year (95% CI, 0.385 to 0.519; $P < .001$) (Fig. 23B). Replication in the French Quinze-Vingts cohort [511 observations from 111 eyes over a median (IQR) follow-up of 5.2 (3.1–8.1) years] yielded a similar estimate [0.443 mm/year (95% CI, 0.394 to 0.491; $P < .001$)], despite a higher mean baseline area (Fig. 23B). The estimated mean MA growth rate using pooled data from both cohorts was 0.447 mm/year (95% CI, 0.406 to 0.488; $P < .001$). This figure confirms that EMAP outpaces the mean growth at 1 year of GA secondary to AMD, estimated at 0.36 mm (95% CI, 0.33 to 0.38) in the prospective Proxima A and B natural history studies (Holekamp et al., 2020). On the other hand, it is closer to the growth rate attributed to pseudodrusen in AMD (0.379 mm/year; 95% CI 0.329 to 0.430) by the AREDS study group (Agrón et al., 2023). This latter observation suggests that the mechanism governing the development and progression of MA may be similar between EMAP and AMD featuring pseudodrusen. Further details on this topic will be discussed in section 7.2 of this review. However, as previously noted, EMAP can potentially progress into vast atrophic lesions due to the widespread distribution of the deposits, and the longer life expectancy and consequently disease course of these patients. Indeed, within the French Quinze-Vingts cohort, 38 eyes from 28 patients developed a MA exceeding 100 mm^2 at a median (IQR) age of 71.5 (66.7–74.8) years, and ranging from 61 to 78 years, reflecting the variable age of onset of the disease. These data were excluded from the statistical analyses presented above because the lesion often surpassed the field-of-view of the Heidelberg SPECTRALIS 55° lens, rendering reproducible measurement nearly impossible, even for the same grader (Supplementary Material). It is thus evident that MA in EMAP continues its expansion even after reaching the proposed last stage, leading to further visual impairment and hindering low vision rehabilitation. Consequently, the growth rate that we reported herein may be an underestimate. In this regard, UWF instruments may prove more appropriate in future research to explore the progression kinetics of retinal atrophy in the severe end of EMAP spectrum and its peripheral component (Battaglia Parodi et al., 2023), similarly to approaches proposed for *ABCA4*-associated retinopathy (Heath Jeffery et al., 2021a, 2021b).

6. Retinal function

6.1. Full-field electroretinogram

Retinal electrophysiology holds key importance in interpreting the symptoms experienced by patients and the functional consequences of imaging features observed in EMAP. Full-field electroretinogram (ERG) is the only investigation that enables an objective and quantitative assessment of retinal function, allowing for the distinction between rod and cone system activity and between photoreceptor and inner retinal function. Current standards recommended by the International Society for Clinical Electrophysiology of Vision (ISCEV) include a minimum of six recordings under dark-adapted (DA) or light-adapted (LA) conditions and using different light flash strengths (Robson et al., 2022). The DA ERGs include responses to flash strengths (in photopic units; phot) of 0.01, 3, and 10 phot $cd{\cdot}s{\cdot}m^{-2}$ (DA 0.01; DA 3; DA 10) and allow assessment of rod system function. Following a minimum period of 20 min of dark adaptation, the DA 0.01 ERG uses a dim flash, below the threshold for the DA cone system, to elicit a single positive waveform arising in the inner retina but depending exclusively on the function of the rod photoceptors. On the contrary, the DA 3 and DA 10 ERGs are in fact mixed rod and cone system responses, but contribution from the rod system dominates in a healthy retina. Both show a negative a-wave generated in the photoreceptors, followed by a larger positive b-wave originating in the inner retina. The LA ERGs are performed following 10 min of light adaptation using a flash strength of 3 phot $cd{\cdot}s{\cdot}m^{-2}$ superimposed on a light-adapting background (luminance 30 cd $s{\cdot}m^{-2}$) as single flashes (LA 3 ERG) and at a 30 Hz frequency (LA 30 Hz ERG). Thus, the rod system is saturated, and specific cone system recordings are obtained (Robson et al., 2022). In this regard, it is essential to remark that, even if the macula is the retinal region with the highest density of cones, ERG signals are generated across the entire retina and the contribution from the macula is minimal. Thus, although ERG changes are part of the normal aging process (Birch and Anderson, 1992), retinal diseases confined to the macula such as AMD are expected to show ERG responses within the age-matched normality range.

In EMAP, an amplitude attenuation of rod-dominated DA responses was observed in all patients included in the original description by Hamel et al. in 2009, along with a milder impairment of cone-driven LA responses (Hamel et al., 2009). Later, Watanabe et al. found ERG alterations in 80% of patients (Watanabe et al., 2023). A study including ISCEV-standard ERGs from 104 eyes of 52 patients belonging to the French Quinze-Vingts cohort (Bianco et al., under review) found that the mean response attenuation was between 80 and 90% of lower limit of normal (LLN) for DA ERGs, and only subnormal (90–100% of LLN) for LA ones. Furthermore, advanced EMAP cases showing MA beyond the temporal vascular arcades had a more severe attenuation of both DA and LA ERG responses. As an example, Fig. 18 illustrates how waveform amplitudes are progressively affected as MA expands toward the mid-periphery. Overall, 31% of eyes had severe rod-cone dysfunction, 29% moderate rod-cone dysfunction, 17% isolated rod dysfunction, while the remaining 23% had a normal retinal function on ERG. Almost 90% of patients with normal ERG had early-stage EMAP. Anyhow, EMAP appears to be characterized by a generalized dysfunction of retinal photoreceptors in the majority of cases, with a prevailing involvement of the rod system, and should not be therefore considered a macular disease. Indeed, rod system dysfunction in EMAP has been demonstrated also by more sensitive techniques, such as dark adaptometry and scotopic microperimetry (Hamel et al., 2009; Romano et al., 2023a). This is in keeping with the fact that the majority of EMAP patients experience some degree of night blindness (56% in the initial cohort reported by Hamel et al. and 95% in the cohort of Watanabe et al.), even before the development of a central/paracentral scotoma and loss of visual acuity. We believe that the rod system dysfunction observed in EMAP can be attributed – perhaps partially and before widespread chorioretinal atrophy develops – to a slowdown of

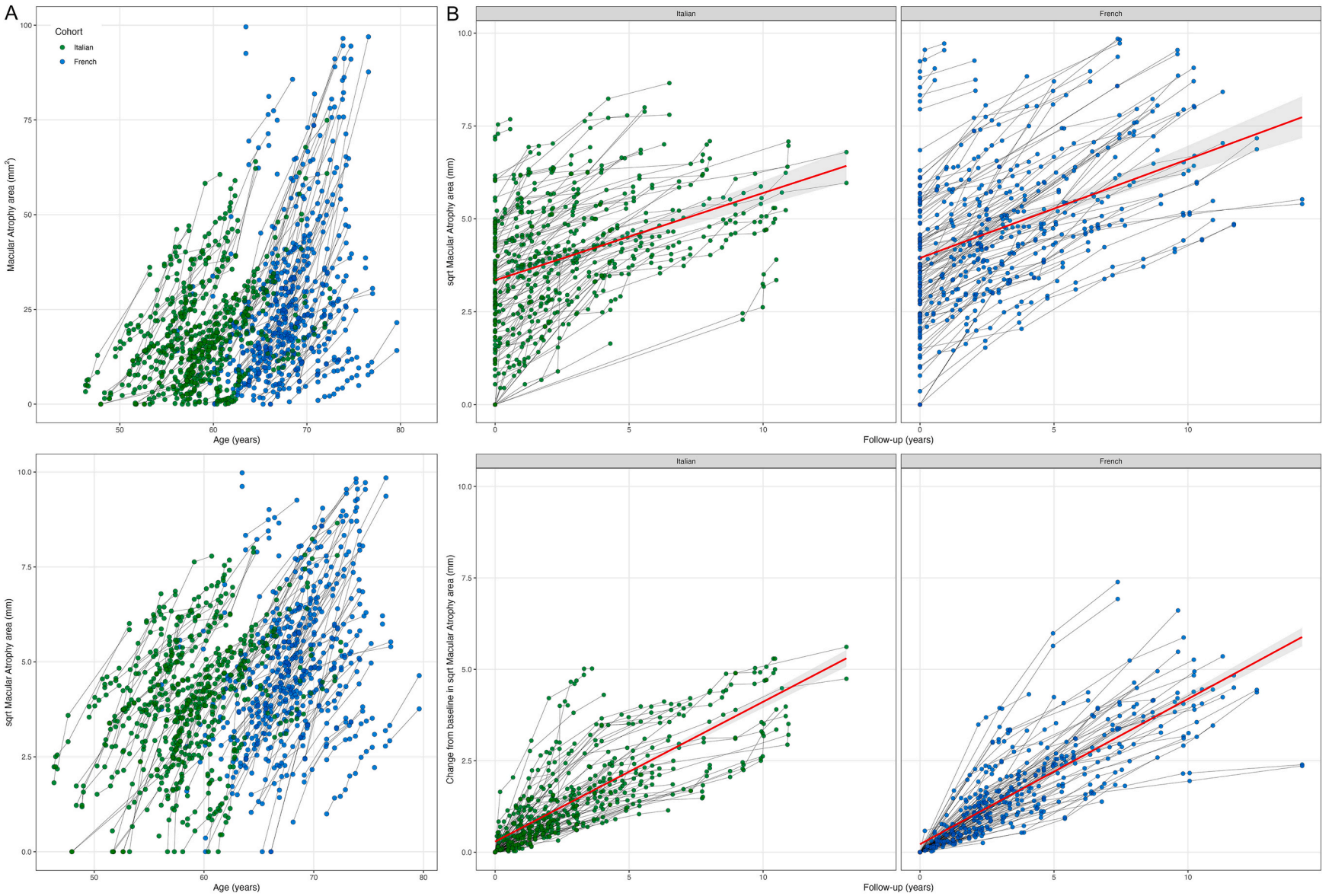

Fig. 23. *Progression of macular atrophy in EMAP cases from the Italian and French Quinze-Vingts cohorts.* (A) Scatterplot of age and macular atrophy area in EMAP. (B) Growth of macular atrophy area (square-root transformed; mm) over the follow-up in the Italian and French cohorts (upper panels) and change form baseline in macular atrophy (lower panels). Measurements from the same eye are connected by a black line. A best-fit linear regression line along with its standard error is shown in each panel. Despite the Italian cohort being younger age and with a smaller lesion area at baseline, the annual growth rate is similar between the two cohorts.

phototransduction kinetics. Indeed, a dramatic DA 0.01 ERG b-wave recovery after prolonged dark adaptation was observed by Douillard et al., although not systematically reported in every patient (Douillard et al., 2018), and all the putative EMAP cases from the series reported by Tsunoda et al. showed either a partial or complete recovery after 180 min of dark-adaptation (Tsunoda et al., 2019). Furthermore, similar electrophysiological findings can be observed in retinal diseases with an acquired (vitamin A deficiency) or inherited (*RDH5, RLBP1, C1QTNF5, TIMP3*) impairment of the RPE visual cycle (discussed in section 8). Whether this slowdown is due to a local retinoid deficiency due to hindered transport by the sub-RPE deposits deserves to be investigated in future research using retinal electrophysiology. In any case, our findings prove the usefulness of ERG for prognostic purposes (Fig. 24) and in the differential diagnosis with other GA secondary to AMD (Fig. 25).

6.2. Microperimetry

Microperimetry (also known as 'fundus-controlled perimetry') is an increasingly recognized tool for assessing spatially-resolved retinal sensitivity under various illumination conditions, including mesopic and dark-adapted scotopic testing (Pfau et al., 2021). Recent technological advances have led to devices with enhanced tracking capabilities, broader dynamic range, and the ability to selective test different photoreceptor types (e.g., S-, L-, M-cones, and rods). Consequently, microperimetry has found widespread application in a variety of retinal conditions for both clinical assessment and research. Romano F et al. employed mesopic and scotopic microperimetry to validate the proposed three-stage clinical classification (Fig. 4) (Romano et al., 2023a). While mesopic retinal sensitivity significantly decreased across the disease stages, no differences in scotopic retinal sensitivity were found between stages 2 and 3, particularly in the macular region. Mesopic sensitivity reduction was significantly associated with the presence of foveal atrophy, non-neovascular fibrosis, and a larger extent of RPE atrophy. In contrast, the lack of meaningful associations between impaired responses to red scotopic stimuli and imaging biomarkers was attributed to the profound rod impairment characteristic of the disease, resulting in a floor effect. Although cyan scotopic microperimetry, which selectively tests rod function, was not performed, the authors highlighted a severe rod impairment in the paramacular are of stage 1 eyes by reporting the scotopic sensitivity loss (i.e., the difference in sensitivity between mesopic and red scotopic stimuli). These findings align with observations from other macular disorders, such as PXE and advanced AMD, where severe degenerative changes at the level of the BM impede effective exchange with the outer retina. Furthermore, the same authors recently corroborated these findings using dark-adapted two-color scotopic microperimetry in four stage 1 eyes (Romano et al., 2023b). After 30 min of dark adaptation, cyan scotopic sensitivity was abolished in eyes exhibiting only RPE-BM separation without RPE atrophy. This finding suggests that even the ~20% of cases with early stage EMAP and normal DA ERG amplitudes can still have substantial rod dysfunction, though full-field tests may not be sensitive enough to detect early changes. However, studies comparing ERG, scotopic microperimetry, and dark adaptometry across different EMAP stages are currently lacking.

7. Phenotypic overlap with age-related macular degeneration

The definition of AMD varies slightly among the various proposed classification systems. According to the Beckman classification, which is the most commonly used in clinical practice, the diagnosis of AMD requires the presence of medium-sized drusen (63–125 μm) and/or

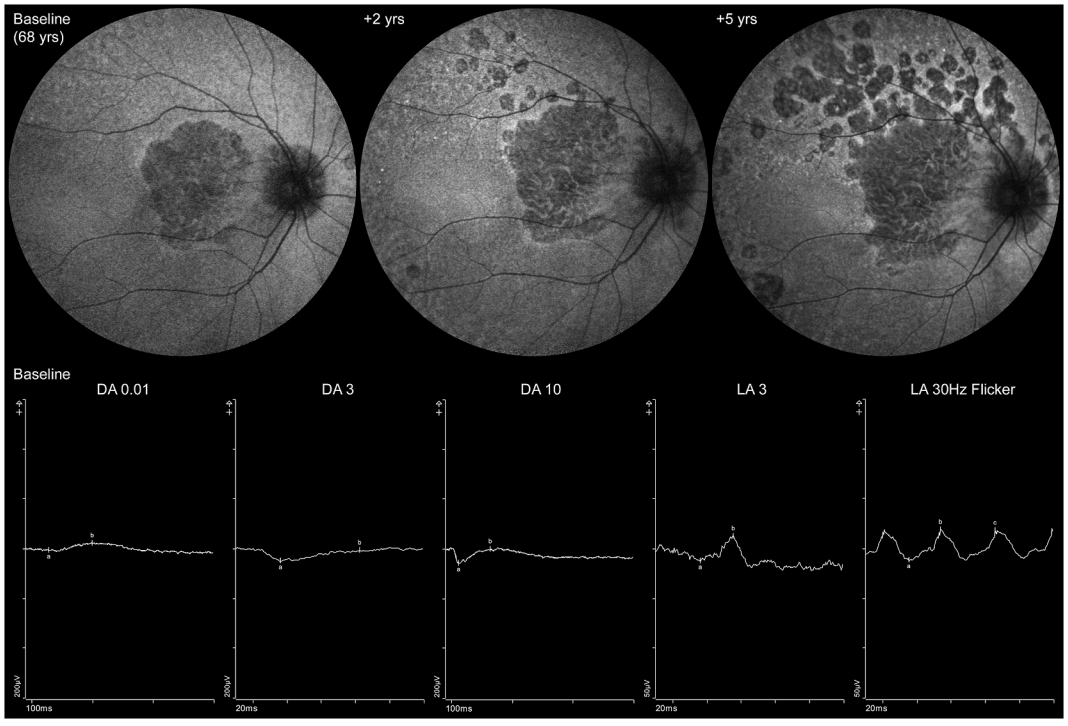

Fig. 24. *Prognostic relevance of full-field electroretinogram (ERG) in predicting expansion of macular atrophy in a patient with early-stage EMAP.* At baseline, a 68-years old female affected by EMAP showing a central patch of MA with "grayish" hypoAF appearance surrounded by granular hyperAF changes on SW-AF. Despite the patient being relatively aged and the MA area smaller than typical cases, the corresponding ERG (lower panel) demonstrates typical findings for EMAP. Indeed, the rod-specific DA 0.01 recording shows a substantial decrease in the b-wave amplitude, with only a mild decrease in LA cone-driven responses. The DA 10 ERG response has a pseudo-electronegative configuration attributable to the exposure of responses from dark-adapted cones subject to the "photopic hill" phenomenon in an almost "rod-free" retina. After 2 years of follow-up, isolated circular hypoAF atrophic patches developed outside the macula along the temporal vascular arcades. At the 5th year of follow-up, clear expansion of MA toward the retinal mid-periphery is seen, along with the delineation of the typical temporal sparing.

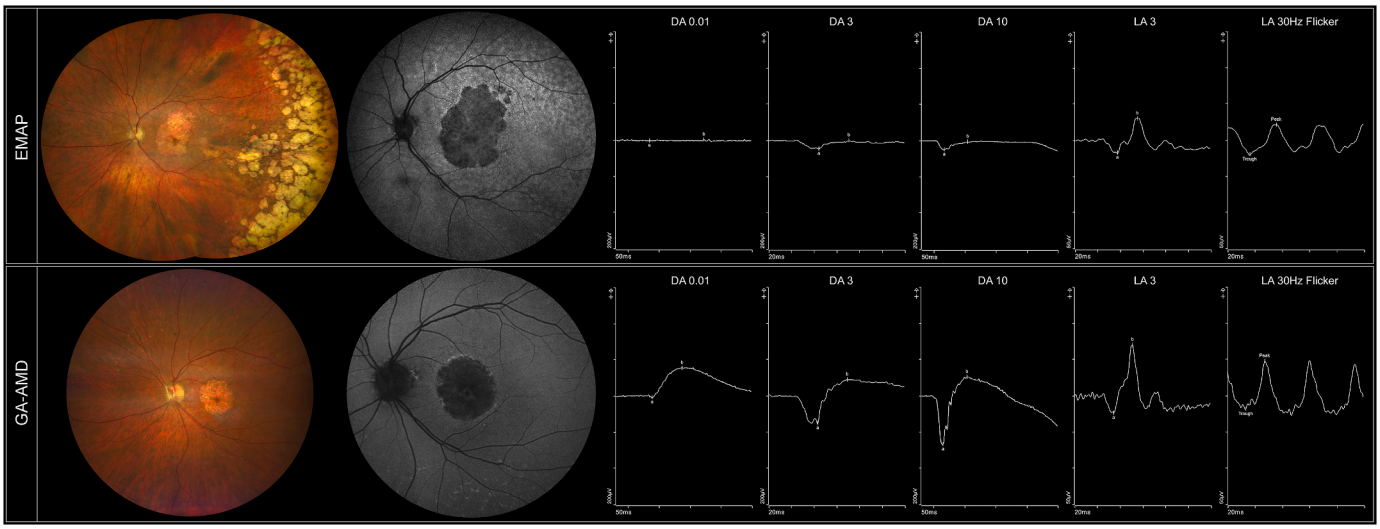

Fig. 25. *Role of full-field electroretinogram (ERG) in the differential diagnosis between EMAP and geographic atrophy (GA) secondary to age-related macular degeneration (AMD).* (Upper panel) The patient affected by EMAP shows an atrophic lesion still confined within the temporal vascular arcades despite being relatively aged. A lattice of pseudodrusen-like deposits covers the entire posterior pole and mid-periphery. These are also visible on SW-AF as faintly hyperAF lesions arranged in a reticular pattern around the atrophic lesion. Pavingstone-like degeneration is present and best seen in the temporal sector, having reached the equator and projecting into the mid-periphery along the horizontal meridian. ERG shows an undetectable b-wave on DA 0.01 response, a pseudo-electronegative DA 10 response dominated by DA cones, and mildly abnormal cone-driven LA ERGs. (Lower panel) Paradoxically, the patient affected by GA secondary to AMD is younger (67 years-old) than that affected by EMAP. A circular area of macular atrophy is seen, very similar to that of EMAP in terms of size, along with small peripheral drusen but no pseudodrusen-like deposits. As expected, ERG shows normal waveforms under all adaptation and stimulus conditions.

pigment abnormalities (Ferris et al., 2013). Conversely, while RPD have recently been acknowledged as a third hallmark of AMD and are associated with an increased risk of progression to late AMD, their isolated presence has not yet been incorporated in any classification scheme to date (Agrón et al., 2022; Huisingh et al., 2016). GA represents the advanced dry form of AMD and is characterized by the progressive loss of photoreceptors, RPE cells and the underlying choriocapillaris (Sarks et al., 1988). Despite being detectable using various imaging modalities, the identification of GA has historically relied on CFPs due to its widespread adoption in epidemiologic studies and disease classifications. GA is defined as a sharply delineated round or oval area of hypopigmentation, with increased visibility of the choroidal vessels and a minimum linear dimension of 170–350 μm, depending on the classification system (Bird et al., 1995; Klein et al., 1991). However, CFP has limitations in identifying certain features of GA lesions, leading to the use of novel imaging modalities for clinical and research purposes. As we mentioned earlier in this review (sections 4.1.1 and 5.3), SW-AF is now considered the predominant modality for assessing GA size and progression and is accepted by most regulatory agencies as a structural endpoint for clinical trials. Nonetheless, SW-AF has its limitations, including challenges in evaluating foveal involvement due to its hypoAF appearance caused by the luteal pigment (Moritz Lindner et al., 2015). Consequently, there has been an increasing focus on identifying more sensitive biomarkers based on OCT imaging. The term "nascent GA" was first introduced in 2014 to describe the OCT precursors of GA, characterized by subsidence of the outer plexiform layer (OPL) and the inner nuclear layer, and/or the identification of a hyporeflective wedge in the OPL (Wu et al., 2014). More recently, the classification of atrophy meeting (CAM) initiative used OCT as the reference imaging technique to define cRORA as the simultaneous attenuation or loss of RPE and photoreceptors, accompanied by posterior hypertransmission greater than 250 μm (Sadda et al., 2018). In this context, the authors advocated for the use of the term cRORA, particularly in the absence of MNV, rather than GA, which represents a typical presentation of AMD-related cRORA on CFP and SW-AF, as proposed in a previous CAM (Sadda et al., 2018; Schmitz-Valckenberg et al., 2016a). Bearing in mind these definitions, various multimodal imaging characteristics can be utilized to differentiate EMAP from AMD. These characteristics include the absence of drusen, the continuous RPE-BM separation across the macular area, and the consistent MDAF pattern on SW-AF. At the beginning of this review, we mentioned that the description of EMAP occurred almost simultaneously with that of DTGA as the most aggressive SW-AF pattern of GA in the context of the FAM-study (Holz et al., 2007). Differentiating between these two entities based exclusively on multimodal imaging posed a substantial challenge, as they exhibit nearly identical features on both OCT and SW-AF (Bianco et al., 2023). Curiously, in the CAM report number 3, the DTGA pattern represented the only exception to the SW-AF description of cRORA, although this was not further discussed (Sadda et al., 2018). A few years following their initial descriptions, the striking similarities between EMAP and DTGA in terms of progression and imaging features emerged. This observation sparked a debate about whether the two conditions belonged to a common clinical spectrum or rather represent the same condition. In the following sections, we will review the similarities and differences between EMAP and DTGA, as well as the functional significance of RPD in AMD.

7.1. *Diffuse trickling geographic atrophy (DTGA)*

The "Diffuse-Trickling" pattern has been originally identified as the most aggressive SW-AF pattern of GA secondary to AMD (Fleckenstein et al., 2014; Holz et al., 2007), only two years before the first description of EMAP (Hamel et al., 2009). In this study, the authors aimed to investigate whether the different pattern at the border of MA ("junctional pattern") on SW-AF were associated with different GA growth rates. One of these patterns, the "diffuse" one, was further branched in five sub-patterns based on the distribution of the hyperAF signal beyond the atrophic area. The DTGA sub-pattern was identified in 9 eyes with younger age and unique GA characteristics. Between 2011 and 2016, the same authors published further studies on DTGA, delving deeper into its multimodal imaging findings, and associated risk factors, from both clinical and genetic standpoints (Fleckenstein et al., 2016, 2014, 2011; Lindner et al., 2015). Although the initial results of the "EMAP Case-Control National Clinical Trial" were published almost in parallel in 2016 (Douillard et al., 2016), the multimodal imaging characteristics

of EMAP were thoroughly explored only recently (Antropoli et al., 2023; Battaglia Parodi et al., 2023; Bianco et al., 2023; Romano et al., 2023c; Romano et al., 2021). Over time, a growing body of literature has corroborated the hypothesis that EMAP and DTGA share more similarities than DTGA does with other patterns of GA secondary to AMD (Antropoli et al., 2023; Bianco et al., 2023; Fleckenstein et al., 2014; Romano et al., 2021). It is important to note that while "EMAP" denotes a clinical diagnosis, the term "diffuse-trickling" was conceived to describe the pattern of hyperAF surrounding GA lesions (Holz et al., 2007). Indeed, a "DTGA" pattern on SW-AF could result from several diseases, including L-ORD, SFD, and also EMAP, rather than being exclusive for a subtype of GA secondary to AMD (Fleckenstein et al., 2016). Shortly after the description of DTGA, the focus rapidly shifted from the SW-AF pattern towards ancillary imaging features, alongside the clinical characteristics, and the genetic and acquired risk factors of the affected patients. In the forthcoming sections, we will present the published literature on DTGA, intertwining the comparison of its similarities and differences with EMAP throughout the discussion.

7.1.1. Macular atrophy characteristics

On multimodal imaging, DTGA displays the same key characteristics of EMAP, including the MDAF ("grayish") SW-AF signal, multilobular borders, initial sparing of the fovea, and potential to extend beyond the vascular arcades up to the nasal retina adjacent to the optic disc (Fleckenstein et al., 2011). While no data on their frequency is available in literature, it is worth noting that drusen were infrequent in DTGA in published cases, whereas a background of RPD was common. Additionally, on fundus examination, granular pigmentary changes in the foveal region and at the atrophy boundaries have been described as a frequent characteristic of DTGA. The same alterations have been described in EMAP as well (Puech et al., 2014), particularly in the early stages using NIR-AF (Romano et al., 2023b). Initially estimated at 3.02 mm^2/year based on 9 eyes in the FAM-study (Holz et al., 2007), the growth rate of DTGA was refined 7 years later in 50 eyes of 29 patients (Fleckenstein et al., 2014). The authors reported a median (IQR) growth rate of 2.9 (2.11–3.83) mm^2/year, which aligns more closely with the rate estimated for EMAP than with non-DTGA patterns of GA secondary to AMD. (Antropoli et al., 2023; Bianco et al., 2023; Romano et al., 2023c; Romano et al., 2021). Noteworthy, in some cases the atrophic areas exceeded the SW-AF image frames and could not be measured. In 2011, Fleckenstein et al. described the OCT features of DTGA and identified a diffuse RPE-BM separation, similar to that depicted as a hallmark of EMAP, as a common finding (Fleckenstein et al., 2011). This previously unreported sign was also observed when examining all the borders of MA in non-DTGA cases, but it was frequently too thin for quantification. Specifically, out of 240 borders from 60 eyes with a non-DTGA pattern, the separation was identified in only 33 (14% of cases), with merely 5 of these being sufficiently thick for measurement. In contrast, a conspicuous and measurable RPE-BM separation was consistently present in all 240 borders in DTGA, ranging from 10 to 50 μm in thickness (Fleckenstein et al., 2011). More recently, two studies directly compared EMAP and DTGA by means of SW-AF and OCT, confirming the absence of significant differences between these two entities for what concerns macular findings (Antropoli et al., 2023; Bianco et al., 2023). In detail, MA from EMAP and DTGA could not be distinguished on SW-AF even with the aid of quantitative shape descriptors (Bianco et al., 2023), unlike non-DTGA patterns. The MA growth rates were comparable (3.6 versus 3.25 mm^2/year, respectively), both being significantly faster than non-DTGA patterns (1.65 mm^2/year). In addition, compared to non-DTGA, these two groups had a thinner choroid and displayed a more widespread RPE-BM separation on OCT (Antropoli et al., 2023; Lindner et al., 2015). Thus, EMAP and DTGA can be easily differentiated from non-DTGA patterns without the need for more complex image analysis techniques (Chouraqui et al., 2023). By contrast, these two entities could only be distinguished by considering patients' age, which however was constrained by the study's own inclusion criteria (Antropoli et al., 2023; Bianco et al., 2023).

7.1.2. Cardiovascular risk factors

The literature suggests that EMAP and DTGA differ in some demographic features, including the prevalence of cardiovascular risk factors, the age of onset, and the risk of MNV (Douillard et al., 2016; Fleckenstein et al., 2014). However, a closer look may reveal a more intricate picture. Focusing on the cardiovascular risk factors, Fleckenstein et al. reported an increased rate of hospitalization due to cardiovascular diseases in patients younger than 65 years (Fleckenstein et al., 2014). Specifically, females had a high prevalence of hospitalization for hypertensive crisis, while many males had been hospitalized for myocardial infarction. Consequently, there was significant decrease in the proportion of males after the age of 65 in the DTGA group, perhaps suggesting a higher mortality. On the other hand, no association with cardiovascular risk factors was found in the "EMAP Case-Control National Clinical Trial" (Douillard et al., 2016). However, 70 out of the 115 EMAP patients in this cohort were females, and the overall mean age was 63.1 years, which is nearly identical to the average age of 64.6 years of the FAM-study. Notably, the FAM-study found no differences in the prevalence of cardiovascular risk factors between DTGA and non-DTGA when considering the entire patient cohort, while no sub-analyses were conducted in the EMAP case-control study on patients younger than 65 years. It is possible that such a subdivision might have revealed a link with cardiovascular disorders within this cohort as well, potentially exacerbating the disparity in the male-to-female ratio, similar to the switch observed in the FAM-study. In keeping with this theory, smaller and younger cohorts may not show a female predominance (Antropoli et al., 2023; Bianco et al., 2023). In conclusion, to date there is insufficient evidence suggesting that DTGA patients have a higher cardiovascular risk compared to those with EMAP.

7.1.3. Age of onset

Similar to the previously discussed 65-year-old cut-off (Fleckenstein et al., 2014), the frequently cited 55-year-old threshold used for EMAP study was also arbitrary (Hamel et al., 2009). In the original series by Hamel et al., patients were retrospectively identified at a reference center for genetic sensory diseases, potentially introducing a selection bias. Even though the age of onset reported in this paper ranged from 41 to 54 years (Hamel et al., 2009), there is insufficient evidence to assert that all EMAP cases must manifest before the age of 55. Conversely, patients in the FAM-study were required to be older than 50 years at the time of inclusion (Fleckenstein et al., 2014). Nonetheless, the onset of visual symptoms ranged from 46 to 83 years. Early in this review, we chose age at first presentation as the least biased method of assessing the age range in which the disease is most common and noticed a considerable proportion of patients being 56–69 years old, but already showing extensive MA. Furthermore, the time taken from the MA to involve the fovea or to expand beyond the central 30° and 55° field of view is not influenced by age at presentation, indicating that cases with earlier or later onset are in fact part of the same disease spectrum (Antropoli et al., 2024). Indeed, evidence for the existence of "late-onset" EMAP cases - compared with the original description - has been presented throughout this review (Figs. 7, 8 and 16, and 25). Taking the case from Fig. 24 as an example, we showed a 68-year-old patient with MA confined within the vascular arcades but severely altered ERG. After 5 years of follow-up, MA rapidly expanded beyond the posterior pole, gaining a more typical EMAP configuration. Based on these findings, we can assert that a functional onset before the age of 55 should be considered a suggestive but not necessary feature for the diagnosis of EMAP. The absence of studies exploring the retinal periphery or investigating the electrophysiological findings in DTGA, coupled with the identical MA features, suggests that many cases of DTGA may actually be EMAP.

7.1.4. Macular neovascularization

MNV is a possible albeit uncommon complication of EMAP (Battaglia Parodi and Querques, 2015; Bianco et al., 2023; Kamami-Levy et al., 2014; Romano et al., 2023c). Despite the absence of MNV cases in the series by Hamel et al., no specific data regarding MNV occurrence were reported in the larger case-control study (Douillard et al., 2016, 2018; Hamel et al., 2009). The first study on neovascular complications in EMAP was conducted by Kamami-Levy et al. (2014), who reported a prevalence of ~10% of the eyes. As detailed in section 4.6.1, the incidence of MNV was recently assessed in the Italian EMAP cohort (Trinco et al., under review). An MNV developed in 8.9% (14/158) of eyes, with an estimated cumulative incidence of 6.1% at one year and 15.2% at 4 years. After excluding left-censored data, the median incidence rate was estimated to be 2.3 events per 100 person-years. Neovascular complications were instead present in 14.9% of the eyes at the last recorded visit in the French Quinze-Vingts cohort (Antropoli et al., 2024). In summary, MNV occurs in approximately 9–15% of EMAP patients, that is lower but not drastically different from the 25–33% reported for DTGA (Fleckenstein et al., 2011, 2014). Hence, we discourage discarding the diagnosis of EMAP based on the uncommon, yet possible, occurrence of MNV.

7.1.5. Genetic characterization

The genetic background of both EMAP and DTGA has been investigated, either by searching for single nucleotide polymorphisms (SNPs) associated with AMD, or pathogenic variants in genes already linked with IRDs (Douillard et al., 2018; Fleckenstein et al., 2016). In two independent studies, the prevalence of variants considered as risk factors for AMD was compared between EMAP and healthy subjects, and between DTGA, non-DTGA patients and healthy subjects (Douillard et al., 2018; Fleckenstein et al., 2016). It was found that the *ARMS2*_rs10490924 variant was more prevalent in DTGA patients compared to healthy controls, but there was no significant difference when compared to non-DTGA patients (Fleckenstein et al., 2016). In contrast, the frequency of the same *ARMS2*_rs10490924 variant in EMAP patients was similar to the one observed in controls (Douillard et al., 2018). However, the reference databases used for these analyses varied in their sample sizes: the DTGA comparison included data from 267 European subjects from the 1000G database (http://www.1000genomes.org), while the EMAP comparison drew on data from over 33,000 individuals from the ExAC database (now available at https://gnomad.broadinstitute.org/), therefore making a direct comparison between the results challenging. On the other hand, the C3_rs2230199 variant was found to be more prevalent in EMAP patients than in controls (Douillard et al., 2018). A similar trend was observed in DTGA, but when compared to the other non-DTGA patterns, no statistically significant difference was observed (Fleckenstein et al., 2016). However, since the serum levels of C3 were found to be elevated in EMAP, the possibility that chronic systemic inflammation plays a pivotal role in the etiopathogenesis of this disease deserves further investigation (Douillard et al., 2016). In conclusion, the C3_rs2230199 risk allele seems to be equally prevalent in EMAP, DTGA, and other GA subtypes, while no definitive conclusions can be drawn for *ARMS2*_ rs10490924. Conversely, the *CFH*_rs1061170 and *CFH*_rs800292 variants seem to be more represented in non-DTGA than EMAP and DTGA (Douillard et al., 2018; Fleckenstein et al., 2016).

Concerned by the similarities between EMAP and IRDs including SFD and L-ORD (Boon et al., 2009), in the EMAP Case-Control National Clinical Trial a total of 65 patients underwent whole exome sequencing (WES). However, no pathogenic variant in genes already associated with IRDs was identified (Douillard et al., 2018). Similarly, screening for *C1QTNF5* and *TIMP3* through direct Sanger sequencing did not reveal any rare variant among 58 EMAP patients from the French Quinze-Vingts cohort (Antropoli et al., 2024). On the contrary, in DTGA patients the *C1QTNF5* gene associated with L-ORD was specifically sequenced (Fleckenstein et al., 2016). Interestingly, one patient was found to be affected with L-ORD, confirming the similarities between these conditions (see section 8.2).

7.1.6. Summary and conclusions

In summary, we describe EMAP as a disease spectrum, while DTGA initially referred to a junctional SW-AF pattern showing a "grayish" signal within the atrophic lesion, multilobular borders and diffusely hyperAF background. The frequent confusion between the two arises from the later clinical characterization of patients displaying features such as younger age, fast progression, RPE-BM separation and prevalence of pseudodrusen. This has led to a recognized spectrum overlap between DTGAs presumably linked to AMD and conditions such as L-ORD, SFD, and EMAP. A review of all published DTGA images in the literature reveals numerous examples of these remarkable similarities (Douillard et al., 2016; Fleckenstein et al., 2011; Holz et al., 2007). Consequently, while molecular testing can straightforwardly rule out L-ORD and SFD, establishing diagnostic criteria for EMAP is a crucial step for accurate differential diagnosis based on clinical features, as discussed in Section 8.2.

7.2. Reticular pseudodrusen

Since RPD were first described in AMD (Mimoun et al., 1990) and later characterized as SDDs using OCT (Zweifel et al., 2010), a large body of literature has emerged on this topic and has been recently reviewed by others (Wu et al., 2022). Notably, RPD are found in approximately 30% of AMD patients, who tend to be older and exhibit larger drusen in terms of size and area compared to those without (Domalpally et al., 2019). Their presence is strongly associated with the *ARMS2*_rs10490924 risk allele (Ueda-Arakawa et al., 2013), while this polymorphism in EMAP is as frequent as in healthy controls (Douillard et al., 2018). Nonetheless, the hypothesis that RPD may constitute a distinct AMD phenotype with a different pathogenesis from that associated with soft drusen has been already proposed in the past (Smith et al., 2009; Spaide, 2018; Xu et al., 2013), without achieving a universal acceptance. Indeed, as per most classifications, classic drusen are necessary for the diagnosis of AMD (Ferris et al., 2013) while RPD alone are not sufficient, and are considered only an additional risk factor for the progression to GA (Huisingh et al., 2016).

For the scope of this review, we will focus on the relationship between RPD and impairment of rod function, which appears to be most evident similarity between EMAP and AMD. Indeed, multiple research groups have shown evidence of impaired dark adaptation in AMD, with the greatest severity observed in eyes with RPD (Flamendorf et al., 2015; Tan et al., 2019). Furthermore, RPD are more frequent in regions with higher rod density like the perifovea (Curcio et al., 2013), while regression of RPD is associated with the development of outer retinal atrophy (Spaide, 2013). Additionally, a recent investigation using qAF found that GA lesions with RPD as precursor lesion had a higher mean AF signal and a greater prevalence of RPE-BM separation when compared with GA preceded by soft drusen (Wei et al., 2023). Thus, the presence of RPD was posited to signal a distinct pathogenetic pathway involving exaggerated accumulation of BLamD (Wei et al., 2023). Pfau et al. conducted two clinical trials (NCT03478865, NCT03478878) to evaluate the impact of low-dose vitamin A supplementation on dark adaptation kinetics in AMD with and without RPD (Pfau et al., 2023). Surprisingly, only the latter group had significant improvement following supplementation, while the former group showed no benefit. The authors hypothesized that the presence of RPD may indicate a level of rod impairment beyond recovery, or that the lack of response could be due to impaired vitamin A delivery to the RPE (Pfau et al., 2023). In fact, IRDs characterized by alterations in the RPE-BM complex, such as PXE and SFD, exhibit both RPD and delayed dark adaptation, which can be improved with extremely high doses of vitamin A (*see* section 7). Thus, the possibility that a similar mechanism may be in play in AMD cannot be dismissed. Moreover, the presence of generalized rod (or even cone)

dysfunction was not ascertained, as further electrophysiological assessments were not pursued in this study. Indeed, the literature on this topic is relatively scant and, as a further layer of complexity, many studies fail to disclose the specific number of patients exhibiting *exclusively* RPD, which in turn could not be formally classified as AMD. Only a recent study employed ERG to investigate rod and cone function among eyes with different RPD burden (Kong et al., 2018). The authors found that eyes with localized RPD (confined to the central 50°) had a reduction of waveforms amplitude only in scotopic ERGs, while eyes with diffuse RPD (present in the majority of mid-peripheral sectors) had severely decreased responses under both scotopic and photopic conditions. Curiously, a previous publication from the same group (Lee et al., 2012) reported a 40% prevalence of GA in eyes with diffuse RPD compared to only 4% in those with localized ones.

In summary, RPD are considered a strong risk factor for the progression of AMD to GA and there is currently strong evidence to suggest that RPD in AMD flag a dysfunction of rod photoreceptors. Whether this dysfunction is reversible with extended dark adaptation or high-dose vitamin A supplementation remains to be elucidated. Similar findings can be observed in EMAP with a different degree of severity and underlying etiology, considering that the prevalence of RPD increases with age in patients affected by AMD (Buitendijk et al., 2016; Cleland et al., 2021). However, a common degenerative pathway may be already in place once RPD are detected, leading to the development of outer retinal atrophy and progression to MA in both AMD and EMAP.

8. Phenotypic overlap with inherited retinal diseases (IRDs)

We defined EMAP as a retinal disease featuring MA with distinct phenotypic features and both diffuse SDDs and pseudodrusen-like deposits, with variable age of onset and severity. However, numerous other IRDs can present with such clinical imaging characteristics, and thus EMAP remains a diagnosis of exclusion (i.e. after a negative genetic testing). Nonetheless, we aim to take advantage of these similarities to interpret the key findings of EMAP through the lens of IRDs featuring SDDs, since monogenic eye diseases represent a natural occurring model to study acquired conditions that share a similar pathogenesis. A similar approach has proven useful to investigate the relationship between acquired myopia and light exposure by studying the mechanisms occurring in a human genetic disease characterized by a transmission defect in bipolar cells (complete congenital stationary night blindness) with development of high myopia (Zeitz et al., 2023). As a matter of fact, EMAP is to this date an orphan disease with unknown etiopathogenesis, and such speculations may provide guidance for future research. Several genetically characterized monogenic IRDs feature diffuse SDDs and retinal atrophy. The formation of SDDs in these IRDs indicates a failure in the visual cycle of the RPE, either primary due to mutations in proteins expressed in the RPE [e.g. fundus albipunctatus (FA) and retinitis punctata albescens (RPA)] or secondary due to the accumulation of mutated proteins within the BM, leading to limited delivery of retinoids to the outer retina (e.g. L-ORD, SFD). Below, we will delve into the similarities, differences, and pathogenesis of SDDs in each of these IRDs, with the aim to translate this knowledge to EMAP.

8.1. *Fundus albipunctatus (RDH5) & retinitis punctata albescens (RLBP1)*

The perception of light by the retina depends on the interaction between photons and light-sensitive chromophores bound to opsins within photoreceptor outer segments. The major chromophore is 11-*cis*-retinal, which undergoes isomerization to all-*trans*-retinal upon light-absorption and then induces conformational changes in the opsin with subsequent initiation of the phototransduction cascade. The complex series of reactions and transport mechanisms to regenerate and deliver 11-*cis*-retinal to photoreceptors is collectively referred to as the "visual cycle". While only the reduction of all-*trans*-retinal to all-*trans*-retinol takes place in photoreceptors (Haeseleer et al., 1998), the RPE plays a pivotal role in regenerating and shuttling 11-*cis*-retinal back to photoreceptors. Indeed, after the first reduction reaction, all-*trans*-retinol is shuttled to the RPE. Once inside, all-*trans*-retinol is processed by lecithin retinol acyl transferase (LRAT) enzyme (Saari, 1982) and esterified to produce all-*trans*-retinyl esters (Saari and Bredberg, 1989). Dietary all-*trans*-retinol transported in the systemic circulation by the retina-specific carrier protein encoded by the *RBP4* gene is conveyed to the RPE at this stage of the visual cycle. The isomerohydrolase encoded by the *RPE65* gene then catalyzes the formation of 11-*cis*-retinol, which binds to retinaldehyde binding protein 1 (CRALBP) encoded by the *RLBP1* gene to facilitate its oxidation back into 11-*cis*-retinal by the dehydrogenase encoded by the *RDH5* gene. Furthermore, CRALBP performs additional functions in the visual cycle, including reduces product inhibition of the upstream *RPE65* isomerohydrolase and ensuring continuous production of 11-cis-retinol (Saari and Crabb, 2005; Stecher et al., 1999), as well as preventing the precocious re-isomerization of 11-*cis*-retinal in the presence of light (He et al., 2009; Parker et al., 2011; Saari and Bredberg, 1987; von Lintig et al., 2010). Pathogenic variants in the genes mentioned above result in loss-of-function of key proteins involved in the RPE visual cycle and thus cause autosomal recessive IRDs when present in homozygosity or compound heterozygosity. These are characterized by a variable age of onset, severity of the clinical manifestations, and prognosis. Still, these diseases share some common phenotypic features with EMAP, including a prevailing dysfunction of the rod system and the presence of SDDs (often referred to as "white dots" in the literature regarding these IRDs).

Failure to convert 11-*cis*-retinol to 11-*cis*-retinal due to biallelic *RDH5* variants is the pathophysiologic basis of FA. Similarly, a defective or absent function of the RLBP1 carrier implies a decreased regeneration of 11-*cis*-retinal, which is the cause of RPA, a form of rod-cone dystrophy that features white dots and lacks the "bone spicule" pigmentation typical of retinitis pigmentosa (Maw et al., 1997; Morimura et al., 1999). RPA phenotypes were identified in association with highly prevalent *RLBP1* variants in geographic isolates such as the Gulf of Bothnia in Northern Sweden (Burstedt et al., 1999) and the Newfoundland island in Canada (Eichers et al., 2002). In FA, the delayed regeneration of bleached photoreceptor visual pigments manifests with abolished or severely reduced DA rod responses on ERG after the standard dark-adaptation protocol. However, a substantial recovery can be seen after prolonged dark adaptation (3–4 h). Similarly, in patients affected by RPA rod responses on ERG are characteristically undetectable and some degree of amplitude recovery is possible only after extremely long (8 h and beyond) dark-adaptation protocols in early disease stages before irreversible photoreceptor degeneration occurs. Still, hypomorphic *RLBP1* variants may cause a mild phenotype that is more similar to FA than to RPA (Bianco et al., 2024). Anyhow, SDDs are present in almost all cases of FA/*RDH5*-associated retinopathy, and using multimodal imaging these lesions can be seen as white dots starting in the perifoveal region and diffusing toward the retinal mid-periphery. The foveal and parafoveal region are usually spared from such lesions (Fig. 26). Confocal NIR allows to highlight a target appearance of these lesions, with a highly reflective core surrounded by a hyporeflective halo (Newman et al., 2022). On OCT, these appear as discrete conical or nodular SDDs often breaching the ellipsoid zone. Furthermore, SW-AF imaging reveals low background fluorescence in FA, in keeping with the long-standing slowdown of the visual cycle and consequent reduced accumulation of lipofuscin, with foci of weakly increased signal associated with only some of the white dots (Sergouniotis et al., 2011). Similarly, such SDDs dots are also present in RPA/*RLBP1*-associated retinopathy (Fig. 27), but since chorioretinal atrophy ensues early in the disease course these lesions are seen in only 50% of eyes (Bianco et al., 2024). This is confirmed by the fact that the phenotype associated with hypomorphic *RLBP1* is characterized by an extensive and interlacing network of SDDs outside the posterior pole without any atrophic region even in patients in their 6th decade (Bianco et al., 2024) (Fig. 27).

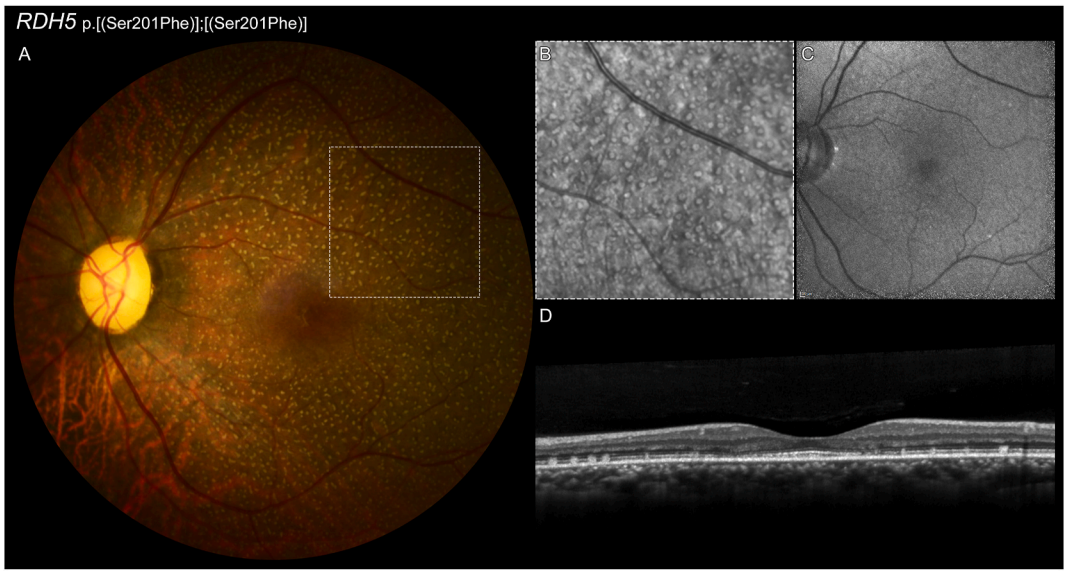

Fig. 26. *Multimodal retinal imaging in RDH5-associated retinopathy.* (A) Color fundus photography. (B) Infrared reflectance. (C) Short-wavelength fundus autofluorescence. (D) Optical Coherence Tomography scan passing vertically through the macula.

Interestingly, pathogenic variants in *LRAT* and *RPE65* result in more severe phenotypes of Leber congenital amaurosis or early-onset retinal degeneration with congenital night blindness and abolished rod responses. A markedly reduced SW-AF signal is a signature of IRDs caused by those genotypes, indicating an almost complete depletion of lipofuscin in the RPE. However, variants in these genes may occasional result in milder phenotypes with abundant SDDs and resembling FA or RPA (Littink et al., 2012; Schatz et al., 2011; Yang et al., 2017) (Fig. 28). Furthermore, biallelic *RBP4* variants that impair vitamin A delivery to the RPE result in a similar phenotype (Smirnov et al., 2022).

Thus, the consequence of a slowdown or blockage of the RPE's visual cycle as a result of mutations in its key proteins results in a rod system dysfunction associated with the formation of SDDs. These two features are common to EMAP, providing evidence for an involvement of the RPE in the pathogenesis of this retinopathy. On the other hand, EMAP shows a distinct RPE-BM separation, which is generally not seen in IRDs due to mutation in visual cycle genes. Furthermore, these show a diminished SW-AF signal because of a decrease lipofuscin burden in the RPE, which is not seen in EMAP. Indeed, a visual cycle slowdown can be primary or secondary to the accumulation of aberrant compounds above or within the BM, limiting the diffusion of vitamin A to the RPE.

8.2. Diseases of the Bruch's membrane

The BM is a pentalaminar, extracellular matrix located between the RPE and choriocapillaris layer of the choroid that plays a key role in retinal homeostasis (Booij et al., 2010). Beyond its role as physical barrier between the retina and choroid, the BM functions as a specialized vessel wall (i.e., a subendothelial space) with transport functions, and is a substrate for RPE attachment as well (Booij et al., 2010). At its core, the BM consists of an elastic layer encased by two collagenous layers, which are in turn separated from the RPE and choriocapillaris from their homonymous basement membranes (Hogan, 1961). In AMD, the pathological processes that culminate with drusen formation are preceded by the accumulation of subclinical deposits in the macular region, where the elastic lamina of the BM is thinner and prone to disease (Chong et al., 2005). These deposits can be classified based on their location relative to the basement membrane of the RPE. Basal linear deposits (BLinD) are found below the RPE basement membrane, while BLamD are located above it (Khan et al., 2016). Thus, the former are found within the BM itself, culminating with the formation of drusen in AMD (Chen et al., 2021), while the latter are external. Alternatively, drusenoid material may also accumulate in the subretinal space (SDDs), corresponding to RPD (Zweifel et al., 2010). Unlike BLinD, which concentrate in the subfoveal region where cone density is highest, SDDs are predominantly located superior to the fovea in AMD, closely following the distribution of rods (Curcio et al., 2013). For a detailed description of the BM, its structure and function, as well as modifications with aging and role in drusen and pseudodrusen formation, we refer the readers to previous reviews that discussed these topics thoroughly (Booij et al., 2010; Chen et al., 2020, 2021; Khan et al., 2016; Sura et al., 2020; Wu et al., 2022).

In this section, we will explore monogenic diseases of the BM, which can feature a variable combination of sub-RPE deposits and SDDs. Specifically, we will discuss L-ORD, SFD and PXE, three potential differential diagnoses of EMAP that need to be excluded through genetic testing. We will briefly touch upon their pathogenesis and subsequently shift our focus to examining the shared clinical and imaging characteristics they may exhibit with EMAP.

8.2.1. Sorsby fundus dystrophy (SFD)

Initially described in 1949 (Sorsby and Mason, 1949), SFD is an autosomal dominant IRD caused by pathogenic variants in the *TIMP3* gene (Weber et al., 1994). It typically manifests between the 4th and 6th decades with delayed dark adaptation or visual loss due to MNV formation, progressing to fibrovascular scarring at the posterior pole and widespread chorioretinal atrophy (Gliem et al., 2015c). The *TIMP3* gene encodes for an homonymous protein, mainly expressed by the RPE, which acts as an inhibitor of matrix metalloproteinases (MMPs) (Christensen et al., 2017) and serves other functions, including angiogenesis inhibition (Qi et al., 2003). With the exception of mutations that alter the signal peptide sequence (Guan et al., 2022), leading to a peculiar macular dystrophy, virtually all TIMP3 mutations result in dimerization or multimerization of the protein through disulfide bonds. This, in turn, significantly impairs its ability to inhibit the proangiogenic growth factor receptor VEGFR2 (Alsaffar et al., 2023; Christensen et al., 2017), with important clinical consequences discussed later. Despite the physiological presence of TIMP3 in the BM, its dimers and multimers exhibit increased resistance to turnover, which leads to their accumulation and subsequent formation of drusen-like deposits (Langton et al., 2005). Although the composition of sub-RPE deposits in EMAP remains unknown, histological studies on SFD provide some insights, allowing us to compare these findings with *in vivo* observations obtained through

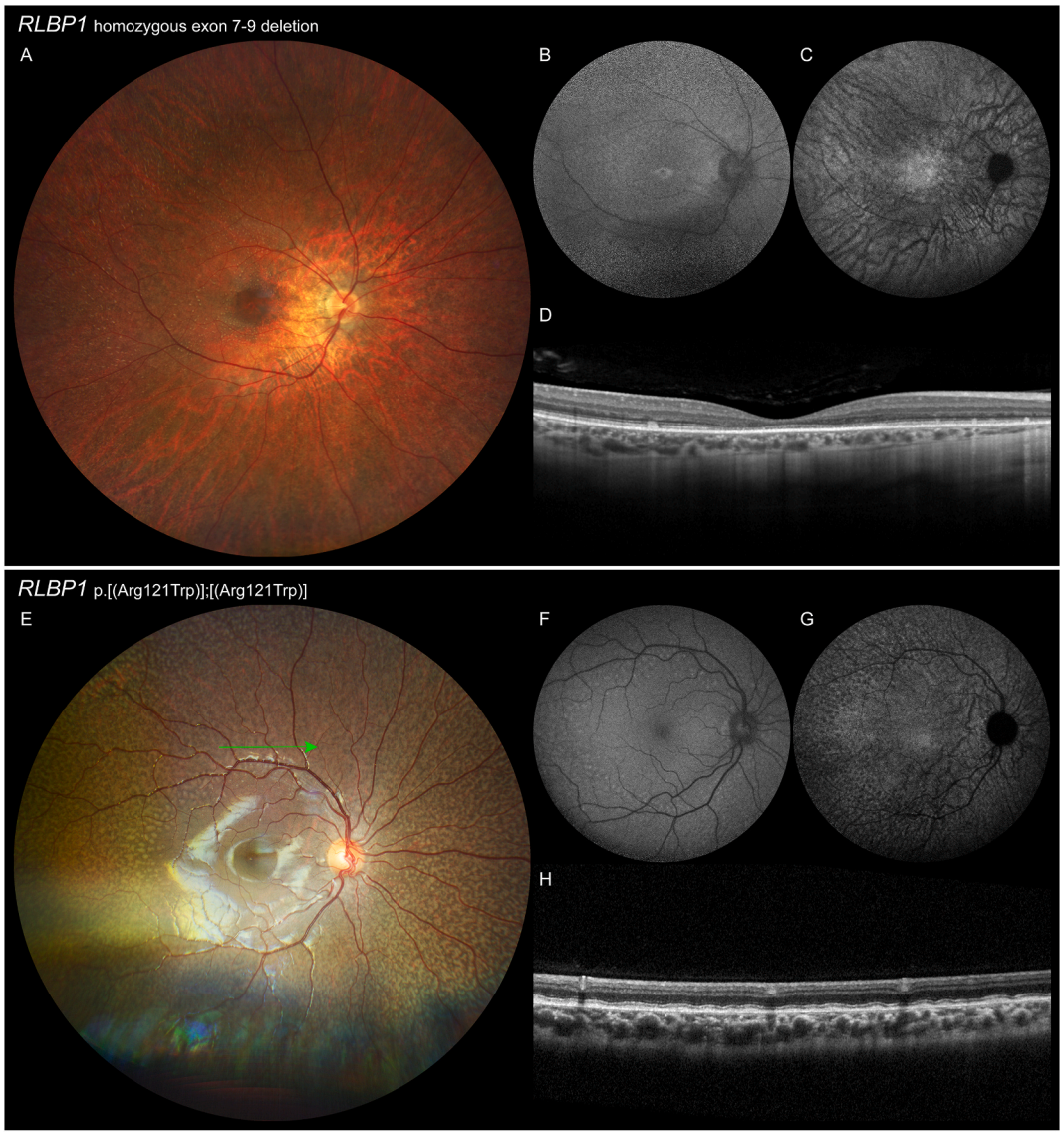

Fig. 27. *Multimodal retinal imaging in RLBP1-associated retinopathy*. (Upper panel) A 37-years-old male patient carrying the 7.36-kb deletion encompassing the exons 7 to 9 in homozygosity. The full-field electroretinogram showed undetectable waveforms under all adaptation and stimulus conditions, indicating a severe form of photoreceptor degeneration. (A) The widefield color retinography demonstrates mid-peripheral and peripheral chorio-retinal atrophy, with a relative preservation of the macula. No intraretinal "bony spiculae" pigmentation is seen. Some white dots/pseudodrusen are still visible in the parafovea and in the temporal-midperiphery. (B) Short-wavelength fundus autofluorescence shows the characteristic overall decreased signal. (C) Near-infrared fundus autofluorescence is characterized by a reduced signal with increased visibility of choroidal vessels, but with normal foveal hyperautofluorescence. (D) Optical Coherence Tomography scan passing horizontally through the macula demonstrates attenuation of the ellipsoid zone in the parafovea and confirms that the white dots/pseudodrusen correspond to subretinal drusenoid deposits.

OCT. The first histological study on eyes from subjects with a well-documented autosomal dominant pedigree was published by Capon et al., in 1989, featuring both light and electron microscopy (Capon et al., 1989). With light microscopy, there was a striking deposition of eosinophilic material, up to 30 μm in thickness, between the BM and the RPE. The same deposits were also observed in areas devoid of RPE, although their identification was less immediate. Electron microscopy enabled a more accurate localization of the deposits, which were situated between the RPE cell body and its basement membrane (i.e., the same location of BLamD). Occasionally, glial cells that infiltrated the deposits extended towards the scleral side of the BM, invading the inner collagenous layer to lie upon an irregular elastic lamina. Positive immunostaining of the deposits for mutated TIMP3 was subsequently demonstrated (Chong et al., 2000). Interestingly, TIMP3 not only colocalized with the sub-RPE deposits, but also with elastin, in the context of a disorganized and frequently broken BM elastic layer. In summary, in SFD, most deposits - consisting of mutated TIMP3 protein with impaired antiangiogenic activity - are secreted by the RPE and accumulate between the BM and the RPE, in the same location of BLamD. Some deposits also infiltrate the BM, leading to thickening and breaks of the elastic lamina, which result in secondary damage to the BM.

8.2.1.1. Clinical and imaging findings. The visualization of the sub-RPE deposits is possible *in vivo* with modern OCTs, that, when high-resolution technology is available, are also capable of distinguishing several components based on their reflectivity (Romano et al., 2023b). Several authors investigated the alterations of the RPE-BM complex in SFD, with the aim of visualizing and/or quantifying the thickening of the BM (Iyer et al., 2022; Khan et al., 2020). This is only possible in pathological conditions where the physical separation between the BM and the RPE becomes sufficiently wide that it can be detected with the axial

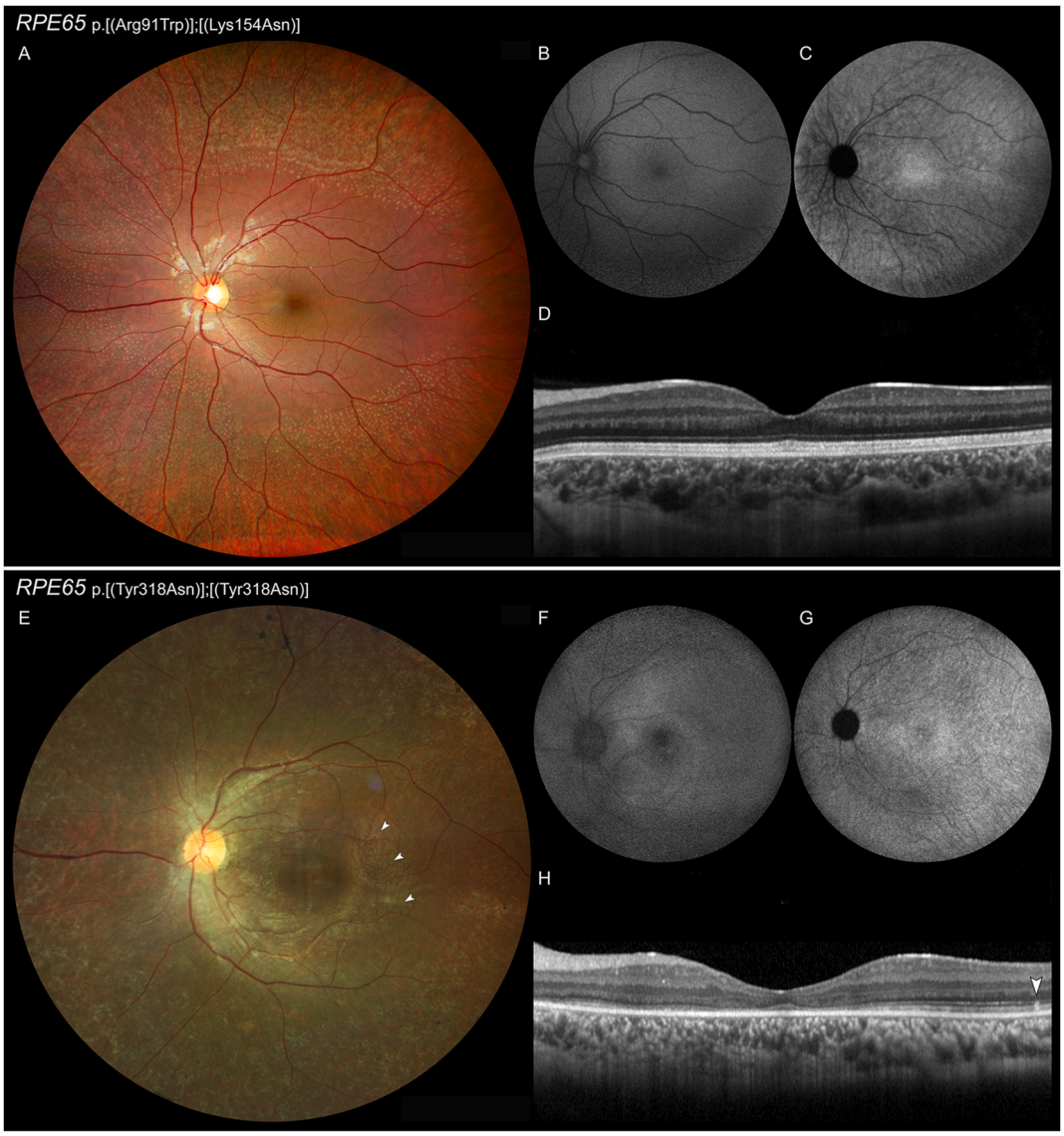

Fig. 28. *Multimodal retinal imaging in milder phenotypes of RPE65-associated retinopathy associated with missense variants*. (Upper panel) A 6-years-old female patient carrying the c.271C > T p.(Arg91Trp) & c.462G > C p.(Lys154Asn) in compound heterozygosity. The patient had night blindness from birth, and the corresponding full-field electroretinogram traces showed absence of any response from the rod system but normal light-adapted cone responses. (A) The widefield color retinography demonstrates that, anteriorly to the posterior pole, the fundus is strewed with yellowish subretinal dots and flecks. (B) Short-wavelength fundus autofluorescence shows the characteristic overall decreased signal, without any recognizable focal lesion. (C) Near-infrared fundus autofluorescence is characterized by a reduced signal with increased visibility of choroidal vessels. (D) Optical Coherence Tomography scan passing horizontally through the macula confirms a normal configuration of outer retinal bands in the macula. (Lower panel) A 27-years-old male patient carrying the c.982 T > A p.(Tyr318Asn) in homozygosity. The corresponding full-field electroretinogram traces showed undetectable waveforms under all adaptation and stimulus conditions, indicating a severe form of photoreceptor degeneration. (E) The widefield color retinography demonstrates several depigmented lesions outside the posterior pole arranged in a mottled or reticular pattern. Scant intraretinal pigment migration is seen. (F) Short-wavelength fundus autofluorescence shows the characteristic overall decreased signal, without any recognizable focal lesion. (G) Near-infrared fundus autofluorescence is characterized by a reduced signal with increased visibility of choroidal vessels. (G) Optical Coherence Tomography scan passing horizontally through the macula demonstrates attenuation of the ellipsoid zone, which is more prominent in the parafovea (as already observed in *RDH5* and *RLBP1*-retinopathies), and confirms that the white dots/pseudodrusen temporally to the macula correspond to subretinal drusenoid deposits.

resolution of currently available OCTs. Nonetheless, achieving precise segmentation of the BM is practically difficult, necessitating surrogate measurements to estimate its thickness. For this purpose, Khan et al. quantified the RPE-BM separation as a proxy for the BM thickness (Khan et al., 2020). The authors demonstrated that one of the early manifestations of SFD is a flat, continuous, and macula-wide RPE-BM separation, similar to that seen in EMAP. It is hypothesized that such deposits are able to cause a local deficit of vitamin A, interfering with its normal transport from the blood circulation. In keeping with that, when present, night blindness is usually referred as the earliest symptom in SFD, and it is unresponsive to vitamin A supplementation, unless extremely high doses are administered (Gliem et al., 2015b; Jacobson et al., 1995). As already discussed earlier in this review, vitamin A deficiency, delayed dark adaptation and SDDs are closely linked to each other. Indeed, another shared feature is the early occurrence of SDDs, which in SFD are the most common drusenoid lesion in the 6th decade, with a frequency of ~70% (Gliem et al., 2015b). They usually precede the onset of severe vision-threatening complications, such as MNV and macular atrophy. Their distribution mirrors that observed in other diseases: they are generally absent in the foveal region, more commonly found in the

superior quadrant of the macula, and can also be located nasal to the optic disc. Both the "dot" and "ribbon" types, as well as "peripheral pseudodrusen" can be seen. This latter type appears to differ from the pseudodrusen-like deposits typical of EMAP, despite sharing the yellowish appearance, confluence and faint hyperAF (Battaglia Parodi et al., 2023; Gliem et al., 2015b). In reference to RPD, "peripheral pseudodrusen" are smaller and tend to cluster along the vascular arcades and nasally to the optic disc, whereas the pseudodrusen-like deposits in EMAP are larger in size and spread more extensively towards the periphery (Gliem et al., 2015b; Hamel et al., 2009; Sivaprasad et al., 2008). Due to lack of familial history, the age of onset of the SDDs in EMAP is currently unknown. Conversely, they can be detected very early in SFD, up to the beginning of the 4th decade (Iyer et al., 2022). Interestingly, late-phase ICGA (30–40 min) can detect multilobulated areas of hypofluorescence even in the absence of obvious funduscopic changes (Gliem et al., 2015c). The extent of hypofluorescence has been observed to progressively expand with increasing disease severity, from mere drusen-like deposits to eventual atrophy. This reduced fluorescence might result either from decreased permeability of the BM, or a defective uptake from functionally damaged RPE cells (Gaudric, 2023; Gliem et al., 2015c). Notably, the shape and distribution of the angiographic changes in patients without fundus abnormalities resembles those of the atrophic lesions in EMAP, that in turn does not exhibit obvious hypofluorescent phenomena beyond the MA (*see* section 4.6). Even though most cases of SFD experience severe visual loss due to the development of MNV with an aggressive course, in the remaining cases the clinical picture is dominated by the development of MA (Sivaprasad et al., 2008) (Fig. 29). Interestingly, in these cases the atrophy exhibits many similarities with EMAP: it can have a MDAF appearance, it can extend beyond the vascular arcades, up to the midperiphery, its margins are multilobulated, and its progression rate is remarkably fast, even though scant quantitative data are available (Gliem et al., 2015c). On the other hand, although a clear differential diagnosis is not always possible with just multimodal imaging, there are some differences that may raise suspicion for SFD rather than EMAP: atrophy distribution deviates from known patterns (Romano et al., 2023c); its margins are still multilobular but with bigger and fewer lobules (Gliem et al., 2015c); in very advanced cases with midperipheral atrophy, the condition is either accompanied by neovascular fibrosis or lacks the typical centripetal progression from the retinal periphery, as commonly observed in EMAP (Battaglia Parodi et al., 2023; Gliem et al., 2015c).

8.2.2. *Late-onset retinal degeneration (L-ORD)*

L-ORD is another autosomal dominant IRD often presenting with nyctalopia in early adulthood (Lando and Borooah, 2022), and numerous RPD located temporally to the macula between the 4th and 6th decades (Borooah et al., 2021). These lesions are precursors of retinal atrophy, which typically involves the fovea when patients reach their sixties. Patients also show a characteristic finding of long anterior zonular insertion and peripupillary iris atrophy (Ayyagari et al., 2005; Subrayan et al., 2005). L-ORD is caused by pathogenic variants in the *C1QTNF5* gene, encoding the C1q and Tumor Necrosis Factor protein 5 (CTRP5), which is expressed by the RPE and ciliary body (Mandal et al., 2006). CTRP5 can self-assemble into multimeric structures, forming hexagonal lattices associated with the RPE lateral membranes, and is apically secreted by the RPE in the interphotoreceptor matrix as well. The CTRP5 has been implicated in regulating fatty acid metabolism and cellular energy homeostasis (Miyagishima et al., 2021), as well as serving as both a substrate and activator for the HTRA1 serine-protease (Chekuri et al., 2019). The first causative variant identified for L-ORD was the founder mutation p.Ser163Arg (Hayward et al., 2003), which remains the most prevalent and extensively studied mutation. Additional variants within the C1q globular domain have been implicated in the disease (Lando and Borooah, 2022), with some, such as the p.(Gln180Glu), leading to atypical retinal phenotypes (Kellner et al., 2021). For the purpose of this review, the following discussion will be focused on the p.Ser163Arg mutation, given the wealth of detailed phenotyping and preclinical research available.

8.2.2.1. Histopathology. The main histological finding in L-ORD is the presence of widespread sub-RPE deposits (Kuntz et al., 1996). Their thickness is directly related to photoreceptor loss, and increases from the

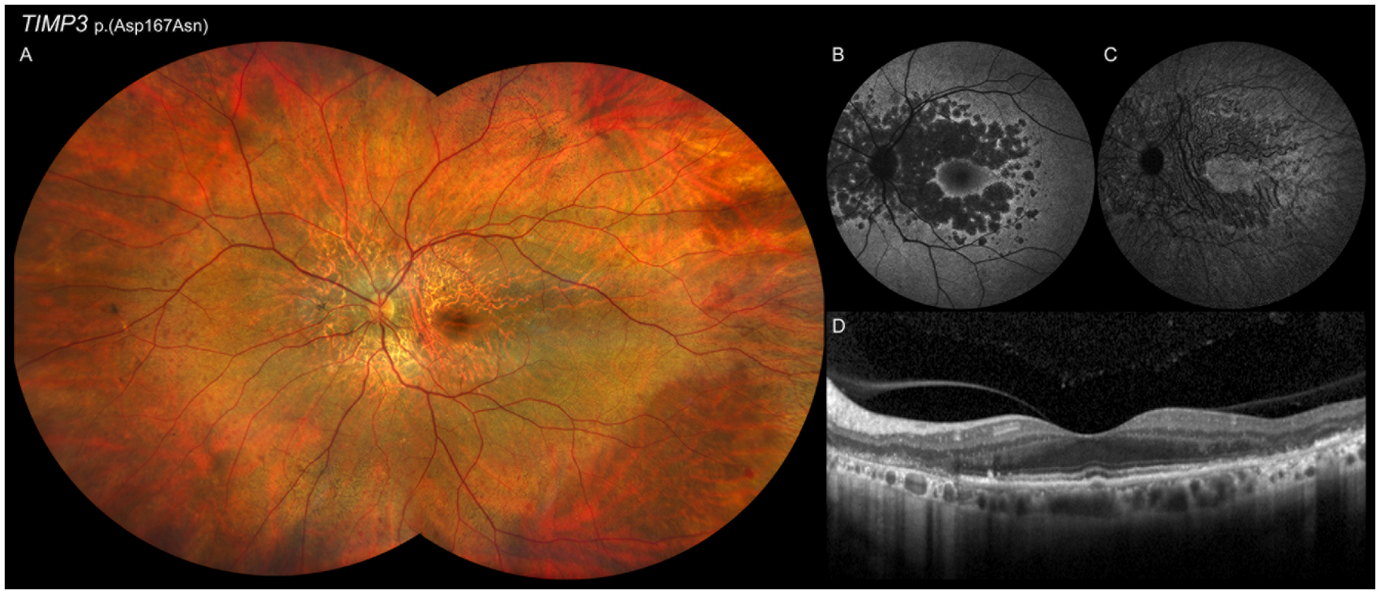

Fig. 29. *Multimodal retinal imaging in Sorsby Fundus Dystrophy (SFD).* (A) Widefield color retinography of a 56-year-old patient carrying the heterozygous c.499G > A p.(Asp167Asn) *TIMP3* variant. An oval area of retinal pigment epithelium (RPE) atrophy centered on the optic nerve head that spares the fovea. A yellowish hue covers the entire posterior pole and mid-periphery, where numerous "classical" and "peripheral" pseudodrusen and scattered drusen are evident. (B) Short-wavelength autofluorescence reveals a well-demarcated, horizontal, multilobular area of hypoautofluorescence. (C) The same area with less defined contours is detected on near-infrared autofluorescence, alongside with abnormally enhanced visibility of the choroidal vessels at the posterior pole. (D) Optical coherence tomography displays a single subfoveal drusen and some SDDs overlying a subtle but continuous separation between the Bruch's membrane (BM) and the intact RPE. Outside the foveal sparing, hyperreflective "debris" lying over the bare BM can be seen.

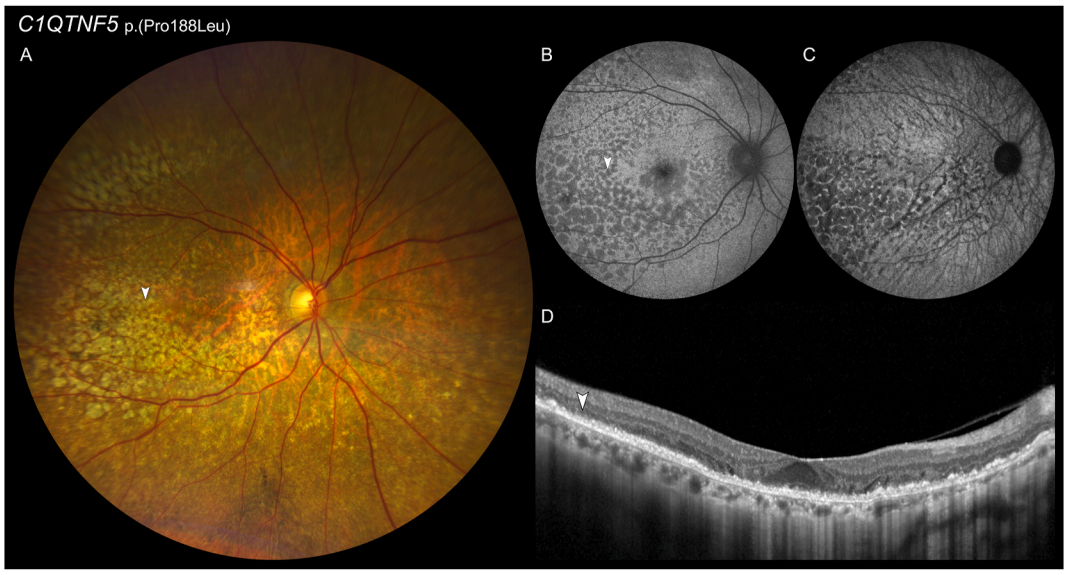

Fig. 30. *Multimodal retinal imaging in Late-Onset Retinal Degeneration (L-ORD).* (A) Widefield color retinography of a 63-year-old patient carrying the heterozygous c.562C > A p.(Pro188Thr) *C1QTNF5* variant. Multilobulated atrophy is evident against a background of diffuse pseudodrusen. Unlike EMAP, the temporal paramacular region is the initial site of involvement, and atrophy extends through distinct foci. (B) The temporal-to-nasal progression of the atrophy characteristic of L-ORD is easily identified on short-wavelength autofluorescence. (C) Due to diffuse hypopigmentation, the atrophy area shows diminished contrast on near-infrared autofluorescence. (D) Optical coherence tomography shows widespread hyperreflective sub-RPE deposits. Diffuse hypertransmission defects flag imminent RPE atrophy.

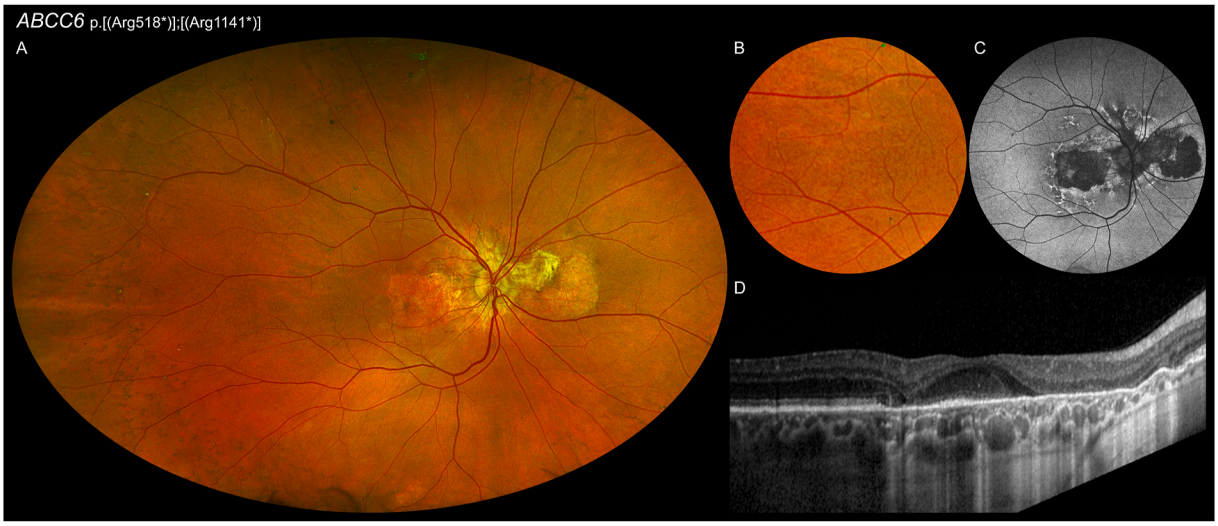

Fig. 31. *Multimodal retinal imaging in Pseudoxanthoma Elasticum (PXE).* (A) Ultra-widefield pseudocolor retinography of a 58-years-old patient carrying the c.1552C > T p.(Arg518*) and the c.3421C > T p.(Arg1141*) variants in compound heterozygosity. The hallmark findings of PXE can be seen: angioid streaks are reddish, jagged lines radiating from the optic disc; in the mid-periphery, *peau d'orange* returns a mottled, whiteish appearance; punctate, small, whiteish "comet" lesions are found in the far periphery of the retina. (B) Close-up of *peau d'orange*. (C) Short-wavelength autofluorescence demonstrates a hypoautofluorescent area of macular atrophy surrounded by typical pattern dystrophy-like alterations. Nasal to the optic disc, a second area of atrophy is detected. (D) Optical coherence tomography: on the nasal side, Bruch's membrane undulation marks the borders of an angioid streak.

macula towards the peripheral retina (Milam et al., 2000). Based on several studies, their composition is likely a combination of lipids, such as esterified and unesterified cholesterol, most likely derived from the RPE (Grubaugh et al., 2024), along with proteins including both wild-type and mutant CTRP5, as well as HTRA1 (Chekuri et al., 2019; Milam et al., 2000). Similarly, diverse mechanisms participate to the formation of these deposits and have been extensively studied both *in vitro* and in animal models. Specifically, due to the p.Ser163Arg mutation, the apically secreted CTRP5 protein is abnormally misrouted towards the basal side of the RPE, leading to the formation of sub-RPE deposits (Xu et al., 2023). Also, multimers of CTRP5 incorporating the mutant protein show reduced cleavage by HTRA1, resulting in their diminished turnover, and also a compromised functionality, including impacting lipid metabolism (Chekuri et al., 2019; Miyagishima et al., 2021).

8.2.2.2. Clinical and imaging findings. From a clinical perspective, L-ORD is extremely similar and somewhat "complementary" to EMAP, as the first involved region locates temporal to the macula, in correspondence of the region of relative sparing that is always noted in EMAP. Moreover, in L-ORD the MA progresses in a horizontal path from temporal to nasal (Cheloni et al., 2023), whereas in EMAP it primarily

follows a vertical trajectory. Nonetheless, from its early phases till the end-stage of the disease, L-ORD shares numerous clinical, imaging, and functional findings with EMAP (Fig. 30). The first ophthalmoscopically visible alterations are perimacular SDDs (Cukras et al., 2016). Before their formation, widespread sub-RPE deposits - undetectable through biomicroscopy - begin to accumulate (Li et al., 2023), corresponding on OCT with an interruption of the overlying EZ (Soumplis et al., 2013). Then, photoreceptor loss starts in the temporal paramacular region around 48 years old (Li et al., 2023). With ageing, SDDs become increasingly prevalent in L-ORD patients, reaching the peak occurrence of 62% in the 6th decade, similar to SFD (Borooah et al., 2021; Gliem et al., 2015b). By the age of 55, atrophic changes temporal to the macula become visible on SW-AF, usually preceded by an EZ disruption that also progresses in a temporal-to-nasal fashion. The same process is delayed in the fovea of about ten years, but progresses at a similar rate thereafter (Li et al., 2023). Once the atrophy begins, it progresses rapidly, estimated at a rate of roughly 0.53 mm/year. Consequently, most patients exhibit widespread retinal atrophy and severe visual impairment by the age of 75 (Cheloni et al., 2023). Like EMAP and SFD, HPS within areas of RPE atrophy may be detected with OCT (Soumplis et al., 2013). The funduscopic and imaging similarities that L-ORD shares with EMAP are also reflected in their functional impairment. L-ORD is characterized by delayed dark adaptation that can be reversed with administration of high doses of vitamin A (Jacobson et al., 2001), as well as exhibiting a greater rod than cone dysfunction on ERG (Soumplis et al., 2013). Moreover, in both conditions the presence of sub-RPE deposits, even before the occurrence of RPE atrophy, proved sufficient to cause a loss of macular sensitivity, as testified by mesopic microperimetry (Alex et al., 2023; Romano et al., 2023a, 2023b). Lastly, a common complication of L-ORD is the development of MNV. These may remain non-exudative, often not necessitating treatment, or can develop in the peripheral retina (Keenan et al., 2021). This behavior contrasts with EMAP, where type 2 MNV is the most frequent subtype and mainly involve the macular or occasionally the peripapillary area (Antropoli et al., 2024). Notably, MNV in L-ORD may resolve spontaneously (Ayyagari et al., 2000), a phenomenon never observed in EMAP. Future studies should investigate whether the instances of presumed “non-neovascular fibrosis” in EMAP result from a similar process.

In conclusion, L-ORD shares several characteristics with EMAP, most importantly a comparable age of onset, diffuse sub-RPE deposits and multilobular retinal atrophy. The key distinction lies in the preferential involvement of the temporal macula, a phenomenon that remains unexplained to date but could hold valuable clues for understanding EMAP. Interestingly, during fetal development, a bulge characterized by remarkable RPE cell density at its apex forms in this location (Streeten, 1969). Over time, this temporal bulge flattens, leaving a slight depression roughly 4 mm from the optic disc, while the RPE cells increase in size. This region is believed to play a pivotal role in macular development, and its abnormalities have been suggested as a potential cause for torpedo maculopathy, a congenital anomaly of the RPE (Shields et al., 2010). One could speculate that these specific RPE cells possess inherent properties that, contrary to L-ORD, make them “resistant” to the yet unidentified pathologic process responsible for EMAP. These considerations might be helpful to identify future research areas and underscore the urgent need for histological studies on EMAP.

8.2.3. *Pseudoxantoma elasticum (PXE)*

PXE is a multisystemic, autosomal recessive disorder, characterized by ectopic calcifications mainly affecting the skin, cardiovascular system, and ocular tissues (Gliem et al., 2013). This condition arises from mutations in the *ABCC6* gene (Bergen et al., 2000), which encodes a transmembrane transporter predominantly expressed in the liver and kidneys (Bisaccia et al., 2021). Its malfunction indirectly leads to a reduction of the circulating levels of inorganic pyrophosphate, which normally prevent ectopic mineralization in target tissues (Jansen et al., 2013).

The ocular phenotype of PXE results from the progressive calcification, in the form of calcium phosphate precipitation, of both the elastic and collagenous layers of the BM (Risseeuw et al., 2024), which starts at the posterior pole and gradually expands in a centrifugal manner (Charbel Issa et al., 2010). Ophthalmoscopically, a mottled, whiteish appearance of the retina characterized by an opaque fundus reflex, known as *peau d’orange*, demarcates the transition zone of BM calcification (Risseeuw et al., 2024). It is within this area that most of the PXE-related retinal changes are found, with the exception of the so-called “comet lesions”, including the most striking finding of angioid streaks (Charbel Issa et al., 2010) (Fig. 31). These have been demonstrated, both histologically and more recently *in vivo* with the aid of OCT, to correspond to pathological ruptures in the BM (Charbel Issa et al., 2009; Hagedoorn, 1975). Angioid streaks represent a predilected path for the ingrowth of fibrovascular tissue, consequently leading to MNV formation and subsequently fibrosis, which are the main causes of visual impairment in PXE (Risseeuw et al., 2019). While the complex retinal phenotype of PXE is often readily distinguishable from EMAP, in this section we will discuss various shared features between the two diseases that offer an interesting interpretative key for understanding EMAP.

As previously mentioned, PXE-related retinal alterations progress centrifugally over time, with the earliest funduscopic alteration being *peau d’orange*. Furthermore, as the disease advances, an area of reduced fluorescence becomes visible at the posterior pole in the late phase of ICGA, while lacking a visible counterpart on fundus examination (Charbel Issa et al., 2010). This likely signifies an area of homogeneous BM mineralization or significant damage to the RPE, resulting in reduced dye uptake. Consequently, two distinct transition zones emerge in PXE: the first, a central transition from reduced to normal fluorescence in ICGA, and the second, a peripheral transition zone best observed using NIR imaging, showing a shift from *peau d’orange* (hyperreflective on NIR) to a normal fundus (isoreflective on NIR). Intriguingly, the *peau d’orange* area has a static anterior border, demarcating a predetermined region for BM mineralization, while its posterior border advances anteriorly (Risseeuw et al., 2021). Consequently, the first transition zone expands centrifugally, whereas the second transition zone narrows over time, possessing a predetermined anterior border and a progressively advancing central border. It is within these two transition zones that an area of preserved fluorescence on ICGA can be observed temporal to the macula, in the very same location of the temporal sparing seen in EMAP. This might represent either a region with a less severely calcified BM or an area of relative RPE preservation. As of today, this phenomenon remains unexplained, although a possible link with the perfusion levels of this specific area has been hypothesized. In a recent work, Risseeuw et al. demonstrated that the mineralization of the BM occurs because of diffuse hydroxyapatite precipitation (Risseeuw et al., 2024). Beyond the posterior pole, this calcification is intermittent, and the hydroxyapatite deposits concentrate above the vascular lumen of the choriocapillaris. Consequently, the authors hypothesized a partial dependance on the choriocapillaris flow for the mineralization process, with the temporal sector of the macula owing its relative sparing to its physiologically inferior choriocapillaris perfusion (Borrelli et al., 2019). However, considering that the perfusion gap between the temporal and central macula is clinically negligible, it is unlikely that the temporal sparing results from perfusion issues in EMAP. Furthermore, in contrast to EMAP, where a preserved area of autofluorescence on SW-AF can be identified even in presence of widespread retinal atrophy, the temporal sparing observed with ICGA in PXE does not last as long (Risseeuw et al., 2021), suggesting that the different mechanisms may be responsible for this phenomenon. Similar to L-ORD, SFD, and EMAP, SDDs occur in roughly half of PXE patients, with their prevalence peaking between the ages of 40 and 50, and declining thereafter (Gliem et al., 2015a). Despite sharing a similar distribution pattern with these other conditions, SDDs exclusively manifest within the area of reduced ICGA fluorescence in PXE. In this

context, the calcification of the BM appears more homogeneous, potentially attributable to increased choriocapillaris fenestration and reduced intercapillary distances, revealing a closer link between reduced BM permeability and SDDs occurrence in PXE (Risseeuw et al., 2024). Expectedly, also these patients experience delayed dark adaptation that partially improves with high doses of vitamin A (Hess et al., 2020a). Vice versa, the mechanism leading to BM ruptures appears to be opposite between EMAP and PXE. Understanding these differences could prove valuable in our efforts to comprehend the etio-pathogenesis of EMAP. On fundus examination, angioid streaks generally appear as reddish, jagged, variably branched lines that radiate from the optic nerve (Gliem et al., 2013). Notably, the RPE overlying an angioid streak can remain normal, while subtle anatomical and functional changes can be detected with OCTA or microperimetry (Hess et al., 2020b; Loewinger et al., 2023), until the occurrence of MNV or MA. As the disease progresses, the choroid progressively thins (Gliem et al., 2014), and the development of pattern dystrophy-like changes may precede the onset of MA (Schoenberger and Agarwal, 2013). Although rare, the natural course of PXE in the absence of neovascular complications presents with a purely atrophic phenotype resembling AMD-related GA, occasionally surrounded by a diffuse hyperAF signal (Schoenberger and Agarwal, 2013). In such cases, the area of MA enlarges rapidly, and angioid streaks within its boundaries become less discernible while remaining detectable on OCT (Gliem et al., 2016a). In a similar fashion, in EMAP, BM openings always occur within the region of MA atrophy, often accompanied by severe choroidal thinning (Antropoli et al., 2024), making them rarely identifiable through fundus examination. In both EMAP and PXE, they remain identifiable with OCT and appear as hyperreflective on IR and hypoAF on SW-AF. With respect to PXE, in EMAP the shape of the BM ruptures is often extremely regular with either a vertical or horizontal orientation, although irregular and branching ruptures resembling angioid streaks can also be seen. For these scenarios, dye angiographies are useful in distinguishing "true" angioid streaks, which are hyperfluorescent in both FA and ICGA, from BM ruptures in EMAP, which hypofluorescent due to the severe choroidal thinning. While in PXE these breaks result from the mechanical stress produced during the ocular movements on the calcified BM (Gliem et al., 2013), the pathogenesis of such breaks in EMAP is unknown. Unlike PXE, where angioid streaks precede MA formation, in EMAP, the BM dehiscence follows this event. Building on prior observations discussed for L-ORD and SFD, sub-RPE deposits may infiltrate the BM also in EMAP. However, the diverse characteristics of BM ruptures in EMAP suggest the presence of additional mechanisms influencing the development and evolution of these defects.

8.3. *Understanding of EMAP through the lens of IRDs with impairment of the visual cycle*

In summary, all IRDs characterized by a dysregulation of the retinoid re-supply route to the RPE - be it primary due to gene variants or secondary to impaired vitamin A delivery through a calcified or infiltrated BM - have common clinical and pathologic features, including delayed dark adaptation, reduced rod function on ERG, and formation of SDDs. Furthermore, EMAP exhibits further phenotypic overlap with L-ORD and SFD in the absence of MNV, possibly attributable to the presence of sub-RPE deposits in all the three conditions. These deposits, appear as a continuous separation between the RPE and BM on OCT, and are found in the same location as BLamD in histological studies. However, to date, no histological studies have been conducted on EMAP, and the composition of both sub-RPE and pseudodrusen-like deposits in this disease remains unknown. For this reason, we recommend using OCT terms such as "sub-RPE deposits", or "RPE-BM separation" when describing this finding.

A more obscure finding is the consistent presence of a temporal sparing, evident both on fundus examination and multimodal imaging. A similar phenomenon can be unmasked in the late phase of ICGA in PXE, where a temporal island of preserved fluorescence appears within a hypofluorescent posterior pole. This ICGA sign is absent in SFD, which nonetheless exhibits a different pattern of hypofluorescence that mimics the multilobular shape of the atrophy in EMAP. Finally, the same region of temporal sparing in PXE and EMAP is, conversely, the first one affected in L-ORD. We must consider that, in PXE, BM mineralization appears sufficient to promote SDDs formation but not the development of sub-RPE deposits. In contrast, in L-ORD and SFD, it is the sub-RPE deposits themselves that are likely responsible for hindering the transport of retinoids from the choriocapillaris to the RPE and precede the formation of SDDs. In both cases, the mutant protein is secreted by the RPE. This secretion process is physiological for TIMP3, which, however, forms pathological aggregates in this context, and it results from misrouted secretion for CTRP5. In this sense, some specific characteristics of the temporal paramacular RPE make this region particularly susceptible to the effects of *C1QTNF5* variants and, at the same time, particularly resistant to BM calcification or its consequences. Table 1 recapitulates the main characteristics of EMAP and its differential diagnoses.

9. A novel retinopathy

9.1. *Key messages for the clinician*

As we hopefully have demonstrated in the previous chapters, EMAP is not an exceptional diagnosis at our centers in Italy and France. The under-recognition of this disease might have contributed to its portrayal as an extremely rare condition confined to Western Europe. Our observations, along with recent case series from other countries, suggest that numerous patients with currently undiagnosed EMAP may exist worldwide. In this review, we aimed to spread awareness and shed light on EMAP by comprehensively recapitulating the knowledge available to date in literature and providing original unpublished data to further characterize its clinical spectrum.

To avoid overlooking the diagnosis of EMAP, the detection of a bilateral MA with MDAF on SW-AF in the absence of drusen should always prompt further investigations. In such cases, it is inadequate to rely only on single fovea-centered OCT scans or standard macular volumes; clinicians must actively search for additional and wider-field signs indicative of EMAP. This begins with a detailed examination of the area surrounding the MA, with a particular emphasis on the superior and inferior margins, where a diffuse RPE-BM separation can be identified, and on the temporal margin, typically spared. Besides the macular findings, the presence of SDDs and pseudodrusen-like deposits surrounding the MA and extending to the mid-periphery is an essential feature. Moreover, the biomicroscopic evaluation of the fundus cannot be considered thorough without a careful inspection of the retinal periphery, particularly in the inferotemporal sector, to assess for pavingstone-like degeneration. However, its absence should not exclude the diagnosis, as the degree of peripheral and central involvement may vary unpredictably across different patients. In a similar manner, various other features may be suggestive of EMAP but are not necessary for establishing its diagnosis. For instance, symptoms like night blindness, due to their subjective nature, should be regarded as helpful indicators, though not consistently reported. Similarly, the age of onset is typically considered to fall within the 6th decade but encompass a wider range than initially thought. Consequently, a judicious interpretation of the area of MA in relation to the patient's age can aid the diagnostic process, particularly in cases with a late onset. Indeed, age thresholds rarely represent an effective way to establish a specific diagnosis, and the same applies to its risk factors, such as cardiovascular events, or complications, like MNV development. These elements, along with age, have been utilized in the past to distinguish between EMAP and DTGA, which is a SW-AF pattern that can accompany MA across a variety of diseases, but remains entangled with AMD. In cases where a differential diagnosis between EMAP and GA secondary to AMD is difficult because

Table 1
Differential diagnosis between EMAP, AMD, and monogenic Bruch's membrane disorders.

	EMAP	GA due to AMD	SFD	L-ORD	PXE
Onset	Between 45 and 60 years with photophobia, night blindness, scotoma, visual acuity loss	~80 years with central or paracentral scotoma and visual loss.	Between 30 and 60 years, with progressive night blindness or visual loss often due to MNV	Between 40 and 60 years, with nyctalopia	Ophthalmological signs are often incidental findings or identified after referral by another specialist diagnosing PXE. Between the 3rd and 6th decade, patients may experience visual loss, metamorphopsia, or photopsia due to MNV development, acute retinopathy resembling MEWDS, or macular atrophy development.
Family history and mode of inheritance	Usually none	Usually none	Autosomal dominant (*TIMP3*)	Autosomal dominant (*C1QTNF5*)	Autosomal recessive (*ABCC6*)
Features of macular atrophy	Multilobular, with major vertical orientation in manifest disease. Moderately decreased autofluorescence (MDAF) signal on SW-AF.	Dark hypoautofluorescent signal with large drusen often preceding cRORA formation.	Lobular, scalloped, and confluent chorioretinal atrophy extending from the macula to the peripheral retina, often accompanied by severe fibrovascular scarring due to MNV.	Multilobular, with onset temporal to the macula, followed by rapid horizontal expansion, leading to widespread retinal atrophy and severe visual impairment by age 75	Multifocal, unifocal or confluent areas of macular chorioretinal atrophy, often accompanied by fibrovascular scarring. Without MNV, macular atrophy progresses more rapidly, and pattern-dystrophy like changes with hypo-/hyperAF signal are frequently observed.
	Onset typically in the superior macula, with initial diffuse RPE-BM separation visible on OCT.	Foveal involvement is present at onset in about one-third of cases, with remaining cases progressing to foveal atrophy within around 5.5 years. Atrophy slowly enlarges over time	Purely atrophic forms without MNV may have multilobular borders lacking a preferred orientation		
	Foveal involvement occurs within ~4 years, followed by rapid progression beyond the vascular arcades, toward the nasal and temporal mid-periphery with relative temporal sparing. Residual hyperreflective debris and BM ruptures within the area of cRORA can be seen on OCT. Conjunction with peripheral pavingstone-like degeneration may occur				
Large drusen[a]	Absent	Present, sometimes regressed	Present from the 3rd decade	Generally absent	Absent
RPD/SDDs and pseudodrusen-like lesions[a]	SDDs are found at early stages, localized over the area of RPE-BM separation in the macula. Mid-peripheral pseudodrusen-like deposits are ubiquitous, corresponding to hyperreflective lesions at the level of the RPE on OCT, though visibility may be limited in myopic eyes	>60% of cases between the 8th and 9th decades	Prevalence ~70% in the 6th decade.	Develop temporally to the macula in the late 40s, with prevalence ~60% in the 6th decade.	~60% in the 5th decade, central to the area of *peau d'orange* (the calcified BM region, hypofluorescent on late-phase ICGA)
Peripheral findings	Ranges from simple RPE alterations to pavingstone-like degeneration and pigmented chorioretinal atrophy, most commonly in the infero-temporal sector	Aspecific hypo-/hyper-pigmentary changes, RPE alterations, pavingstone degeneration, drusenoid lesions and occasional RPD are seen at a higher frequency than the general population	Peripheral RPD, including regions nasal to the optic nerve head and along the vascular arcades	Peripheral RPD	*Peau d'orange*, comet lesions, and linear streaks are characteristic
MNV[a]	~15% within 4 years from diagnosis. Mostly type 2, rarely type 1 MNV	~11% within 4 years from the diagnosis. Mostly type 2, but types 1 and 3 are possible	60–80% of cases, with type 2 > type 1.	Unclear prevalence, type 1 is common, peripheral neovascularization has been documented.	42–86%. Type 1 > type 2. Non-exudative MNV in 33%.

[a] *Adapted from Trinco* et al. *Under review.* EMAP = Extensive macular atrophy with pseudodrusen-like appearance; GA = Geographic atrophy; AMD = Age-related macular degeneration; SFD = Sorsby fundus dystrophy; L-ORD = Late-onset retinal degeneration; PXE = Pseudoxanthoma elasticum; MNV = Macular neovascularization; MEWDS = Multifocal evanescent white-dot syndrome; BM = Bruch's membrane; RPE = Retinal pigment epithelium; SW-AF = Short-wavelength autofluorescence; cRORA = Complete retinal pigment epithelium and outer retinal atrophy; RPD = Reticular pseudodrusen; SDDs = Subretinal drusenoid deposits; OCT = optical coherence tomography.

Table 2
Diagnostic criteria for Extensive Macular Atrophy with Pseudodrusen-like appearance (EMAP).

Mandatory features	
a) Diffuse SDDs and pseudodrusen-like deposits involving the posterior pole and mid-periphery on fundus examination and multimodal *en face* imaging	
b) (1) No evident macular atrophy on SW-AF but diffuse macular RPE-BM separation on OCT ***OR*** *(2)* Moderately hypoautofluorescent ("grayish") macular atrophy on SW-AF[a], surrounded by RPE-BM separation on OCT ***OR*** *(3)* Moderately hypoautofluorescent ("grayish"), multilobular macular atrophy with vertical, "leaf-shaped", or confluent configuration along with "temporal sparing"[‡]	
c) Negative genetic testing for known causes of IRDs	
Complementary features	
Pavingstone-like degeneration	Well-defined, roundish, patches of chorio-retinal atrophy that tend to coalesce,most often found at the inferotemporal sector.However, the full assessment of the entire retinal periphery is required. In the very advanced stage of the disease it may reach the equator, merge with posterior pole atrophy, and develop a coarse pigmentation.
Rod and cone system dysfunction on ERG	The dark-adapted rod-specific (DA 0.01) ERG shows a decrease in b-wave amplitude, while the light-adapted cone-specific 30 Hz flicker ERG is characterized by an implicit time delay that is disproportionate to the reduction in amplitude. In the very advanced stage of the disease, the ERGs can be undetectable under all stimulus conditions.

The diagnosis requires the concurrent presence of "a" + "b1" *or* "b2" *or* "b3" + c in *both* eyes. Complementary findings should be always investigated, as their presence supports the diagnosis, while their absence makes it less likely, particularly for "b1" and "b2".

[a] Effortless distinction of the overlying retinal vessels on confocal SW-AF, with inhomogeneous autofluorescence. [‡]Round or oval region of relatively preserved retinal tissue, located roughly 15° temporal to the macula, and surrounded by chorio-retinal atrophy. CFP = Color fundus photograph; IR = Infrared reflectance; SW-AF = Short-wavelength autofluorescence; OCT = Optical coherence tomography; BM = Bruch's membrane; RPE = Retinal pigment epithelium; IRDs = Inherited retinal diseases; ERG = full-field electroretinography; SDDs = Subretinal drusenoid deposits.

of overlapping clinical features, electrophysiological testing may be helpful. Indeed, ERG is almost invariably altered in EMAP, particularly in rod-dominated DA responses, while it should be *a priori* within the normal limits in GA secondary to AMD or any other maculopathy. This leads to our key message that warrants particular emphasis: EMAP is a panretinal disorder and not a simple maculopathy. In this regard, its name can be somewhat misleading, as it does not acknowledge the generalized photoreceptor dysfunction or the peripheral retinal atrophy.

9.2. Diagnostic criteria

The scrutiny of the large Italian and French Quinze-Vingts EMAP cohorts that we presented herein allowed the identification of some necessary disease features for the diagnosis of EMAP through multimodal imaging and retinal electrophysiology. Thus, in light of the presented imaging and functional data, we propose the first diagnostic criteria for EMAP. For the diagnosis, a detailed fundus examination and multimodal imaging including SW-AF and OCT scans encompassing the entire posterior pole are required. These should be ideally complemented by UWF imaging and ERG. The proposed diagnostic criteria are presented in Table 2.

The first criterion is the presence of diffuse SDDs and pseudodrusen-like deposits on fundus examination and multimodal imaging (*a*). Classic SDDs are typically found in the macular region of early cases, while pseudodrusen-like deposits are more abundant in the mid-periphery. Future studies will be needed to ascertain the nature of pseudodrusen-like deposits on OCT. The second criterion concerns the macular findings on multimodal imaging and envisages three different scenarios (*b1, b2, b3*). In more detail, *b1* refers to the pre-atrophic stage, with just a diffuse thick RPE-BM separation found in the macular region on OCT. Then, *b2* includes all MAs that do not demonstrate the typical orientation and shape of EMAP but show the MDAF pattern on SW-AF surrounded by RPE-BM separation on OCT. Lastly, the *b3* case is for instances with all typical features of MA in EMAP, including the multilobular borders with vertical, "leaf-shaped", or confluent configuration and an identifiable "temporal sparing". Genetic testing negative for known causes of IRDs is the third criterion. A diagnosis of EMAP requires that these criteria are met in both eyes.

We intentionally exclude the presence of pavingstone-like degeneration or proven generalized photoreceptor dysfunction from *mandatory* criteria. In fact, this would require performing ancillary tests which are not readily available in all retina clinics, such as UWF imaging and retinal electrophysiology. Furthermore, although being frequently observed in clinical practice and highly suggestive, definitive data on the prevalence of pavingstone-like degeneration in EMAP are not available. However, these additional findings become increasingly important when the MA lacks some or most of its typical features, such as in *b1* and *b2*. For instance, in a patient over 65 years with a small patch of MA and pseudodrusen-like deposits (scenario *b2*), the diagnosis of EMAP would be more compelling if there is pavingstone-like degeneration in the far periphery or generalized photoreceptor dysfunction on ERG. Conversely, a completely normal ERG would suggest a diagnosis of GA secondary to AMD. Similarly, while finding diffuse pseudodrusen-like deposits and RPE-BM splitting in a 40-year-old patient is clearly pathological and warrants investigation as potential IRD with genetic testing, an older patient falling in the *b1* category will necessitate further investigations, including a careful assessment of the periphery. However, we advise against dismissing a diagnosis of EMAP based solely on the patient's age or symptoms, although these may be suggestive when considered in a broader clinical context.

The strength of our criteria lies in their ability to facilitate the diagnosis of EMAP both in early and late stages, or even when not all elements of the classic clinical triad described by Hamel et al. are present. This approach minimizes misdiagnoses by incorporating complementary tests. Although this review identifies many features characteristic of EMAP, keeping the diagnostic criteria simple is essential for gaining broad acceptance in clinical practice. Nonetheless, the identification of all the corollary features accompanying EMAP across its various stages is entrusted to the retina specialist. Table 3 provides a comprehensive summary of the main findings of EMAP. The next chapter will discuss the practical and therapeutic implications of applying these criteria in the diagnosis of EMAP.

9.3. Therapeutical implications

As of now, no treatment options are available for EMAP, a severely blinding disorder affecting mostly individuals with at least 15–20 years of life expectancy. Considering this, it is imperative to undertake every effort to find therapies that can slow down its progression. The application of diagnostic criteria represents a critical step and aid in identifying patients who may have been included in previous clinical trials for GA secondary to AMD due to phenotypic overlap with the DTGA phenotype. For instance, Pegcetacoplan, a C3 inhibitor developed by Apellis Pharmaceuticals, Waltham, MA, has recently become the first compounds in its class to receive FDA approval (Apellis Pharmaceuticals, Inc, 2023). Concurrently, the 18-month follow-up report of the GATHER1 trial, which investigated Avacincaptad Pegol (IVERIC bio, Inc., Parsippany, NJ), another complement inhibitor targeting C5, was recently published (Patel et al., 2023). In this trial, approximately one-fifth of the patients exhibited a DTGA aspect, but no subgroup

Table 3
Clinical and multimodal retinal imaging features of EMAP.

Patients' characteristics	
Age at first referral	Commonly between the early 50s and mid-60s, but earlier or later presentation is possible.
Symptoms at presentation	Photophobia is most common, often preceded by night blindness. Other symptoms include dyschromatopsia, central scotoma, and visual field loss. Visual acuity loss is rarely the first complaint, and usually co-occurs with other symptoms. Patients do not typically complain of metamorphopsias.
Gender	Female predominance (~60%).
Macular atrophy	
Fundus autofluorescence (SW-AF)	Moderately decreased hypoautofluorescence (MDAF) with multilobular borders.
Optical coherence tomography	Widespread RPE-BM separation with ellipsoid zone attenuation surrounding the atrophic lesion. Hyperreflective "debris" persists within the atrophy even after RPE loss.
Natural history	The onset often involves the superior perifoveal sector. Subsequent growth takes place bilaterally and symmetrically on the vertical axis with multilobular borders and initial foveal sparing. Once surpassed the vascular arcades, the atrophy turns towards the optic disc nasally, and horizontally, leaving a preserved temporal island. At any time, presumed non-neovascular fibrosis at the fovea may follow RPE atrophy, or neovascular complications may occur. Widespread chorio-retinal atrophy and Bruch's membrane ruptures develop in advanced cases.
Growth rate	The mean growth of the square-root transformed areas is estimated at 0.45 mm/year.
Pseudodrusen-like deposits and reticular pseudodrusen	
Types	Reticular pseudodrusen are focal ("dots") or broad lesions forming an interlacing network ("ribbon") in the macular region or immediate surroundings. Pseudodrusen-like deposits are ill-defined yellowish/hypopigmented lesions arranged in a lattice that extends from the outermost boundary of the posterior pole to the equator.
Optical coherence tomography	Reticular pseudodrusen correspond to SDDs, either focal and conical or flat and diffuse. Pseudodrusen-like deposits in the mid-periphery and contouring peripheral pavingstone-like degeneration appear as flat, large, hyperreflective lesions at the level of the RPE.
Fundus autofluorescence (SW-AF)	Reticular pseudodrusen are hypoautofluorescent, while pseudodrusen-like deposits show faint hyperautofluorescence.
Peripheral findings	
Aspect on CFP	Range from simple RPE alterations to pavingstone-like degeneration to pigmented chorioretinal atrophy.
Localization	The inferotemporal sector is the most frequently involved; 360° involvement is possible.
Progression	Peripheral atrophy can develop over areas of RPE alterations; in some cases, it show centripetal progression ultimately merging with macular atrophy.
Fundus autofluorescence	RPE alterations are hyperautofluorescent, peripheral atrophy has often a faint hypoautofluorescent aspect.
Bruch's membrane ruptures	
Aspect on CFP	Pale, linear streaks within the region of macular atrophy. They may cross the macula in a linear fashion, either horizontally or vertically, or take an irregular appearance with no particular orientation.
Fundus autofluorescence (SW-AF)	Hypoautofluorescent, darker than the surrounding MDAF.
Infrared reflectance	More hyperreflective than the surrounding atrophy.
Optical coherence tomography	Focal interruptions to large dehiscences of the BM, leaving the neuroretina in direct contact with the underlying choroid or, when profound chorioretinal atrophy occurs, the sclera.
Dye angiographies	Large ruptures are hypofluorescent with both fluorescein and indocyanine green angiography.
Functional exams	
ERG	Scotopic responses are more severely reduced than photopic ones but delayed LA 30 Hz flicker is often the most evident alteration. In advanced cases, scotopic ERGs may show a pseudo-electronegative waveform in 3.0 and 10.0 DA ERGs before becoming completely undetectable.
Kinetic perimetry	Large central scotomas develop in all patients. Approximately 1 out of 5 patients exhibits peripheral visual field constriction.
Microperimetry	Reduced macular mesopic and scotopic retinal sensitivity, with profound scotopic sensitivity loss from the early stages.

BM = Bruch's membrane; RPE = Retinal pigment epithelium; SDD = Subretinal drusenoid deposit; CFP = Color fundus photograph; ERG = full-field electroretinography; LA = Light-adapted; DA = Dark-adapted.

analyses based on the SW-AF patterns were conducted. Considering that EMAP may present in an age range partially overlapping with AMD, we may hypothesize that some of the patients diagnosed with DTGA might actually be affected by EMAP. Complement inhibitors have been demonstrated to slow GA growth by approximately 30% per year, although no significant differences were observed in terms of visual outcomes. For this reason, some authors have questioned the appropriateness of subjecting an elderly population to the burden of intravitreal injections without expected benefits in vision or quality of life (Spaide and Vavvas, 2023). These pertinent criticisms were followed by the recent refusal by the European Medicines Agency of the marketing approval for Pegcetacoplan (European Medicines Agency, 2024). Therefore, it is crucial to determine whether any patients with EMAP were inadvertently included in these trials. Interestingly, Pegcetacoplan acts by inhibiting the activation of C3 complement factor, whose levels have been found to be elevated in EMAP compared to controls (Douillard et al., 2016), possibly due to the association with the C3_rs2230199 risk allele (Douillard et al., 2018), although the difference was marginal and these results need replication in further studies. Should complement inhibitors prove to be effective in EMAP, there would be grounds for a timely phase II/III trial for this blinding disorder. Moreover, considering the nature of EMAP patients as fast progressors, such reduction in MA growth could be highly meaningful for patients affected by EMAP, potentially preserving many years of useful vision.

10. Conclusions and future directions

This review has summarized all the existing literature on EMAP and presented unpublished data from the two largest cohorts in Europe. We conclude that EMAP is a bilateral and highly symmetric retinopathy characterized by generalized photoreceptor dysfunction and rapidly progressive MA. These characteristics have been distinctly described through multimodal retinal imaging, providing the basis for the set of diagnostic criteria that we proposed here. Despite these advancements, the etiology and pathogenesis of EMAP remain elusive. Future research should aim at unraveling its risk factors, considering the complex interactions between chronic systemic inflammation, complement dysregulation and genetic factors. Additionally, histopathologic studies are warranted to better understand the nature and implications of the widespread deposits observed both above and below the RPE in EMAP. Lastly, *post-hoc* analyses of clinical trial data on complement inhibitors for GA may potentially yield insights into whether effective treatment options are already available for EMAP.

Funding

IHU FOReSIGHT [ANR-18-IAHU-0001] supported by French state funds managed by the Agence Nationale de la Recherche within the Investissements d'Avenir program.

CRediT authorship contribution statement

Alessio Antropoli: Writing – review & editing, Writing – original draft, Visualization, Investigation, Formal analysis, Data curation, Conceptualization. **Lorenzo Bianco:** Writing – review & editing, Writing – original draft, Visualization, Investigation, Formal analysis, Data curation, Conceptualization. **Francesco Romano:** Writing – original draft, Investigation, Data curation. **Andrea Trinco:** Investigation, Data curation. **Alessandro Arrigo:** Investigation. **Amine Benadji:** Investigation. **Raphaël Atia:** Investigation. **Oana Palacci:** Investigation. **Dorothée Dagostinoz:** Investigation. **Céline Devisme:** Investigation. **Christel Condroyer:** Investigation. **Aline Antonio:** Investigation. **Francesca Bosello:** Resources, Investigation. **Stefano Casati:** Resources, Investigation. **Anna Paola Salvetti:** Resources, Investigation. **Chiara Zaffalon:** Resources, Investigation. **Alain Gaudric:** Writing – review & editing. **José-Alain Sahel:** Supervision. **Giovanni Staurenghi:** Writing – review & editing, Resources. **Francesco Bandello:** Supervision, Resources. **Florian Sennlaub:** Writing – review & editing. **Christina Zeitz:** Writing – review & editing, Resources. **Isabelle Meunier:** Writing – review & editing, Supervision. **Maurizio Battaglia Parodi:** Writing – review & editing, Supervision, Resources, Project administration, Conceptualization. **Isabelle Audo:** Writing – review & editing, Supervision, Resources, Project administration, Conceptualization.

Appendix A. Supplementary data

Supplementary data to this article can be found online at https://doi.org/10.1016/j.preteyeres.2024.101320.

Data availability

Data will be made available on request.

References

Agrón, E., Domalpally, A., Cukras, C.A., Clemons, T.E., Chen, Q., Lu, Z., Chew, E.Y., Keenan, T.D.L., AREDS and AREDS2 Research Groups, 2022. Reticular pseudodrusen: the third macular risk feature for progression to late age-related macular degeneration: age-related eye disease study 2 report 30. Ophthalmology 129, 1107–1119. https://doi.org/10.1016/j.ophtha.2022.05.021.

Agrón, E., Domalpally, A., Cukras, C.A., Clemons, T.E., Chen, Q., Swaroop, A., Lu, Z., Chew, E.Y., Keenan, T.D.L., AREDS and AREDS2 Research Groups, 2023. Reticular pseudodrusen status, ARMS2/HTRA1 genotype, and geographic atrophy enlargement: age-related eye disease study 2 report 32. Ophthalmology 130, 488–500. https://doi.org/10.1016/j.ophtha.2022.11.026.

Alex, V., Papastavrou, V., Walker, E.H., Browning, A.C., Dhillon, B., Borooah, S., 2023. Microperimetry in foveal-sparing atrophic late-onset retinal degeneration. Retina 43, 1590. https://doi.org/10.1097/IAE.0000000000003849.

Alsaffar, F.A., Mujamammi, A.H., Aldughaim, M.S.K., Nicklin, M.J.H., Barker, M.D., 2023. Evidence that all Sorsby's fundus dystrophy mutations cause TIMP3 dimerization resulting in impaired inhibition of VEGFR2. Genes Dis 10, 45–47. https://doi.org/10.1016/j.gendis.2022.03.008.

Alten, F., Clemens, C.R., Heiduschka, P., Eter, N., 2014. Characterisation of reticular pseudodrusen and their central target aspect in multi-spectral, confocal scanning laser ophthalmoscopy. Graefes Arch. Clin. Exp. Ophthalmol. 252, 715–721. https://doi.org/10.1007/s00417-013-2525-y.

Antropoli, A., Arrigo, A., Bianco, L., Berni, A., Lamberto, L.F., Saladino, A., Bandello, F., Battaglia Parodi, M., 2023. Quantitative multimodal imaging of extensive macular atrophy with pseudodrusen and geographic atrophy with diffuse trickling pattern. Sci. Rep. 13, 1822. https://doi.org/10.1038/s41598-023-28906-4.

Antropoli, A., Bianco, L., Condroyer, C., Antonio, A., Navarro, J., Dagostinoz, D., Benadji, A., Sahel, J.-A., Zeitz, C., Audo, I., 2024. Extensive Macular Atrophy with Pseudodrusen-like appearance (EMAP): progression kinetics and late-stage findings. Ophthalmology. https://doi.org/10.1016/j.ophtha.2024.04.001, 0.

Apellis Pharmaceuticals, Inc., 2023. FDA Approves SYFOVRE™ (Pegcetacoplan Injection) as the First and Only Treatment for Geographic Atrophy (GA), a Leading Cause of Blindness.

Arrigo, A., Aragona, E., Battaglia Parodi, M., Bandello, F., 2023. Quantitative approaches in multimodal fundus imaging: state of the art and future perspectives. Prog. Retin. Eye Res. 92, 101111. https://doi.org/10.1016/j.preteyeres.2022.101111.

Ayyagari, R., Griesinger, I.B., Bingham, E., Lark, K.K., Moroi, S.E., Sieving, P.A., 2000. Autosomal dominant hemorrhagic macular dystrophy not associated with the TIMP3 gene. Arch. Ophthalmol. 118, 85–92. https://doi.org/10.1001/archopht.118.1.85.

Ayyagari, R., Mandal, M.N.A., Karoukis, A.J., Chen, L., McLaren, N.C., Lichter, M., Wong, D.T., Hitchcock, P.F., Caruso, R.C., Moroi, S.E., Maumenee, I.H., Sieving, P.A., 2005. Late-onset macular degeneration and long anterior lens zonules result from a CTRP5 gene mutation. Invest. Ophthalmol. Vis. Sci. 46, 3363–3371. https://doi.org/10.1167/iovs.05-0159.

Battaglia Parodi, M., Antropoli, A., Bianco, L., Arrigo, A., Pili, L., Saladino, A., Bandello, F., 2023. Peripheral retinal involvement in extensive macular atrophy with pseudodrusen-like deposits. Ophthalmol. Retina 7, 910–917. https://doi.org/10.1016/j.oret.2023.06.020.

Battaglia Parodi, M., Querques, G., 2015. Choroidal neovascularization associated with extensive macular atrophy and pseudodrusen. Optom. Vis. Sci. 92, S51–S54. https://doi.org/10.1097/OPX.0000000000000532.

Ben Moussa, N., Georges, A., Capuano, V., Merle, B., Souied, E.H., Querques, G., 2015. MultiColor imaging in the evaluation of geographic atrophy due to age-related macular degeneration. Br. J. Ophthalmol. 99, 842–847. https://doi.org/10.1136/bjophthalmol-2014-305643.

Bergen, A.A., Plomp, A.S., Schuurman, E.J., Terry, S., Breuning, M., Dauwerse, H., Swart, J., Kool, M., van Soest, S., Baas, F., ten Brink, J.B., de Jong, P.T., 2000. Mutations in ABCC6 cause pseudoxanthoma elasticum. Nat. Genet. 25, 228–231. https://doi.org/10.1038/76109.

Berlin, A., Fischer, N.A., Clark, M.E., Kar, D., Swain, T.A., Martindale, R.M., McGwin, G., Crosson, J.N., Sloan, K.R., Owsley, C., Curcio, C.A., 2024. Quantitative autofluorescence at AMD's beginnings highlights retinal topography and grading system differences: ALSTAR2 baseline. Ophthalmologica 1–13. https://doi.org/10.1159/000538696.

Bianco, L., Antropoli, A., Arrigo, A., Berni, A., La Franca, L., Saladino, A., Bandello, F., Parodi, M.B., 2023. Fundus autofluorescence in extensive macular atrophy with pseudodrusen (EMAP) and diffuse trickling geographic atrophy (DTGA). Retina. https://doi.org/10.1097/IAE.0000000000003733.

Bianco, L., Antropoli, A., Benadji, A., Condroyer, C., Antonio, A., Navarro, J., Sahel, J.-A., Zeitz, C., Audo, I., 2024. RDH5 and RLBP1-associated inherited retinal diseases: refining the spectrum of stationary and progressive phenotypes. Am. J. Ophthalmol. https://doi.org/10.1016/j.ajo.2024.06.016. S0002-9394(24)00261–7.

Birch, D.G., Anderson, J.L., 1992. Standardized full-field electroretinography. Normal values and their variation with age. Arch. Ophthalmol. 110, 1571–1576. https://doi.org/10.1001/archopht.1992.01080230071024.

Bird, A.C., Bressler, N.M., Bressler, S.B., Chisholm, I.H., Coscas, G., Davis, M.D., de Jong, P.T.V.M., Klaver, C.C.W., Klein, B.E.K., Klein, R., Mitchell, P., Sarks, J.P., Sarks, S.H., Soubrane, G., Taylor, H.R., Vingerling, J.R., 1995. An international classification and grading system for age-related maculopathy and age-related macular degeneration. Surv. Ophthalmol. 39, 367–374. https://doi.org/10.1016/S0039-6257(05)80092-X.

Bisaccia, F., Koshal, P., Abruzzese, V., Castiglione Morelli, M.A., Ostuni, A., 2021. Structural and functional characterization of the ABCC6 transporter in hepatic cells: role on PXE, cancer therapy and drug resistance. Int. J. Mol. Sci. 22, 2858. https://doi.org/10.3390/ijms22062858.

Bone, R.A., Landrum, J.T., Fernandez, L., Tarsis, S.L., 1988. Analysis of the macular pigment by HPLC: retinal distribution and age study. Invest. Ophthalmol. Vis. Sci. 29, 843–849.

Bonnet, C., Querques, G., Zerbib, J., Oubraham, H., Garavito, R.B., Puche, N., Souied, E. H., 2014. Hyperreflective pyramidal structures on optical coherence tomography in geographic atrophy areas. Retina 34, 1524. https://doi.org/10.1097/IAE.0000000000000165.

Booij, J.C., Baas, D.C., Beisekeeva, J., Gorgels, T.G.M.F., Bergen, A.a.B., 2010. The dynamic nature of Bruch's membrane. Prog. Retin. Eye Res. 29, 1–18. https://doi.org/10.1016/j.preteyeres.2009.08.003.

Boon, C.J.F., Theelen, T., Hoyng, C.B., 2009. Extensive macular atrophy with pseudodrusen-like appearance: a new clinical entity. Am. J. Ophthalmol. 148, 173–174. https://doi.org/10.1016/j.ajo.2009.03.017.

Borooah, S., Papastavrou, V., Lando, L., Han, J., Lin, J.H., Ayyagari, R., Dhillon, B., Browning, A.C., 2021. Reticular pseudodrusen in late-onset retinal degeneration. Ophthalmol. Retina 5, 1043–1051. https://doi.org/10.1016/j.oret.2020.12.012.

Borrelli, E., Uji, A., Toto, L., Viggiano, P., Evangelista, F., Mastropasqua, R., 2019. In vivo mapping of the choriocapillaris in healthy eyes: a widefield swept-source OCT angiography study. Ophthalmol. Retina 3, 979–984. https://doi.org/10.1016/j.oret.2019.05.026.

Buitendijk, G.H.S., Hooghart, A.J., Brussee, C., de Jong, P.T.V.M., Hofman, A., Vingerling, J.R., Klaver, C.C.W., 2016. Epidemiology of reticular pseudodrusen in age-related macular degeneration: the rotterdam study. Invest. Ophthalmol. Vis. Sci. 57, 5593–5601. https://doi.org/10.1167/iovs.15-18816.

Burstedt, M.S., Sandgren, O., Holmgren, G., Forsman-Semb, K., 1999. Bothnia dystrophy caused by mutations in the cellular retinaldehyde-binding protein gene (RLBP1) on chromosome 15q26. Invest. Ophthalmol. Vis. Sci. 40, 995–1000.

Capon, M.R.C., Marshall, J., Krafft, J.I., Alexander, R.A., Hiscott, P.S., Bird, A.C., 1989. Sorsby's fundus dystrophy: a light and electron microscopic study. Ophthalmology 96, 1769–1777. https://doi.org/10.1016/S0161-6420(89)32664-9.

Charbel Issa, P., Berendschot, T.T.J.M., Staurenghi, G., Holz, F.G., Scholl, H.P.N., 2008. Confocal blue reflectance imaging in type 2 idiopathic macular telangiectasia. Invest. Ophthalmol. Vis. Sci. 49, 1172–1177. https://doi.org/10.1167/iovs.07-0636.

Charbel Issa, P., Finger, R.P., Götting, C., Hendig, D., Holz, F.G., Scholl, H.P.N., 2010. Centrifugal fundus abnormalities in pseudoxanthoma elasticum. Ophthalmology 117, 1406–1414. https://doi.org/10.1016/j.ophtha.2009.11.008.

Charbel Issa, P., Finger, R.P., Holz, F.G., Scholl, H.P.N., 2009. Multimodal imaging including spectral domain OCT and confocal near infrared reflectance for characterization of outer retinal pathology in pseudoxanthoma elasticum. Invest. Ophthalmol. Vis. Sci. 50, 5913–5918. https://doi.org/10.1167/iovs.09-3541.

Chekuri, A., Zientara-Rytter, K., Soto-Hermida, A., Borooah, S., Voronchikhina, M., Biswas, P., Kumar, V., Goodsell, D., Hayward, C., Shaw, P., Stanton, C., Garland, D., Subramani, S., Ayyagari, R., 2019. Late-onset retinal degeneration pathology due to mutations in CTRP5 is mediated through HTRA1. Aging Cell 18, e13011. https://doi.org/10.1111/acel.13011.

Cheloni, R., Venkatesh, A., Rodriguez-Martinez, A.C., Moosajee, M., 2023. Longitudinal changes of retinal structure in molecularly confirmed C1QTNF5 patients with late-onset retinal degeneration. Transl. Vis. Sci. Technol. 12, 14. https://doi.org/10.1167/tvst.12.12.14.

Chen, L., Messinger, J.D., Kar, D., Duncan, J.L., Curcio, C.A., 2021. Biometrics, impact, and significance of basal linear deposit and subretinal drusenoid deposit in age-related macular degeneration. Invest. Ophthalmol. Vis. Sci. 62, 33. https://doi.org/10.1167/iovs.62.1.33.

Chen, L., Messinger, J.D., Zhang, Y., Spaide, R.F., Freund, K.B., Curcio, C.A., 2020. Subretinal drusenoid deposit in age-related macular degeneration: histologic insights into initiation, progression to atrophy, and imaging. Retina 40, 618–631. https://doi.org/10.1097/IAE.0000000000002657.

Chen, L., Zhang, X., Liu, B., Mi, L., Wen, F., 2018. Age-related scattered hypofluorescent spots on late-phase indocyanine green angiography: the multimodal imaging and relevant factors. Clin. Exp. Ophthalmol. 46, 908–915. https://doi.org/10.1111/ceo.13306.

Chong, N.H.V., Alexander, R.A., Gin, T., Bird, A.C., Luthert, P.J., 2000. TIMP-3, collagen, and elastin immunohistochemistry and histopathology of sorsby's fundus dystrophy. Invest. Ophthalmol. Vis. Sci. 41, 898–902.

Chong, N.H.V., Keonin, J., Luthert, P.J., Frennesson, C.I., Weingeist, D.M., Wolf, R.L., Mullins, R.F., Hageman, G.S., 2005. Decreased thickness and integrity of the macular elastic layer of Bruch's membrane correspond to the distribution of lesions associated with age-related macular degeneration. Am. J. Pathol. 166, 241–251. https://doi.org/10.1016/S0002-9440(10)62248-1.

Chouraqui, M., Crincoli, E., Miere, A., Meunier, I.A., Souied, E.H., 2023. Deep learning model for automatic differentiation of EMAP from AMD in macular atrophy. Sci. Rep. 13, 20354. https://doi.org/10.1038/s41598-023-47854-7.

Christensen, D.R.G., Brown, F.E., Cree, A.J., Ratnayaka, J.A., Lotery, A.J., 2017. Sorsby fundus dystrophy - a review of pathology and disease mechanisms. Exp. Eye Res. 165, 35–46. https://doi.org/10.1016/j.exer.2017.08.014.

Cideciyan, A.V., Swider, M., Jacobson, S.G., 2015. Autofluorescence imaging with near-infrared excitation:normalization by reflectance to reduce signal from choroidal fluorophores. Invest. Ophthalmol. Vis. Sci. 56, 3393–3406. https://doi.org/10.1167/iovs.15-16726.

Cleland, S.C., Domalpally, A., Liu, Z., Pak, J.W., Blodi, B.A., Bailey, S., Gehrs, K., Wallace, R., Tinker, L., Mares, J.A., Second Carotenoids in Age-Related Eye Disease Study Investigators, 2021. Reticular pseudodrusen characteristics and associations in the carotenoids in age-related eye disease study 2 (CAREDS2), an ancillary study of the women's health initiative. Ophthalmol. Retina 5, 721–729. https://doi.org/10.1016/j.oret.2020.12.019.

Crincoli, E., De Rosa, I., Miere, A., Colantuono, D., Mehanna, C.J., Souied, E.H., 2022. Comparison of multimodal imaging for the characterization of geographic atrophy. Transl. Vis. Sci. Technol. 11, 21. https://doi.org/10.1167/tvst.11.11.21.

Cukras, C., Flamendorf, J., Wong, W.T., Ayyagari, R., Cunningham, D., Sieving, P.A., 2016. Longitudinal structural changes in late-onset retinal degeneration. Retina 36, 2348–2356. https://doi.org/10.1097/IAE.0000000000001113.

Curcio, C.A., Kar, D., Owsley, C., Sloan, K.R., Ach, T., 2024. Age-related macular degeneration, a mathematically tractable disease. Invest. Ophthalmol. Vis. Sci. 65, 4. https://doi.org/10.1167/iovs.65.3.4.

Curcio, C.A., Messinger, J.D., Sloan, K.R., McGwin, G., Medeiros, N.E., Spaide, R.F., 2013. Subretinal drusenoid deposits in non-neovascular age-related macular degeneration: morphology, prevalence, topography, and biogenesis model. Retina 33, 265–276. https://doi.org/10.1097/IAE.0b013e31827e25e0.

Curcio, C.A., Presley, J.B., Millican, C.L., Medeiros, N.E., 2005. Basal deposits and drusen in eyes with age-related maculopathy: evidence for solid lipid particles. Exp. Eye Res. 80, 761–775. https://doi.org/10.1016/j.exer.2004.09.017.

Delori, F., Greenberg, J.P., Woods, R.L., Fischer, J., Duncker, T., Sparrow, J., Smith, R.T., 2011. Quantitative measurements of autofluorescence with the scanning laser ophthalmoscope. Invest. Ophthalmol. Vis. Sci. 52, 9379–9390. https://doi.org/10.1167/iovs.11-8319.

Domalpally, A., Agrón, E., Pak, J.W., Keenan, T.D., Ferris, F.L., Clemons, T.E., Chew, E. Y., 2019. Prevalence, risk, and genetic association of reticular pseudodrusen in age-related macular degeneration: age-related eye disease study 2 report 21. Ophthalmology 126, 1659–1666. https://doi.org/10.1016/j.ophtha.2019.07.022.

Douillard, A., Picot, M.-C., Delcourt, C., Defoort-Dhellemmes, S., Marzouka, N.A.-D., Lacroux, A., Zanlonghi, X., Drumare, I., Jozefowicz, E., Bocquet, B., Baudoin, C., Perez-Roustit, S., Arsène, S., Gissot, V., Devin, F., Arndt, C., Wolff, B., Mauget-Faÿsse, M., Quaranta, M., Mura, T., Deplanque, D., Oubraham, H., Cohen, S.Y., Gastaud, P., Zambrowski, O., Creuzot-Garcher, C., Saïd, S.M., Sahel, J.-A., Souied, E., Milazzo, S., Garavito, R.B., Kalatzis, V., Puech, B., Hamel, C., Audo, I., Meunier, I., 2018. Dietary, environmental, and genetic risk factors of Extensive Macular Atrophy with Pseudodrusen, a severe bilateral macular atrophy of middle-aged patients. Sci. Rep. 8, 6840. https://doi.org/10.1038/s41598-018-25003-9.

Douillard, A., Picot, M.-C., Delcourt, C., Lacroux, A., Zanlonghi, X., Puech, B., Defoort-Dhelemmes, S., Drumare, I., Jozefowicz, E., Bocquet, B., Baudoin, C., Al-Dain Marzouka, N., Perez-Roustit, S., Arsène, S., Gissot, V., Devin, F., Arndt, C., Wolff, B., Mauget-Faÿsse, M., Quaranta, M., Mura, T., Deplanque, D., Oubraham, H., Cohen, S. Y., Gastaud, P., Zambrowsky, O., Creuzot-Garcher, C., Mohand Saïd, S., Blanco Garavito, R., Souied, E., Sahel, J.-A., Audo, I., Hamel, C., Meunier, I., 2016. Clinical characteristics and risk factors of extensive macular atrophy with pseudodrusen. Ophthalmology 123, 1865–1873. https://doi.org/10.1016/j.ophtha.2016.05.018.

Duncker, T., Greenberg, J.P., Ramachandran, R., Hood, D.C., Smith, R.T., Hirose, T., Woods, R.L., Tsang, S.H., Delori, F.C., Sparrow, J.R., 2014. Quantitative fundus autofluorescence and optical coherence tomography in best vitelliform macular dystrophy. Invest. Ophthalmol. Vis. Sci. 55, 1471–1482. https://doi.org/10.1167/iovs.13-13834.

Duncker, T., Tsang, S.H., Lee, W., Zernant, J., Allikmets, R., Delori, F.C., Sparrow, J.R., 2015. Quantitative fundus autofluorescence distinguishes ABCA4-associated and non-ABCA4-associated bull's-eye maculopathy. Ophthalmology 122, 345–355. https://doi.org/10.1016/j.ophtha.2014.08.017.

Eichers, E.R., Green, J.S., Stockton, D.W., Jackman, C.S., Whelan, J., McNamara, J.A., Johnson, G.J., Lupski, J.R., Katsanis, N., 2002. Newfoundland rod-cone dystrophy, an early-onset retinal dystrophy, is caused by splice-junction mutations in RLBP1. Am. J. Hum. Genet. 70, 955–964. https://doi.org/10.1086/339688.

Elledge, J.A., Davis, M.D., Hubbard, L.D., Reimers, J.L., Fink, C.A., Hafford, D.G., Susman, R.A., 2005. Diameter/area of the standardized optic disc and accurate scaling in retinal images. Invest. Ophthalmol. Vis. Sci. 46, 2583.

Elsner, A.E., Burns, S.A., Weiter, J.J., Delori, F.C., 1996. Infrared imaging of sub-retinal structures in the human ocular fundus. Vis. Res. 36, 191–205. https://doi.org/10.1016/0042-6989(95)00100-e.

European Medicines Agency, 2024. Syfovre.

Ferris, F.L., Wilkinson, C.P., Bird, A., Chakravarthy, U., Chew, E., Csaky, K., Sadda, S.R., 2013. Clinical classification of age-related macular degeneration. Ophthalmology 120, 844–851. https://doi.org/10.1016/j.ophtha.2012.10.036.

Flamendorf, J., Agrón, E., Wong, W.T., Thompson, D., Wiley, H.E., Doss, E.L., Al-Holou, S., Ferris, F.L., Chew, E.Y., Cukras, C., 2015. Impairments in dark adaptation are associated with age-related macular degeneration severity and reticular pseudodrusen. Ophthalmology 122, 2053–2062. https://doi.org/10.1016/j.ophtha.2015.06.023.

Fleckenstein, M., Grassmann, F., Lindner, M., Pfau, M., Czauderna, J., Strunz, T., Von Strachwitz, C., Schmitz-Valckenberg, S., Holz, F.G., Weber, B.H.F., 2016. Distinct genetic risk profile of the rapidly progressing diffuse-trickling subtype of geographic atrophy in age-related macular degeneration (AMD). Invest. Ophthalmol. Vis. Sci. 57, 2463. https://doi.org/10.1167/iovs.15-18593.

Fleckenstein, M., Mitchell, P., Freund, K.B., Sadda, S., Holz, F.G., Brittain, C., Henry, E. C., Ferrara, D., 2018. The progression of geographic atrophy secondary to age-related macular degeneration. Ophthalmology 125, 369–390. https://doi.org/10.1016/j.ophtha.2017.08.038.

Fleckenstein, M., Schmitz-Valckenberg, S., Lindner, M., Bezatis, A., Becker, E., Fimmers, R., Holz, F.G., 2014. The "diffuse-trickling" fundus autofluorescence phenotype in geographic atrophy. Invest. Ophthalmol. Vis. Sci. 55, 2911–2920. https://doi.org/10.1167/iovs.13-13409.

Fleckenstein, M., Schmitz-Valckenberg, S., Martens, C., Kosanetzky, S., Brinkmann, C.K., Hageman, G.S., Holz, F.G., 2011. Fundus autofluorescence and spectral-domain optical coherence tomography characteristics in a rapidly progressing form of geographic atrophy. Invest. Ophthalmol. Vis. Sci. 52, 3761. https://doi.org/10.1167/iovs.10-7021.

Fragiotta, S., Parravano, M., Sacconi, R., Costanzo, E., Viggiano, P., Prascina, F., Capuano, V., Souied, E.H., Querques, G., 2022. A common finding in foveal-sparing extensive macular atrophy with pseudodrusen implicates basal laminar deposits. Retina 42, 1319. https://doi.org/10.1097/IAE.0000000000003463.

Gass, J.D., Sever, R.J., Sparks, D., Goren, J., 1967. A combined technique of fluorescein funduscopy and angiography of the eye. Arch. Ophthalmol. 78, 455–461. https://doi.org/10.1001/archopht.1967.00980030457009.

Gaudric, A., 2023. Value and significance of hypofluorescent lesions seen on late phase indocyanine green angiography. Ophthalmol. Sci. https://doi.org/10.1016/j.xops.2023.100406, 0.

Giani, A., Pellegrini, M., Carini, E., Peroglio Deiro, A., Bottoni, F., Staurenghi, G., 2012. The dark atrophy with indocyanine green angiography in Stargardt disease. Invest. Ophthalmol. Vis. Sci. 53, 3999–4004. https://doi.org/10.1167/iovs.11-9258.

Gliem, M., Fimmers, R., Müller, P.L., Brinkmann, C.K., Finger, R.P., Hendig, D., Holz, F. G., Charbel Issa, P., 2014. Choroidal changes associated with Bruch membrane pathology in pseudoxanthoma elasticum. Am. J. Ophthalmol. 158, 198–207.e3. https://doi.org/10.1016/j.ajo.2014.04.005.

Gliem, M., Hendig, D., Finger, R.P., Holz, F.G., Charbel Issa, P., 2015a. Reticular pseudodrusen associated with a diseased Bruch membrane in pseudoxanthoma elasticum. JAMA Ophthalmol. 133, 581–588. https://doi.org/10.1001/jamaophthalmol.2015.117.

Gliem, M., Müller, P.L., Birtel, J., Hendig, D., Holz, F.G., Charbel Issa, P., 2016a. Frequency, phenotypic characteristics and progression of atrophy associated with a diseased Bruch's membrane in pseudoxanthoma elasticum. Invest. Ophthalmol. Vis. Sci. 57, 3323–3330. https://doi.org/10.1167/iovs.16-19388.

Gliem, M., Müller, P.L., Birtel, J., McGuinness, M.B., Finger, R.P., Herrmann, P., Hendig, D., Holz, F.G., Charbel Issa, P., 2017. Quantitative fundus autofluorescence in pseudoxanthoma elasticum. Invest. Ophthalmol. Vis. Sci. 58, 6159–6165. https://doi.org/10.1167/iovs.17-22007.

Gliem, M., Müller, P.L., Finger, R.P., McGuinness, M.B., Holz, F.G., Charbel Issa, P., 2016b. Quantitative fundus autofluorescence in early and intermediate age-related macular degeneration. JAMA Ophthalmol. 134, 817–824. https://doi.org/10.1001/jamaophthalmol.2016.1475.

Gliem, M., Müller, P.L., Mangold, E., Bolz, H.J., Stöhr, H., Weber, B.H.F., Holz, F.G., Charbel Issa, P., 2015b. Reticular pseudodrusen in Sorsby fundus dystrophy. Ophthalmology 122, 1555–1562. https://doi.org/10.1016/j.ophtha.2015.04.035.

Gliem, M., Müller, P.L., Mangold, E., Holz, F.G., Bolz, H.J., Stöhr, H., Weber, B.H.F., Charbel Issa, P., 2015c. Sorsby fundus dystrophy: novel mutations, novel phenotypic characteristics, and treatment outcomes. Invest. Ophthalmol. Vis. Sci. 56, 2664–2676. https://doi.org/10.1167/iovs.14-15733.

Gliem, M., Zaeytijd, J.D., Finger, R.P., Holz, F.G., Leroy, B.P., Charbel Issa, P., 2013. An update on the ocular phenotype in patients with pseudoxanthoma elasticum. Front. Genet. 4, 14. https://doi.org/10.3389/fgene.2013.00014.

Grubaugh, C.R., Dhingra, A., Prakash, B., Montenegro, D., Sparrow, J.R., Daniele, L.L., Curcio, C.A., Bell, B.A., Hussain, M.M., Boesze-Battaglia, K., 2024. Microsomal triglyceride transfer protein is necessary to maintain lipid homeostasis and retinal function. Faseb. J. 38, e23522. https://doi.org/10.1096/fj.202302491R.

Guan, B., Huryn, L.A., Hughes, A.B., Li, Z., Bender, C., Blain, D., Turriff, A., Cukras, C.A., Hufnagel, R.B., 2022. Early-onset TIMP3-related retinopathy associated with impaired signal peptide. JAMA Ophthalmol. 140, 730–733. https://doi.org/10.1001/jamaophthalmol.2022.1822.

Haeseleer, F., Huang, J., Lebioda, L., Saari, J.C., Palczewski, K., 1998. Molecular characterization of a novel short-chain dehydrogenase/reductase that reduces all-trans-retinal. J. Biol. Chem. 273, 21790–21799. https://doi.org/10.1074/jbc.273.34.21790.

Hagedoorn, A., 1975. Angioid streaks and traumatic ruptures of Bruch's membrane. Br. J. Ophthalmol. 59, 267. https://doi.org/10.1136/bjo.59.5.267.

Hamel, C.P., Meunier, I., Arndt, C., Salah, S.B., Lopez, S., Bazalgette, Christian, Bazalgette, Cécile, Zanlonghi, X., Arnaud, B., Defoort-Dellhemmes, S., Puech, B., 2009. Extensive macular atrophy with pseudodrusen-like appearance: a new clinical entity. Am. J. Ophthalmol. 147, 609–620. https://doi.org/10.1016/j.ajo.2008.10.022.

Hayward, C., Shu, X., Cideciyan, A.V., Lennon, A., Barran, P., Zareparsi, S., Sawyer, L., Hendry, G., Dhillon, B., Milam, A.H., Luthert, P.J., Swaroop, A., Hastie, N.D., Jacobson, S.G., Wright, A.F., 2003. Mutation in a short-chain collagen gene, CTRP5, results in extracellular deposit formation in late-onset retinal degeneration: a genetic model for age-related macular degeneration. Hum. Mol. Genet. 12, 2657–2667. https://doi.org/10.1093/hmg/ddg289.

He, X., Lobsiger, J., Stocker, A., 2009. Bothnia dystrophy is caused by domino-like rearrangements in cellular retinaldehyde-binding protein mutant R234W. Proc. Natl. Acad. Sci. USA 106, 18545–18550. https://doi.org/10.1073/pnas.0907454106.

Heath Jeffery, R.C., Thompson, J.A., Lamey, T.M., McLaren, T.L., McAllister, I.L., Constable, I.J., Mackey, D.A., De Roach, J.N., Chen, F.K., 2021a. Classifying ABCA4 mutation severity using age-dependent ultra-widefield fundus autofluorescence-derived total lesion size. Retina 41, 2578–2588. https://doi.org/10.1097/IAE.0000000000003227.

Heath Jeffery, R.C., Thompson, J.A., Lo, J., Lamey, T.M., McLaren, T.L., McAllister, I.L., Mackey, D.A., Constable, I.J., De Roach, J.N., Chen, F.K., 2021b. Atrophy expansion rates in Stargardt disease using ultra-widefield fundus autofluorescence. Ophthalmol. Sci. 1, 100005. https://doi.org/10.1016/j.xops.2021.100005.

Hess, K., Gliem, M., Birtel, J., Müller, P., Hendig, D., Andrews, C., Murray, I.J., Holz, F.G., Charbel Issa, P., 2020a. Impaired dark adaptation associated with a diseased bruch membrane in pseudoxanthoma elasticum. Retina 40, 1988–1995. https://doi.org/10.1097/IAE.0000000000002689.

Hess, K., Gliem, M., Charbel Issa, P., Birtel, J., Müller, P.L., von der Emde, L., Herrmann, P., Holz, F.G., Pfau, M., 2020b. Mesopic and scotopic light sensitivity and its microstructural correlates in pseudoxanthoma elasticum. JAMA Ophthalmol. 138, 1–9. https://doi.org/10.1001/jamaophthalmol.2020.4335.

Hogan, M.J., 1961. Ultrastructure of the choroid. Its role in the pathogenesis of chorioretinal disease. Trans. Pac. Coast Oto Ophthalmol. Soc. Annu. Meet. 42, 61–87.

Holekamp, N., Wykoff, C.C., Schmitz-Valckenberg, S., Monés, J., Souied, E.H., Lin, H., Rabena, M.D., Cantrell, R.A., Henry, E.C., Tang, F., Swaminathan, B., Martin, J., Ferrara, D., Staurenghi, G., 2020. Natural history of geographic atrophy secondary to age-related macular degeneration: results from the prospective Proxima A and B clinical trials. Ophthalmology 127, 769–783. https://doi.org/10.1016/j.ophtha.2019.12.009.

Holz, F.G., Bindewald-Wittich, A., Fleckenstein, M., Dreyhaupt, J., Scholl, H.P.N., Schmitz-Valckenberg, S., 2007. Progression of geographic atrophy and impact of fundus autofluorescence patterns in age-related macular degeneration. Am. J. Ophthalmol. 143, 463–472.e2. https://doi.org/10.1016/j.ajo.2006.11.041.

Huisingh, C., McGwin Jr., G., Neely, D., Zarubina, A., Clark, M., Zhang, Y., Curcio, C.A., Owsley, C., 2016. The association between subretinal drusenoid deposits in older adults in normal macular health and incident age-related macular degeneration. Invest. Ophthalmol. Vis. Sci. 57, 739–745. https://doi.org/10.1167/iovs.15-18316.

Iyer, P.G., Zhou, H., Zhang, Q., Chu, Z., Shen, M., Shi, Y., Liu, J., Trivizki, O., Lam, B.L., Wang, R.K., Gregori, G., Rosenfeld, P.J., 2022. Swept-source optical coherence tomography detection of bruch membrane and choriocapillaris abnormalities in sorsby macular dystrophy. Retina 42, 1645–1654. https://doi.org/10.1097/IAE.0000000000003515.

Jacobson, S.G., Cideciyan, A.V., Regunath, G., Rodriguez, F.J., Vandenburgh, K., Sheffield, V.C., Stone, E.M., 1995. Night blindness in Sorsby's fundus dystrophy reversed by vitamin A. Nat. Genet. 11, 27–32. https://doi.org/10.1038/ng0995-27.

Jacobson, S.G., Cideciyan, A.V., Wright, E., Wright, A.F., 2001. Phenotypic marker for early disease detection in dominant late-onset retinal degeneration. Invest. Ophthalmol. Vis. Sci. 42, 1882–1890.

Jansen, R.S., Küçükosmanoglu, A., de Haas, M., Sapthu, S., Otero, J.A., Hegman, I.E.M., Bergen, A.A.B., Gorgels, T.G.M.F., Borst, P., van de Wetering, K., 2013. ABCC6 prevents ectopic mineralization seen in pseudoxanthoma elasticum by inducing cellular nucleotide release. Proc. Natl. Acad. Sci. U.S.A. 110, 20206–20211. https://doi.org/10.1073/pnas.1319582110.

Kamami-Levy, C., Querques, G., Rostaqui, O., Blanco-Garavito, R., Souied, E.-H., 2014. Choroidal neovascularization associated with extensive macular atrophy with pseudodrusen-like appearance. J. Fr. Ophtalmol. 37, 780–786. https://doi.org/10.1016/j.jfo.2014.06.003.

Karlin, D.B., Curtin, B.J., 1976. Peripheral chorioretinal lesions and axial length of the myopic eye. Am. J. Ophthalmol. 81, 625–635. https://doi.org/10.1016/0002-9394(76)90129-X.

Keenan, T.D.L., Vanderford, E.K., de Silva, T., Sieving, P.A., Cukras, C.A., 2021. Massive advancing nonexudative type 1 choroidal neovascularization in CTRP5 late-onset retinal degeneration: longitudinal findings on multimodal imaging and implications for age-related macular degeneration. Retina 41, 2236–2245. https://doi.org/10.1097/IAE.0000000000003205.

Keilhauer, C.N., Delori, F.C., 2006. Near-infrared autofluorescence imaging of the fundus: visualization of ocular melanin. Invest. Ophthalmol. Vis. Sci. 47, 3556–3564. https://doi.org/10.1167/iovs.06-0122.

Kellner, U., Weisschuh, N., Weinitz, S., Farmand, G., Deutsch, S., Kortüm, F., Mazzola, P., Schäferhoff, K., Marino, V., Dell'Orco, D., 2021. Autosomal dominant gyrate atrophy-like choroidal dystrophy revisited: 45 Years follow-up and association with a novel C1QTNF5 missense variant. Int. J. Mol. Sci. 22, 2089. https://doi.org/10.3390/ijms22042089.

Khan, K.N., Borooah, S., Lando, L., Dans, K., Mahroo, O.A., Meshi, A., Kalitzeos, A., Agorogiannis, G., Moghimi, S., Freeman, W.R., Webster, A.R., Moore, A.T., McKibbin, M., Michaelides, M., 2020. Quantifying the separation between the retinal pigment epithelium and Bruch's membrane using optical coherence tomography in patients with inherited macular degeneration. Translat. Vis. Sci. Technol. 9, 26. https://doi.org/10.1167/tvst.9.6.26.

Khan, K.N., Mahroo, O.A., Khan, R.S., Mohamed, M.D., McKibbin, M., Bird, A., Michaelides, M., Tufail, A., Moore, A.T., 2016. Differentiating drusen: drusen and drusen-like appearances associated with ageing, age-related macular degeneration, inherited eye disease and other pathological processes. Prog. Retin. Eye Res. 53, 70–106. https://doi.org/10.1016/j.preteyeres.2016.04.008.

Kim, H.J., Sparrow, J.R., 2018. Novel bisretinoids of human retina are lyso alkyl ether glycerophosphoethanolamine-bearing A2PE species. J. Lipid Res. 59, 1620–1629. https://doi.org/10.1194/jlr.M084459.

Klein, R., Davis, M.D., Magli, Y.L., Segal, P., Klein, B.E., Hubbard, L., 1991. The Wisconsin age-related maculopathy grading system. Ophthalmology 98, 1128–1134. https://doi.org/10.1016/s0161-6420(91)32186-9.

Kong, M., Yoon, J., Ham, D.-I., 2018. Electrophysiological function in eyes with reticular pseudodrusen according to fundus distribution. PLoS One 13, e0203146. https://doi.org/10.1371/journal.pone.0203146.

Kotnala, A., Senthilkumari, S., Wu, G., Stewart, T.G., Curcio, C.A., Halder, N., Singh, S.B., Kumar, A., Velpandian, T., 2022. Retinal pigment epithelium in human donor eyes contains higher levels of bisretinoids including A2E in periphery than macula. Invest. Ophthalmol. Vis. Sci. 63, 6. https://doi.org/10.1167/iovs.63.6.6.

Kuntz, C.A., Jacobson, S.G., Cideciyan, A.V., Li, Z.Y., Stone, E.M., Possin, D., Milam, A.H., 1996. Sub-retinal pigment epithelial deposits in a dominant late-onset retinal degeneration. Invest. Ophthalmol. Vis. Sci. 37, 1772–1782.

Laíns, I., Wang, J.C., Cui, Y., Katz, R., Vingopoulos, F., Staurenghi, G., Vavvas, D.G., Miller, J.W., Miller, J.B., 2021. Retinal applications of swept source optical coherence tomography (OCT) and optical coherence tomography angiography (OCTA). Prog. Retin. Eye Res. 84, 100951. https://doi.org/10.1016/j.preteyeres.2021.100951.

Lando, L., Borooah, S., 2022. Late-onset retinal degeneration: clinical perspectives. Clin. Ophthalmol. 16, 3225–3246. https://doi.org/10.2147/OPTH.S362691.

Langton, K.P., McKie, N., Smith, B.M., Brown, N.J., Barker, M.D., 2005. Sorsby's fundus dystrophy mutations impair turnover of TIMP-3 by retinal pigment epithelial cells. Hum. Mol. Genet. 14, 3579–3586. https://doi.org/10.1093/hmg/ddi385.

Lee, M.Y., Yoon, J., Ham, D.-I., 2012. Clinical features of reticular pseudodrusen according to the fundus distribution. Br. J. Ophthalmol. 96, 1222–1226. https://doi.org/10.1136/bjophthalmol-2011-301207.

Li, R.T.H., Roman, A.J., Sumaroka, A., Stanton, C.M., Swider, M., Garafalo, A.V., Heon, E., Vincent, A., Wright, A.F., Megaw, R., Aleman, T.S., Browning, A.C., Dhillon, B., Cideciyan, A.V., 2023. Treatment strategy with gene editing for late-onset retinal degeneration caused by a founder variant in C1QTNF5. Invest. Ophthalmol. Vis. Sci. 64, 33. https://doi.org/10.1167/iovs.64.15.33.

Lindner, M., Bezatis, A., Czauderna, J., Becker, E., Brinkmann, C.K., Schmitz-Valckenberg, S., Fimmers, R., Holz, F.G., Fleckenstein, M., 2015. Choroidal thickness in geographic atrophy secondary to age-related macular degeneration. Invest. Ophthalmol. Vis. Sci. 56, 875–882. https://doi.org/10.1167/iovs.14-14933.

Lindner, Moritz, Böker, A., Mauschitz, M.M., Göbel, A.P., Fimmers, R., Brinkmann, C.K., Schmitz-Valckenberg, S., Schmid, M., Holz, F.G., Fleckenstein, M., Fundus Autofluorescence in Age-Related Macular Degeneration Study Group, 2015. Directional kinetics of geographic atrophy progression in age-related macular degeneration with foveal sparing. Ophthalmology 122, 1356–1365. https://doi.org/10.1016/j.ophtha.2015.03.027.

Littink, K.W., van Genderen, M.M., van Schooneveld, M.J., Visser, L., Riemslag, F.C.C., Keunen, J.E.E., Bakker, B., Zonneveld, M.N., den Hollander, A.I., Cremers, F.P.M., van den Born, L.I., 2012. A homozygous frameshift mutation in LRAT causes retinitis punctata albescens. Ophthalmology 119, 1899–1906. https://doi.org/10.1016/j.ophtha.2012.02.037.

Loewinger, A.-S., Pfau, M., Herrmann, P., Holz, F.G., Pfau, K., 2023. Choriocapillaris flow signal impairment in patients with pseudoxanthoma elasticum. Invest. Ophthalmol. Vis. Sci. 64, 21. https://doi.org/10.1167/iovs.64.2.21.

Mandal, M.N.A., Vasireddy, V., Reddy, G.B., Wang, X., Moroi, S.E., Pattnaik, B.R., Hughes, B.A., Heckenlively, J.R., Hitchcock, P.F., Jablonski, M.M., Ayyagari, R., 2006. CTRP5 is a membrane-associated and secretory protein in the RPE and ciliary body and the S163R mutation of CTRP5 impairs its secretion. Invest. Ophthalmol. Vis. Sci. 47, 5505–5513. https://doi.org/10.1167/iovs.06-0312.

Maw, M.A., Kennedy, B., Knight, A., Bridges, R., Roth, K.E., Mani, E.J., Mukkadan, J.K., Nancarrow, D., Crabb, J.W., Denton, M.J., 1997. Mutation of the gene encoding

cellular retinaldehyde-binding protein in autosomal recessive retinitis pigmentosa. Nat. Genet. 17, 198–200. https://doi.org/10.1038/ng1097-198.
Midena, E., Torresin, T., Velotta, E., Pilotto, E., Parrozzani, R., Frizziero, L., 2021. Hyperreflective retinal foci in diabetic retinopathy: a semi-automatic detection comparative study. Front. Immunol. 12, 613051. https://doi.org/10.3389/fimmu.2021.613051.
Milam, A.H., Curcio, C.A., Cideciyan, A.V., Saxena, S., John, S.K., Kruth, H.S., Malek, G., Heckenlively, J.R., Weleber, R.G., Jacobson, S.G., 2000. Dominant late-onset retinal degeneration with regional variation of sub-retinal pigment epithelium deposits, retinal function, and photoreceptor degeneration. Ophthalmology 107, 2256–2266. https://doi.org/10.1016/s0161-6420(00)00419-x.
Mimoun, G., Soubrane, G., Coscas, G., 1990. Macular drusen [article in French]. J. Fr. Ophtalmol. 13, 511–530.
Miyagishima, K.J., Sharma, R., Nimmagadda, M., Clore-Gronenborn, K., Qureshy, Z., Ortolan, D., Bose, D., Farnoodian, M., Zhang, C., Fausey, A., Sergeev, Y.V., Abu-Asab, M., Jun, B., Do, K.V., Kautzman Guerin, M.-A., Calandria, J., George, A., Guan, B., Wan, Q., Sharp, R.C., Cukras, C., Sieving, P.A., Hufnagel, R.B., Bazan, N.G., Boesze-Battaglia, K., Miller, S., Bharti, K., 2021. AMPK modulation ameliorates dominant disease phenotypes of CTRP5 variant in retinal degeneration. Commun. Biol. 4, 1–16. https://doi.org/10.1038/s42003-021-02872-x.
Moreira-Neto, C.A., Schmidt Andujar, R.A., Chao, J.C.T., Vasconcelos, H., Alves, F.E.E., Rodrigues, G.D., Hirt, B., Arana, J., Souza, E.C., Maia, A., Sallum, J.M.F., Moreira, C. A., 2024. Rheumatic fever and long-term use of benzathine penicillin as possible risk factors for extensive macular atrophy with pseudodrusen in a Brazilian cohort. Int. J. Retina Vitr. 10, 75. https://doi.org/10.1186/s40942-024-00592-y.
Morimura, H., Berson, E.L., Dryja, T.P., 1999. Recessive mutations in the RLBP1 gene encoding cellular retinaldehyde-binding protein in a form of retinitis punctata albescens. Invest. Ophthalmol. Vis. Sci. 40, 1000–1004.
Müller, P.L., Gliem, M., McGuinnes, M., Birtel, J., Holz, F.G., Charbel Issa, P., 2021. Quantitative fundus autofluorescence in ABCA4-related retinopathy -functional relevance and genotype-phenotype correlation. Am. J. Ophthalmol. 222, 340–350. https://doi.org/10.1016/j.ajo.2020.08.042.
Newman, H., Perlman, I., Pras, E., Rozenberg, A., Ben-Yosef, T., Iovino, C., Simonelli, F., Di Iorio, V., Rotenstreich, Y., Katzburg, E., Ehrenberg, M., Iglicki, M., Zur, D., 2022. The target sign: a near infrared feature and multimodal imaging in a pluri-ethnic cohort with RDH5-related fundus albipunctatus. Retina 42, 1364–1369. https://doi.org/10.1097/IAE.0000000000003466.
O'Malley, P., Raymond, A.A., Bradley, R.S., 1965. Paving-stone degeneration of the retina. Arch. Ophthalmol. 73, 169–182. https://doi.org/10.1001/archopht.1965.00970030171006.
Pang, C.E., Freund, K.B., 2014. Ghost maculopathy: an artifact on near-infrared reflectance and multicolor imaging masquerading as chorioretinal pathology. Am. J. Ophthalmol. 158, 171–178.e2. https://doi.org/10.1016/j.ajo.2014.03.003.
Parker, R., Wang, J.-S., Kefalov, V.J., Crouch, R.K., 2011. Interphotoreceptor retinoid-binding protein as the physiologically relevant carrier of 11-cis-Retinol in the cone visual cycle. J. Neurosci. 31, 4714–4719. https://doi.org/10.1523/JNEUROSCI.3722-10.2011.
Parrulli, S., Cozzi, M., Airaldi, M., Romano, F., Viola, F., Sarzi-Puttini, P., Staurenghi, G., Invernizzi, A., 2022. Quantitative autofluorescence findings in patients undergoing hydroxychloroquine treatment. Clin. Exp. Ophthalmol. 50, 500–509. https://doi.org/10.1111/ceo.14090.
Patel, S.S., Lally, D.R., Hsu, J., Wykoff, C.C., Eichenbaum, D., Heier, J.S., Jaffe, G.J., Westby, K., Desai, D., Zhu, L., Khanani, A.M., 2023. Avacincaptad pegol for geographic atrophy secondary to age-related macular degeneration: 18-month findings from the GATHER1 trial. Eye. https://doi.org/10.1038/s41433-023-02497-w.
Pfau, K., Jeffrey, B.G., Cukras, C.A., 2023. Low-dose supplementation with retinol improves retinal function in eyes with age-related macular degeneration but without reticular pseudodrusen. Retina 43, 1462–1471. https://doi.org/10.1097/IAE.0000000000003840.
Pfau, M., Jolly, J.K., Wu, Z., Denniss, J., Lad, E.M., Guymer, R.H., Fleckenstein, M., Holz, F.G., Schmitz-Valckenberg, S., 2021. Fundus-controlled perimetry (microperimetry): application as outcome measure in clinical trials. Prog. Retin. Eye Res. 82, 100907. https://doi.org/10.1016/j.preteyeres.2020.100907.
Pilotto, E., Parolini, F., Midena, G., Cosmo, E., Midena, E., 2024. Small Hyperreflective Retinal Foci as *in vivo* imaging feature of resident microglia activation in geographic atrophy. Exp. Eye Res. 248, 110064. https://doi.org/10.1016/j.exer.2024.110064.
Puech, B., De Laey, J.-J., Holder, G.E. (Eds.), 2014. Inherited Chorioretinal Dystrophies: A Textbook and Atlas. Springer Berlin Heidelberg, Berlin, Heidelberg. https://doi.org/10.1007/978-3-540-69466-3.
Qi, J.H., Ebrahem, Q., Moore, N., Murphy, G., Claesson-Welsh, L., Bond, M., Baker, A., Anand-Apte, B., 2003. A novel function for tissue inhibitor of metalloproteinases-3 (TIMP3): inhibition of angiogenesis by blockage of VEGF binding to VEGF receptor-2. Nat. Med. 9, 407–415. https://doi.org/10.1038/nm846.
Rabiolo, A., Sacconi, R., Cicinelli, M.V., Querques, L., Bandello, F., Querques, G., 2017. Spotlight on reticular pseudodrusen. Clin. Ophthalmol. 11, 1707–1718. https://doi.org/10.2147/OPTH.S130165.
Rajabian, F., Arrigo, A., Bordato, A., Mercuri, S., Bandello, F., Battaglia Parodi, M., 2020. Optical coherence tomography angiography in extensive macular atrophy with pseudodrusen-like appearance. Trans. Vis. Sci. Tech. 9, 2. https://doi.org/10.1167/tvst.9.3.2.
Risseeuw, S., Ossewaarde-van Norel, J., Klaver, C.C.W., Colijn, J.M., Imhof, S.M., van Leeuwen, R., 2019. Visual acuity in pseudoxanthoma elasticum. Retina 39, 1580–1587. https://doi.org/10.1097/IAE.0000000000002173.
Risseeuw, S., Pilgrim, M.G., Bertazzo, S., Brown, C.N., Csincsik, L., Fearn, S., Thompson, R.B., Bergen, A.A., ten Brink, J.B., Kortvely, E., Spiering, W., Ossewaarde–van Norel, J., van Leeuwen, R., Lengyel, I., 2024. Bruch's membrane calcification in pseudoxanthoma elasticum: comparing histopathology and clinical imaging. Ophthalmol. Sci. 4, 100416. https://doi.org/10.1016/j.xops.2023.100416.
Risseeuw, S., van Leeuwen, R., Imhof, S.M., Spiering, W., Norel, J.O., 2021. The natural history of Bruch's membrane calcification in pseudoxanthoma elasticum. Ophthalmol. Sci. 1, 100001. https://doi.org/10.1016/j.xops.2020.100001.
Robson, A.G., Frishman, L.J., Grigg, J., Hamilton, R., Jeffrey, B.G., Kondo, M., Li, S., McCulloch, D.L., 2022. ISCEV Standard for full-field clinical electroretinography (2022 update). Doc. Ophthalmol. 144, 165–177. https://doi.org/10.1007/s10633-022-09872-0.
Romano, D., Colombo, L., Maltese, P., Bertelli, M., Rossetti, L.M., 2023. Bruch membrane rupture and choroidal neovascularization complicating extensive macular atrophy with pseudodrusen-like appearance: a case report. Retin. Cases Brief Rep. 17, 557–561. https://doi.org/10.1097/ICB.0000000000001236.
Romano, F., Airaldi, M., Cozzi, M., Oldani, M., Riva, E., Bertoni, A.I., Dautaj, A., Bertelli, M., Staurenghi, G., Salvetti, A.P., 2021. Progression of atrophy and visual outcomes in extensive macular atrophy with pseudodrusen-like appearance. Ophthalmol. Sci. 1, 100016. https://doi.org/10.1016/j.xops.2021.100016.
Romano, F., Boon, C.J.F., Invernizzi, A., Bosello, F., Casati, S., Zaffalon, C., Riva, E., Bertoni, A.I., Agarwal, A., Kalra, G., Cozzi, M., Staurenghi, G., Salvetti, A.P., 2023a. Correlation between microperimetry and imaging in extensive macular atrophy with pseudodrusen-like appearance (EMAP). Retina. https://doi.org/10.1097/IAE.0000000000003951, 10.1097/IAE.0000000000003951.
Romano, F., Cozzi, M., Casati, S., Bosello, F., Zaffalon, C., Trinco, A., Pellegrini, M., Invernizzi, A., Staurenghi, G., Salvetti, A.P., 2023b. Unveiling the hidden: early manifestations of extensive macular atrophy with pseudodrusen-like appearance. Retin. Cases Brief Rep. https://doi.org/10.1097/ICB.0000000000001513, 10.1097/ICB.0000000000001513.
Romano, F., Cozzi, M., Monteduro, D., Oldani, M., Boon, C.J.F., Staurenghi, G., Salvetti, A.P., 2023c. Natural course and classification of extensive macular atrophy with pseudodrusen-like appearance. Retina 43, 402. https://doi.org/10.1097/IAE.0000000000003683.
Romano, F., Cozzi, M., Salvetti, A.P., 2023d. Multimodal imaging of extensive macular atrophy with pseudodrusen-like appearance. Ophthalmol. Retina 7, 332. https://doi.org/10.1016/j.oret.2023.01.004.
Saari, J.C., 1982. Isolation of cellular retinoid-binding proteins from bovine retina with bound endogenous ligands. Methods Enzymol. 81, 819–826. https://doi.org/10.1016/s0076-6879(82)81109-9.
Saari, J.C., Bredberg, D.L., 1989. Lecithin:retinol acyltransferase in retinal pigment epithelial microsomes. J. Biol. Chem. 264, 8636–8640.
Saari, J.C., Bredberg, D.L., 1987. Photochemistry and stereoselectivity of cellular retinaldehyde-binding protein from bovine retina. J. Biol. Chem. 262, 7618–7622.
Saari, J.C., Crabb, J.W., 2005. Focus on molecules: cellular retinaldehyde-binding protein (CRALBP). Exp. Eye Res. 81, 245–246. https://doi.org/10.1016/j.exer.2005.06.015.
Sadda, S.R., Guymer, R., Holz, F.G., Schmitz-Valckenberg, S., Curcio, C.A., Bird, A.C., Blodi, B.A., Bottoni, F., Chakravarthy, U., Chew, E.Y., Csaky, K., Danis, R.P., Fleckenstein, M., Freund, K.B., Grunwald, J., Hoyng, C.B., Jaffe, G.J., Liakopoulos, S., Monés, J.M., Pauleikhoff, D., Rosenfeld, P.J., Sarraf, D., Spaide, R.F., Tadayoni, R., Tufail, A., Wolf, S., Staurenghi, G., 2018. Consensus definition for atrophy associated with age-related macular degeneration on OCT: classification of atrophy report 3. Ophthalmology 125, 537–548. https://doi.org/10.1016/j.ophtha.2017.09.028.
Sarks, J.P., Sarks, S.H., Killingsworth, M.C., 1988. Evolution of geographic atrophy of the retinal pigment epithelium. Eye 2 (Pt 5), 552–577. https://doi.org/10.1038/eye.1988.106.
Sato, S., Morimoto, T., Fujikado, T., Tanaka, S., Tsujikawa, M., Nishida, K., 2022a. Extensive macular atrophy with pseudodrusen in a Japanese patient evaluated by wide-field OCTA. Case Rep. Ophthalmol. 13, 847–854. https://doi.org/10.1159/000526970.
Sato, S., Morimoto, T., Fujikado, T., Tanaka, S., Tsujikawa, M., Nishida, K., 2022b. Extensive macular atrophy with pseudodrusen in a Japanese patient evaluated by wide-field OCTA. Case Rep. Ophthalmol. 13, 847–854. https://doi.org/10.1159/000526970.
Schatz, P., Preising, M., Lorenz, B., Sander, B., Larsen, M., Rosenberg, T., 2011. Fundus albipunctatus associated with compound heterozygous mutations in RPE65. Ophthalmology 118, 888–894. https://doi.org/10.1016/j.ophtha.2010.09.005.
Schmetterer, L., Scholl, H., Garhöfer, G., Janeschitz-Kriegl, L., Corvi, F., Sadda, S.R., Medeiros, F.A., 2023. Endpoints for clinical trials in ophthalmology. Prog. Retin. Eye Res. 97, 101160. https://doi.org/10.1016/j.preteyeres.2022.101160.
Schmitz-Valckenberg, S., Brinkmann, C.K., Alten, F., Herrmann, P., Stratmann, N.K., Göbel, A.P., Fleckenstein, M., Diller, M., Jaffe, G.J., Holz, F.G., 2011. Semiautomated image processing method for identification and quantification of geographic atrophy in age-related macular degeneration. Invest. Ophthalmol. Vis. Sci. 52, 7640–7646. https://doi.org/10.1167/iovs.11-7457.
Schmitz-Valckenberg, S., Pfau, M., Fleckenstein, M., Staurenghi, G., Sparrow, J.R., Bindewald-Wittich, A., Spaide, R.F., Wolf, S., Sadda, S.R., Holz, F.G., 2021. Fundus autofluorescence imaging. Prog. Retin. Eye Res. 81, 100893. https://doi.org/10.1016/j.preteyeres.2020.100893.
Schmitz-Valckenberg, S., Sadda, S., Staurenghi, G., Chew, E.Y., Fleckenstein, M., Holz, F. G., CAM (Classification of Atrophy Meeting)-Group, 2016a. Geographic atrophy: semantic considerations and literature review. Retina 36, 2250–2264. https://doi.org/10.1097/IAE.0000000000001258.
Schmitz-Valckenberg, S., Sahel, J.-A., Danis, R., Fleckenstein, M., Jaffe, G.J., Wolf, S., Pruente, C., Holz, F.G., 2016b. Natural history of geographic atrophy progression secondary to age-related macular degeneration (geographic atrophy progression

study). Ophthalmology 123, 361–368. https://doi.org/10.1016/j.ophtha.2015.09.036.
Schoenberger, S.D., Agarwal, A., 2013. Geographic chorioretinal atrophy in pseudoxanthoma elasticum. Am. J. Ophthalmol. 156, 715–723. https://doi.org/10.1016/j.ajo.2013.05.034.
Sergouniotis, P.I., Sohn, E.H., Li, Z., McBain, V.A., Wright, G.A., Moore, A.T., Robson, A.G., Holder, G.E., Webster, A.R., 2011. Phenotypic variability in RDH5 retinopathy (fundus albipunctatus). Ophthalmology 118, 1661–1670. https://doi.org/10.1016/j.ophtha.2010.12.031.
Shields, C.L., Guzman, J.M., Shapiro, M.J., Fogel, L.E., Shields, J.A., 2010. Torpedo maculopathy at the site of the fetal "bulge.". Arch. Ophthalmol. 128, 499–501. https://doi.org/10.1001/archophthalmol.2010.29.
Sivaprasad, S., Webster, A.R., Egan, C.A., Bird, A.C., Tufail, A., 2008. Clinical course and treatment outcomes of Sorsby fundus dystrophy. Am. J. Ophthalmol. 146, 228–234. e2. https://doi.org/10.1016/j.ajo.2008.03.024.
Smirnov, V.M., Wilmet, B., Nassisi, M., Condroyer, C., Antonio, A., Andrieu, C., Devisme, C., Sancho, S., Sahel, J.-A., Zeitz, C., Audo, I., 2022. Large benefit from simple things: high-dose vitamin A improves RBP4-related retinal dystrophy. Int. J. Mol. Sci. 23, 6590. https://doi.org/10.3390/ijms23126590.
Smith, R.T., Sohrab, M.A., Busuioc, M., Barile, G., 2009. Reticular macular disease. Am. J. Ophthalmol. 148, 733–743.e2. https://doi.org/10.1016/j.ajo.2009.06.028.
Sorsby, A., Mason, M.E.J., 1949. A fundus dystrophy with unusual features. Br. J. Ophthalmol. 33, 67–97. https://doi.org/10.1136/bjo.33.2.67.
Soumplis, V., Sergouniotis, P.I., Robson, A.G., Michaelides, M., Moore, A.T., Holder, G.E., Webster, A.R., 2013. Phenotypic findings in C1QTNF5 retinopathy (late-onset retinal degeneration). Acta Ophthalmol. 91, e191–e195. https://doi.org/10.1111/aos.12010.
Spaide, R.F., 2018. Improving the age-related macular degeneration construct: a new classification system. Retina 38, 891–899. https://doi.org/10.1097/IAE.0000000000001732.
Spaide, R.F., 2013. Outer retinal atrophy after regression of subretinal drusenoid deposits as a newly recognized form of late age-related macular degeneration. Retina 33, 1800–1808. https://doi.org/10.1097/IAE.0b013e31829c3765.
Spaide, R.F., Fujimoto, J.G., Waheed, N.K., Sadda, S.R., Staurenghi, G., 2018. Optical coherence tomography angiography. Prog. Retin. Eye Res. 64, 1–55. https://doi.org/10.1016/j.preteyeres.2017.11.003.
Spaide, R.F., Vavvas, D.G., 2023. Complement inhibition for geographic atrophy: review of salient functional outcomes and perspective. Retina 43, 1064–1069. https://doi.org/10.1097/IAE.0000000000003796.
Sparrow, J.R., Duncker, T., Schuerch, K., Paavo, M., de Carvalho, J.R.L., 2020. Lessons learned from quantitative fundus autofluorescence. Prog. Retin. Eye Res. 74, 100774. https://doi.org/10.1016/j.preteyeres.2019.100774.
Stecher, H., Gelb, M.H., Saari, J.C., Palczewski, K., 1999. Preferential release of 11-cis-retinol from retinal pigment epithelial cells in the presence of cellular retinaldehyde-binding protein. J. Biol. Chem. 274, 8577–8585. https://doi.org/10.1074/jbc.274.13.8577.
Strauss, R.W., Kong, X., Ho, A., Jha, A., West, S., Ip, M., Bernstein, P.S., Birch, D.G., Cideciyan, A.V., Michaelides, M., Sahel, J.-A., Sunness, J.S., Traboulsi, E.I., Zrenner, E., Pitetta, S., Jenkins, D., Hariri, A.H., Sadda, S., Scholl, H.P.N., ProgStar Study Group, 2019. Progression of Stargardt disease as determined by fundus autofluorescence over a 12-month period: ProgStar report No. 11. JAMA Ophthalmol. 137, 1134–1145. https://doi.org/10.1001/jamaophthalmol.2019.2885.
Strauss, R.W., Muñoz, B., Ho, A., Jha, A., Michaelides, M., Cideciyan, A.V., Audo, I., Birch, D.G., Hariri, A.H., Nittala, M.G., Sadda, S., West, S., Scholl, H.P.N., ProgStar Study Group, 2017. Progression of Stargardt disease as determined by fundus autofluorescence in the retrospective progression of Stargardt disease study (ProgStar report No. 9). JAMA Ophthalmol. 135, 1232–1241. https://doi.org/10.1001/jamaophthalmol.2017.4152.
Streeten, B.W., 1969. Development of the human retinal pigment epithelium and the posterior segment. Arch. Ophthalmol. 81, 383–394. https://doi.org/10.1001/archopht.1969.00990010385017.
Subrayan, V., Morris, B., Armbrecht, A.M., Wright, A.F., Dhillon, B., 2005. Long anterior lens zonules in late-onset retinal degeneration (L-ORD). Am. J. Ophthalmol. 140, 1127–1129. https://doi.org/10.1016/j.ajo.2005.06.023.
Sura, A.A., Chen, L., Messinger, J.D., Swain, T.A., McGwin, G., Freund, K.B., Curcio, C.A., 2020. Measuring the contributions of basal laminar deposit and Bruch's membrane in age-related macular degeneration. Invest. Ophthalmol. Vis. Sci. 61, 19. https://doi.org/10.1167/iovs.61.13.19.
Suzuki, M., Sato, T., Spaide, R.F., 2014. Pseudodrusen subtypes as delineated by multimodal imaging of the fundus. Am. J. Ophthalmol. 157, 1005–1012. https://doi.org/10.1016/j.ajo.2014.01.025.
Tan, A.C.S., Fleckenstein, M., Schmitz-Valckenberg, S., Holz, F.G., 2016. Clinical application of multicolor imaging technology. Ophthalmologica 236, 8–18. https://doi.org/10.1159/000446857.
Tan, A.C.S., Pilgrim, M.G., Fearn, S., Bertazzo, S., Tsolaki, E., Morrell, A.P., Li, M., Messinger, J.D., Dolz-Marco, R., Lei, J., Nittala, M.G., Sadda, S.R., Lengyel, I., Freund, K.B., Curcio, C.A., 2018. Calcified nodules in retinal drusen are associated with disease progression in age-related macular degeneration. Sci. Transl. Med. 10, eaat4544. https://doi.org/10.1126/scitranslmed.aat4544.
Tan, R.S., Guymer, R.H., Aung, K.-Z., Caruso, E., Luu, C.D., 2019. Longitudinal assessment of rod function in intermediate age-related macular degeneration with and without reticular pseudodrusen. Invest. Ophthalmol. Vis. Sci. 60, 1511–1518. https://doi.org/10.1167/iovs.18-26385.
Tsunoda, K., Fujinami, K., Yoshitake, K., Iwata, T., 2019. Late-onset night blindness with peripheral flecks accompanied by progressive trickle-like macular degeneration. Doc. Ophthalmol. 139, 171–184. https://doi.org/10.1007/s10633-019-09705-7.
Ueda-Arakawa, N., Ooto, S., Nakata, I., Yamashiro, K., Tsujikawa, A., Oishi, A., Yoshimura, N., 2013. Prevalence and genomic association of reticular pseudodrusen in age-related macular degeneration. Am. J. Ophthalmol. 155, 260–269.e2. https://doi.org/10.1016/j.ajo.2012.08.011.
Vatavuk, Z., Andrijević Derk, B., Knežević, T., Belak, M., Milošević, M., Friberg, T.R., 2018. Morphological and angiographic peripheral retinal changes in patients with age-related macular degeneration. Ophthalmol. Retina 2, 201–208. https://doi.org/10.1016/j.oret.2017.06.013.
Verbakel, S.K., van Huet, R.A.C., Boon, C.J.F., den Hollander, A.I., Collin, R.W.J., Klaver, C.C.W., Hoyng, C.B., Roepman, R., Klevering, B.J., 2018. Non-syndromic retinitis pigmentosa. Prog. Retin. Eye Res. 66, 157–186. https://doi.org/10.1016/j.preteyeres.2018.03.005.
Vilela, M.A.P., Battaglia Parodi, M., 2022. Extensive macular atrophy with pseudodrusen-like: case series and review. Eur. J. Ophthalmol. 11206721221102269. https://doi.org/10.1177/11206721221102269.
von Lintig, J., Kiser, P.D., Golczak, M., Palczewski, K., 2010. The biochemical and structural basis for trans-to-cis isomerization of retinoids in the chemistry of vision. Trends Biochem. Sci. 35, 400–410. https://doi.org/10.1016/j.tibs.2010.01.005.
Watanabe, S.E.S., Quercia, A.Z.F., Sacai, P.Y., 2023. Electrophysiological findings in extensive macular atrophy with pseudodrusen. Doc. Ophthalmol. https://doi.org/10.1007/s10633-023-09941-y.
Weber, B.H., Vogt, G., Pruett, R.C., Stöhr, H., Felbor, U., 1994. Mutations in the tissue inhibitor of metalloproteinases-3 (TIMP3) in patients with Sorsby's fundus dystrophy. Nat. Genet. 8, 352–356. https://doi.org/10.1038/ng1294-352.
Wei, W., Mazzola, M., Otero-Marquez, O., Tong, Y., Souied, E., Querques, G., Bailey Freund, K., Theodore Smith, R., 2023. Two potentially distinct pathways to geographic atrophy in age-related macular degeneration characterized by quantitative fundus autofluorescence. Eye 37, 2281–2288. https://doi.org/10.1038/s41433-022-02332-8.
Wu, Z., Fletcher, E.L., Kumar, H., Greferath, U., Guymer, R.H., 2022. Reticular pseudodrusen: a critical phenotype in age-related macular degeneration. Prog. Retin. Eye Res. 88, 101017. https://doi.org/10.1016/j.preteyeres.2021.101017.
Wu, Z., Luu, C.D., Ayton, L.N., Goh, J.K., Lucci, L.M., Hubbard, W.C., Hageman, J.L., Hageman, G.S., Guymer, R.H., 2014. Optical coherence tomography–defined changes preceding the development of drusen-associated atrophy in age-related macular degeneration. Ophthalmology 121, 2415–2422. https://doi.org/10.1016/j.ophtha.2014.06.034.
Xu, L., Blonska, A.M., Pumariega, N.M., Bearelly, S., Sohrab, M.A., Hageman, G.S., Smith, R.T., 2013. Reticular macular disease is associated with multilobular geographic atrophy in age-related macular degeneration. Retina 33, 1850–1862. https://doi.org/10.1097/IAE.0b013e31828991b2.
Xu, L., Ruddick, W.N., Bolch, S.N., Klingeborn, M., Dyka, F.M., Kulkarni, M.M., Simpson, C.P., Beltran, W.A., Bowes Rickman, C., Smith, W.C., Dinculescu, A., 2023. Distinct phenotypic consequences of pathogenic mutants associated with late-onset retinal degeneration. Am. J. Pathol. 193, 1706–1720. https://doi.org/10.1016/j.ajpath.2022.10.004.
Yang, G., Liu, Z., Xie, S., Li, C., Lv, L., Zhang, M., Zhao, J., 2017. Genetic and phenotypic characteristics of four Chinese families with fundus albipunctatus. Sci. Rep. 7, 46285. https://doi.org/10.1038/srep46285.
Yates, J.R.W., Sepp, T., Matharu, B.K., Khan, J.C., Thurlby, D.A., Shahid, H., Clayton, D.G., Hayward, C., Morgan, J., Wright, A.F., Armbrecht, A.M., Dhillon, B., Deary, I.J., Redmond, E., Bird, A.C., Moore, A.T., Genetic Factors in AMD Study Group, 2007. Complement C3 variant and the risk of age-related macular degeneration. N. Engl. J. Med. 357, 553–561. https://doi.org/10.1056/NEJMoa072618.
Yehoshua, Z., Rosenfeld, P.J., Gregori, G., Feuer, W.J., Falcão, M., Lujan, B.J., Puliafito, C., 2011. Progression of geographic atrophy in age-related macular degeneration imaged with spectral domain optical coherence tomography. Ophthalmology 118, 679–686. https://doi.org/10.1016/j.ophtha.2010.08.018.
Zeitz, C., Roger, J.E., Audo, I., Michiels, C., Sánchez-Farías, N., Varin, J., Frederiksen, H., Wilmet, B., Callebert, J., Gimenez, M.-L., Bouzidi, N., Blond, F., Guilllonneau, X., Fouquet, S., Léveillard, T., Smirnov, V., Vincent, A., Héon, E., Sahel, J.-A., Kloeckener-Gruissem, B., Sennlaub, F., Morgans, C.W., Duvoisin, R.M., Tkatchenko, A.V., Picaud, S., 2023. Shedding light on myopia by studying complete congenital stationary night blindness. Prog. Retin. Eye Res. 93, 101155. https://doi.org/10.1016/j.preteyeres.2022.101155.
Zweifel, S.A., Spaide, R.F., Curcio, C.A., Malek, G., Imamura, Y., 2010. Reticular pseudodrusen are subretinal drusenoid deposits. Ophthalmology 117, 303–312.e1. https://doi.org/10.1016/j.ophtha.2009.07.014.